UNIVERSITÀ DEGLI STUDI DI MILANO

Scuola di Dottorato in Scienze Biologiche e Molecolari

XXVII Ciclo

Molecular characterization of membrane-bound glycoproteins involved in human diseases and potential targets for new therapies

Genny Degani

PhD Thesis

Scientific tutor: Prof.ssa Laura Popolo

Scientific co-tutors: Prof. Giancarlo Aldini

Prof. Guenter Fritz

Academic year: 2013-2014

SSD: BIO/11 and BIO/10

Thesis performed at the Department of Biosciences and at the Department of Pharmaceutical Sciences of the University of Milan, and at the Institute of Pathology of the Universitätsklinicum, Department of Neuropathology, Freiburg, Germany

Contents

PART I

Abstract

The present thesis is focused on the molecular characterization of two eukaryotic membrane glycoproteins that are promising candidates for new therapeutic approaches to human diseases.

The first glycoprotein is the human Receptor for the Advanced Glycation End products (hRAGE), a member of the immunoglobulin superfamily. RAGE is a type I transmembrane glycoprotein that is beneficial in normal physiological conditions but it is also a key player in the etiology and progression of several chronic pathologies such as neurodegenerative disorders (Alzheimer), atherosclerosis, cancer and complications of metabolic diseases such as diabetes, by exacerbating the inflammatory response. A variety of ligands sharing an acidic charge, as the advanced glycation End products (AGEs), S100 proteins, HMGB1, Aβ-amyloids, bind to the extracellular V or VC1 domains of RAGE. These domains are N-glycosylated and stabilized by disulphide bonds. To overcome the tendency to aggregate of the V and VC1 domains expressed in bacteria, in this work V and VC1 domains were expressed as secreted proteins in the methylotrophic yeast *Pichia pastoris*. While VC1 was secreted into the culture medium and was functional, the V domain was retained intracellularly, providing the first *in vivo* indication that V requires C1 to fold into a structurally stable domain. The glycosylation pattern of VC1 reflects the glycosylation of RAGE isolated from mammalian sources. A simple procedure for the purification to homogeneity of VC1 from the medium was generated and the folded state of the purified protein was assessed by thermal shift assays. The protein showed a remarkable improved thermal stability compared to VC1 expressed in bacteria. The stability and full solubility of glycosylated VC1 may be beneficial for *in vitro* studies aimed at the identification of new ligands or inhibitors of RAGE.

The second object of this thesis was the Phr family of *Candida albicans*, a dimorphic fungal pathogen responsible of life-threatening invasive infections. These glycoproteins are anchored to the plasma membrane through a GPI. Phr proteins belong to family GH72 of cell wall glucan remodelling enzymes that are unique to fungi and essential for morphogenesis, cell wall integrity and virulence. For these reasons, these enzymes are targets for inhibitors of the cell wall formation to be used in therapy, similarly to what penicillins have been for bacteria. The catalytic properties of Phr proteins were studied using a new fluorescent assay. Phr1p and Phr2p are specific for β-1,3-glucan, the pH optimum was 5.8 for Phr1p and 3 for Phr2p and the temperature optimum was 30°C. Pga4p was inactive suggesting that it turned out into a structural cell wall protein. Finally, we studied the transcriptome of cells lacking β-1,3-glucan remodelling (*phr1*Δ cells) after induction of growth as hypha, the invasive form of this pathogen. About 310 genes were modulated and genetic analysis showed that chitin synthesis by the Chs3p isoform is essential for viability of *phr1*Δ cells.

Introduction

In pharmaceutical research, the identification and validation of a target involved in a particular pathology are the first steps in the process of target-based drug discovery. When the identified target is a protein, its recombinant production is mandatory for the entire process of drug development. The majority of the drugs are inhibitors that block the action of target proteins. The isolation of the protein is required to perform structural and biochemical studies providing results that could drive the design of the drug and the set-up of *in vitro* assays. Moreover, the recombinant protein could be used also for preliminary screenings to identify inhibitors from libraries of different compounds.

The potential candidates as targets for therapy are often glycoproteins and namely hormones, growth factors, membrane-bound receptors, extracellular enzymes and antibodies. It has been estimated that about 30% of the human proteins are directed to the secretory pathway and the majority of them are glycosylated, often contain disulphide bonds and are endowed of complex folding [2]. Protein glycosylation has multiple functions in the cell. For instance, in the endoplasmic reticulum glycosylation is used to monitor protein folding, acting as a quality control system that guarantees only properly folded proteins to translocate to the Golgi apparatus. Moreover, the sugar added to soluble proteins can be recognized by specific receptors in the Golgi promoting their transport to the final destination. Since sugars are hydrophilic, glycans improve the solubility of the proteins and their steric hindrance protects proteins from the attack by extracellular proteases and also confers resistance to denaturation [3, 4].

The most common host cell for the expression of recombinant proteins is *Escherichia coli*. However, bacteria are unable to carry out post-translational modifications and also proteins with complex folding are difficult to express in this microorganism. The aim of the present thesis has been the molecular characterization of two types of eukaryotic membrane-bound glycoproteins that are promising candidates for new therapeutic approaches of human diseases. In order to obtain soluble and glycosylated versions of these proteins and of their domains for the intended biochemical studies, we aimed at the heterologous expression in the eukaryotic methylotrophic yeast *Pichia pastoris*.

The first glycoprotein that is object of this thesis is the human Receptor for the Advanced Glycation End products, hRAGE. This trans-membrane glycoprotein is a multi-ligand receptor with a modular organization of its domains. hRAGE plays a crucial role in several aspects of human physiology but it is also involved in the establishment and progression of several diseases like neurodegenerative disorders, chronic inflammation, and also complications deriving from metabolic diseases. At this regard, hRAGE contributes to the complications of diabetes especially to the chronic pathologies

affecting the microvascular system such as retinopathy. Studies of the interaction of hRAGE with its ligands can prove useful for future identification of antagonists. Therefore, this thesis focused on the ligand-binding domains of the receptor.

The second subject of this work has been the family of Phr glycoproteins that are anchored to the plasma membrane of *Candida albicans* through a GPI (glycosyl phosphatidyl inositol). This microorganism is a common commensal of human mucosae that can turn into a pathogen and cause life-threatening invasive infections in immunocompromised patients. Phr proteins are transglycosylases belonging to family GH72. The work of this thesis focused on these enzymes because they are unique to fungi and are essential for cell wall assembly, morphogenesis, virulence and cell viability and therefore represent promising target for new drugs directed against the fungal cell wall. Since the armamentarium of antifungal agents is still limited, studies on the GH72 enzymes can contribute to the identification of new inhibitors of cell wall formation, which could have an impact similarly to penicillins antibacterial treatment.

hRAGE

The human Receptor for Advanced Glycation End products

The human Receptor for Advanced Glycation End products (hRAGE) is a multi-ligand receptor described as a PRR (Pattern Recognition Receptor) since it binds different ligands sharing a common pattern. It was originally identified and characterized by Neeper and Schmidt in 1992 [5, 6] on the basis of its ability to bind AGE-BSA, an Advanced Glycation End product (AGE) and representative of a large and heterogeneous group of molecules formed by non enzymatic reactions of proteins with sugars [1]. Besides, subsequent studies showed that hRAGE also binds calgranulin/S100 protein family [1, 7], amyloid-β peptide (Aβ) and β-sheet fibrils [8], High Mobility Group protein Box-1 (HMGB1) [9] and other ligands reported in **Table 1**. Even if RAGE ligands do not display amino acid sequence similarity, they all share a net negative charge at neutral pH, in contrast with the positive charge of the domain of RAGE involved in the ligand binding [1].
The binding of a ligand to RAGE leads to the activation of different signal transduction pathways depending on cell type, context and ligand. RAGE is highly expressed at the mRNA and protein levels in early developmental stages, but in adult cells (except in the lung) its expression is very low [10]. Under pathogenic scenarios, such as diabetic vascular disease, accelerated atherosclerosis, cardiovascular disorders, nephropathy and chronic inflammation, a sustained up-regulation of RAGE levels was observed in concomitance with the accumulation of its ligands [1].

As shown in **Figure 1** RAGE is a type I glycoprotein with a single membrane spanning domain and is a member of the immunoglobulin superfamily of cell surface receptors [11]. Its extracellular portion contains one V-type immunoglobulin domain and two consecutive C-type immunoglobulin-like domains (C1 and C2). The V-C1 domains are involved in ligand binding and they are believed to form together an integrated structural and functional unit. The V-C1 domain is connected to the C2 domain through a flexible linker and C2 constitutes another independent unit. The short cytoplasmic tail of RAGE is devoid of any enzymatic activity and any defined structure, but is essential for signal transduction [1].

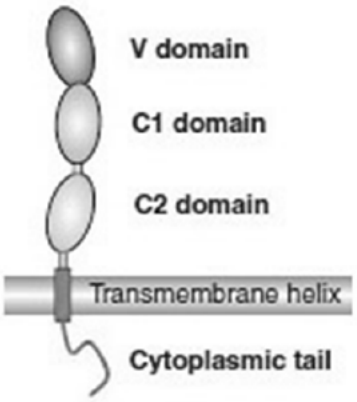

Figure 1. Schematic representation of hRAGE [1]

RAGE: from gene to protein

The human *RAGE* gene (also termed *AGER*) is located on the chromosome 6, in the major histocompatibility complex (MHC) class III region [12]. *AGER* is composed of 11 exons and 10 short introns, a 5'flanking region that regulates its transcription and overlaps the 3'-UTR of *PBX2* (pre-B-cell leukaemia homeobox 2) gene, and a 3'-UTR (**Figure 2**) [12].

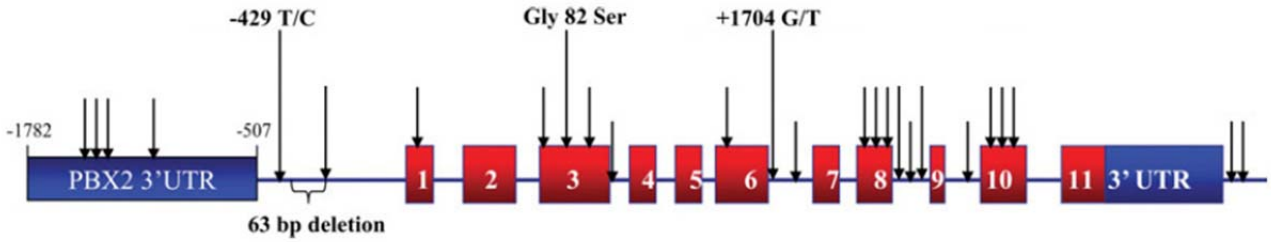

Figure 2. Structure of *AGER* gene. The gene is composed of a 5'-flanking region that overlaps with the *PBX2* gene 3'-UTR, 11 exons (red boxes) and a 3'-UTR. Arrows indicate the identified polymorphisms, the best known being -429T/C, Gly82Ser and +1704G/T [13].

Approximatly 30 single nucleotide polymorphisms (SNP) were identified in *AGER* resulting in changes in the amino acid sequence or non coding changes in exons or changes in introns and in the 5'-flanking region. The polymorphisms -429 T/C, Gly82Ser (resulting in the amino acid substitution of glycine with serine at position 82) and +1704 G/T are the most interesting because they proved to be rather common and associated with diseases [14].

The Gly82Ser polymorphism was one of the first identified polymorphisms of *AGER* and occurs in the ligand binding V domain of RAGE. This is the only frequent coding-change polymorphism in the *AGER*. The association between Gly82Ser polymorphism and the N-glycosylation of Asn81 will be discussed below (section "RAGE is a glycoprotein").

The expression of *AGER* is tightly controlled at multiple levels in different cell type, both in physiological and pathological conditions. Different transcription factor binding sites, as well as silencing/enhancing regulatory mechanisms, were discovered [6]. The nuclear factor-κB (NF-*κ*B), specificity protein 1 (SP-1), activator proteins 1 and 2 (AP-1 and AP-2), E-twenty-six 1 factor (Ets-1), Hypoxia-inducible factor-1 (HIF-1), Early growth response transcription factor 1 (Egr-1) and Thyroid transcription factor-1 (TFF-1) putatively regulate the transcription of *AGER*, since the binding sites of these factors were found in the regulatory 5'-flanking region. An epigenetic regulation of *AGER* expression also occurs via methylation of cytosines in the AP-2 and SP-1 binding elements of the *AGER* promoter [6, 15]. Further, the 3'-UTR of the *AGER* mRNA is differentially polyadenylated to regulate the stability of the mRNA and the 3'UTR has also a target site for mir-30 miRNA, able to affect the *AGER* mRNA stability when necessary [15].

Alternative splicing extensively modulate the *AGER* transcript, resulting in different translation products [12].

The most abundant protein form encoded by the *AGER* is the full-length RAGE (fl-RAGE). It consists of 404 amino acids, including the signal peptide (amino acids 1-23) that is removed during the co-translational translocation of RAGE precursor into the ER membrane, the full ectodomain, the transmembrane domain (TMD, amino acids 340-361) and a cytoplasmic tail (amino acids 362-404) as reported in scheme of **Figure 1** and **Figure 3** [16].

Besides the fl-RAGE, 19 naturally occurring splicing variants were described in humans, but only a minor fraction is translated into proteins [17]. It has been estimated that about 50% of the alternative splicing products in humans are targeted to the nonsense-mediated mRNA decay (NMD) degradation pathway, resulting in the reduction of the total number of functional RAGE transcripts [12, 17]. The major splicing products of RAGE pre-mRNA are represented in **Figure 3**.

RAGE with the deletion of the V domain is unable to interact with its ligands and is unresponsive to any stimulus, whereas RAGE without the cytoplasmic tail functions as a "decoy" receptor with dominant negative effects (called dominant negative RAGE, DN-RAGE). It competes with the endogenous fl-RAGE for ligand binding, but is unable to transmit signal transduction activated by RAGE [17, 18]. Another splicing variant is the soluble form of RAGE (sRAGE) which lacks the TMD and the C-terminal tail. sRAGE is secreted into the extracellular space and there it can act as scavenger preventing ligands to interact with fl-RAGE or with other cell surface receptors. Another mechanism to generate sRAGE is by proteolytic cleavage of fl-RAGE through the action of the metalloproteinases ADAM10 and MMP9. sRAGE is the most studied isoform of RAGE, since the decrease of the circulating levels of sRAGE was reported in several RAGE-associated pathological disorders [17].

All these isoforms are thought to be possible regulators of the fl-RAGE, either by the competition for ligand binding or by replacing the full-length receptor in the membrane [19].

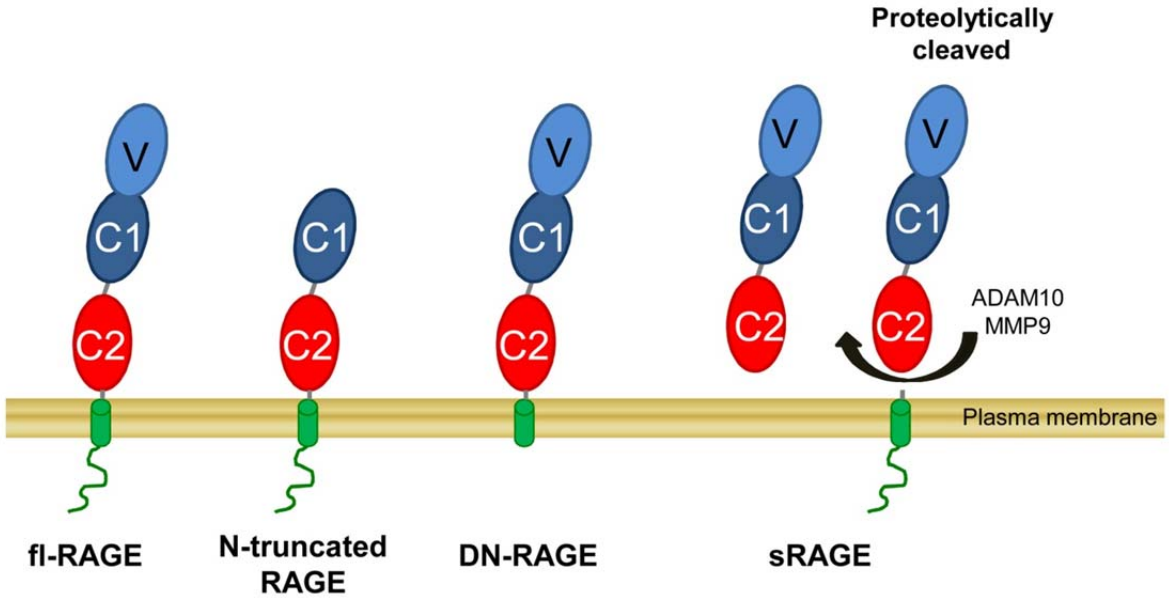

Figure 3. Schematic representation of RAGE variants produced by alternative splicing of *AGER* pre-mRNA or proteolytic cleavage.

Protein structure and surface properties

The structure of the RAGE appears to be a very interesting topic considering the number of protein resolved structures deposited on the Protein Data Bank (PDB, http://www.rcsb.org/pdb/home/home.do) during the last years (18 structures of RAGE on April 2015). The V, C1 and C2 domains form an elongated structure [16]. Since the isolated V or C1 domains produced in bacteria have an intrinsic instability and a highly dynamic conformation compared to the VC1 domain, it has been proposed that V and C1 form a single integrated domain [16]. The VC1 domain and the C2 domain are connected by a segment of several amino acid residues with no apparent secondary structure forming a flexible linker. NMR studies show that VC1 moves as a single unit with respect to the C2 domain [1, 16]. The boundaries of the domains were defined: V (residue 23-119), C1 domain (residue 120-233) and C2 domain (residue 234-325). Since the tandem VC1 domain is involved in the ligand binding, it was subjected to different structural studies, as demonstrated by two papers appeared in 2010 reporting the crystal structure of VC1, solved at 1.85 Å and 1.5 Å respectively [20, 21].

VC1 forms an elongated structure with an angle of 145° between the two Ig-like domains [20]. A specific interface between the domains is observed and includes several interdomain hydrogen bonds and hydrophobic interactions [20].

Although, on the basis of sequence alignments, the V domain had been assigned to the Variable domain (V-set) of immunoglobulins, once the structure was determined it revealed features typical of Intermediate topology (I-set) which is characteristic of cell adhesion molecules or muscle

proteins. Even if more correctly classified as an I-domain, V nomenclature remains in the literature [1].

The V domain is composed of eight β-strands (A, C, C_0, F, G, B, D, E) connected by seven loops to form two β-sheets. A, C, C_0, F, and G form one β-sheet, while strands B, D, and E form the second β-sheet. The two β-sheets are oriented in opposite manner (**Figure 4**). β-strands B and F are connected by a conserved disulphide bond (Cys38-Cys99). A short 3_{10} helix exists in the structure of the V domain (between strands E and F). The loops are well structured through extensive intramolecular hydrogen bonds [20, 21].

The C1 domain fits with the C1-set of Ig molecules, with strands A, B, D, and E forming the back β-sheet and strands C, C_0, F, and G forming the front sheet of the β-sandwich. RAGE C1 domain has a unique topology distinct from other Ig fold sets: it contains two additional β-strands, A_0 and G_0, which form a small parallel β-sheet. This additional β-sheet stabilizes the C-terminus of the domain. Moreover, a hydrogen bond between Arg198 (in a loop in C1 domain) and Pro232 (in the linker between C1 and C2) stabilizes the C-terminus of C1 domain (**Figure 4**) [20, 21]. A disulphide bond connects Cys144 with Cys208.

In the high-resolution structure, an extension of 10 well-ordered residues was observed at the C-terminal of C1 (Glu231-Leu240) and this segment constitutes the linker to the C2 domain [16]. The C1-C2 linker confers a high degree of mobility to the C2 domain (in the isolated protein) relatively to the VC1 rigid block, allowing free rotation of the C2 domain around the VC1 domain [20, 21].

The C2 domain adopts an Ig folds that belongs to the S-type and its structure is depicted in **Figure 5**. C2 domain is composed of 8 β-strands, connected by unstructured loops. Beyond the hydrogen bonds, there is an internal disulphide bond between Cys259 (in strand B) and Cys301 (in strand F) that stabilizes the C2 domain [22].

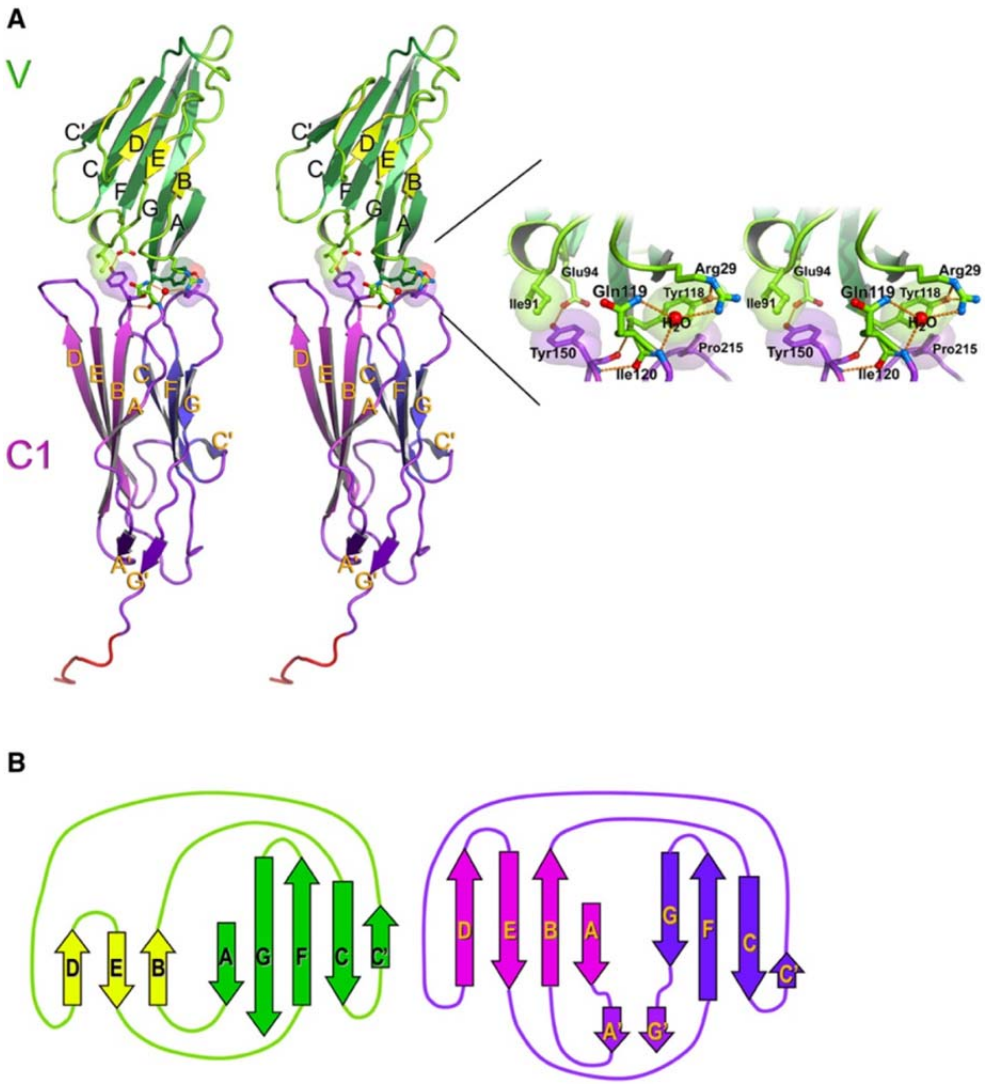

Figure 4. Structure of VC1 Domains of hRAGE. A. Ribbon diagram of the VC1 structure with V in green and C1 in magenta. B. Topology diagram of VC1 with the β-strands coloured as in the upper panel [20].

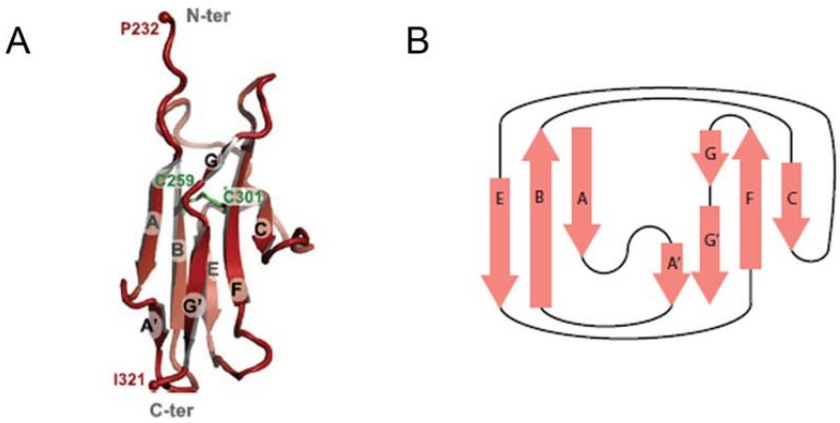

Figure 5. Structure of C2 domain of RAGE. A. Ribbon diagram of C2 structure. B. Topology diagram of C2 domain [22]

The charge properties of the extracellular portion of RAGE clearly define the separation of the ectodomain into VC1 and C2 domains. The V domain has an unusually high content of arginine and lysine residues, which carry a positive charge at neutral pH (pI=10.5). A patch of positively charged electrostatic surface was also identified on C1 [1, 20]. Thus, the entire V and the majority of C1, form a large area of positive surface that fits well to the acidic (negative) charge of the diverse RAGE ligands. In contrast to the VC1 domain, the C2 domain has mainly acidic residues on its surface and is negatively charged (**Figure 6**) [20]. This subdivision of the RAGE ectodomain into VC1 and C2 domains is fully reflected in the ligand binding properties of the different domains [1, 20].

RAGE is able to recognize ligands that have different size, fold or symmetry. The structure and in particular the surface properties of the ligand binding domain (VC1) suggest that the receptor is an electrostatic trap for negatively charged ligands (**Figure 7**) [1, 20]. Moreover, the area is very shallow and the binding could involve several low affinity binding sites whose pattern is recognized by the ligand.

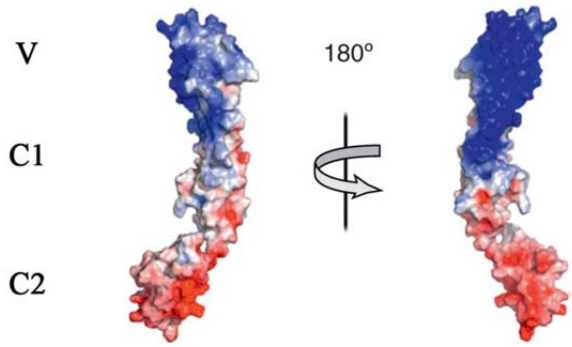

Figure 6. **Surface representation of the ectodomain of RAGE with the electrostatic potential mapped on the surface.** Blue represents positively charged areas and red represents negative charge [1].

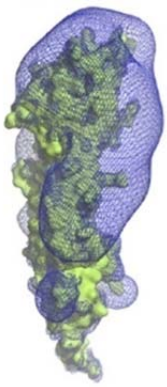

Figure 7. Surface analysis of VC1. In blue are shown the positive electrostatic isopotential surfaces at 0.8 kT/e [20].

RAGE is a glycoprotein

RAGE has two sites for *N*-glycosylation at Asn25 and Asn81, respectively. Both the glycosylation sites are in the V module but their occupancy is different. While the Asn25 is fully occupied, the Asn81 is only partially glycosylated in WT RAGE and further unglycosylated Asn81 undergoes spontaneous deamidation [23]. Asn25 is located in a β-strand, whereas Asn81 is in a loop. The particular microenvironment and the local structure are probably responsible for the different efficiency oligosaccharyltranferases (OST1 and OST2) have for these two sites.

A naturally occurring polymorphism (occurs with a prevalence of 5%, becoming 20% in Asian population) has been identified and results in a glycine to serine substitution in amino acid 82. Gly82Ser polymorphism influences RAGE glycosylation pattern since the replacements of glycine in position 82 with a serine residue promotes the glycosylation of Asn81 [23]. Modification of the glycosylation pattern has been proposed to affect ligand binding and signaling. Some ligands have increased affinity for a recombinant version of the receptor produced in bacteria that lacks of glycans, while other ligands were shown to bind prevalently to glycosylated RAGE [24].

In Chinese population, the genotype G/G, G/S with respect to S/S, is correlated with an increase of the risk of diabetic retinopathy (DR) and increased levels of circulating sRAGE [25].

RAGE oligomerization

In the absence of the ligands, RAGE has been proposed to exist in a dynamic equilibrium among monomer, dimers and multimers. The multimers include at least four RAGE molecules [26, 27]. The binding of multimeric ligands stabilizes the RAGE multimers and shifts the equilibrium toward the formation of oligomers. The advantage of receptor preassembly is that the affinity for ligands increases and receptor signaling is more effective [28]. Indeed, the formation of large ligand-receptor complexes probably results into conformational changes in the cytoplasmic tail, triggering the activation of signaling pathways mediated by RAGE (**Figure 8 A**). This process leads to the expression of RAGE itself, increasing the number of receptor molecules that assemble in the plasma membrane and, upon ligand binding, activate signal transduction [29]. Thus, a positive feedback loop amplifies and perpetuates the original signal, manifesting a chronic state of inflammation [29]. The receptor assembly is stabilized by the high concentration of RAGE on plasma membrane and by the binding to multimeric ligands. Several mechanisms control the surface concentration of RAGE. A mechanism to down-regulate the signaling consists in the internalization of the active receptor/ligand complex in vesicular or granular structures [29, 30]. On the contrary, to increase immediately the surface concentration of RAGE, vesicles containing the recycled receptor are fused with the cytoplasmic membrane [29]. Receptor endocytosis and recycling are described for a number of other receptors and are tightly regulated processes. Deregulation of these processes can result in different disorders, including cancer [31]. Another way to modulate RAGE signaling is the formation of heterocomplexes with the full-length RAGE and sRAGE and/or DN-RAGE (paragraph "RAGE: from gene to protein", **Figure 3**). These heterocomplexes result in assemblies that are able to bind ligands, but are not signaling-competent (**Figure 8 B** and **C**) [1, 29].

Different molecular mechanisms for promoting oligomerization of RAGE molecules were proposed. The interaction could take place prevalently though V-V domain contacts with parallel side-by-side arrangements (like in **Figure 8**) [29]. Other homodimerization modes are represented in **Figure 9** [22]. RAGE self-association may occur through C1-C1 or C2-C2 domain contacts or TMD helix dimerization [22]. Moreover, it has been recently shown that RAGE forms stable hexamers in the presence of heparan sulphate [32]. All the proposed modes of interaction between RAGE molecules may indicate a multiple oligomerization strategy [22]. Association between RAGE molecules by the formation of a C2-C2 disulphide bond is still controversial [22, 33]. All these homodimerization strategies were demonstrated singularly, but it is not known if all of them can exist at a single time [22].

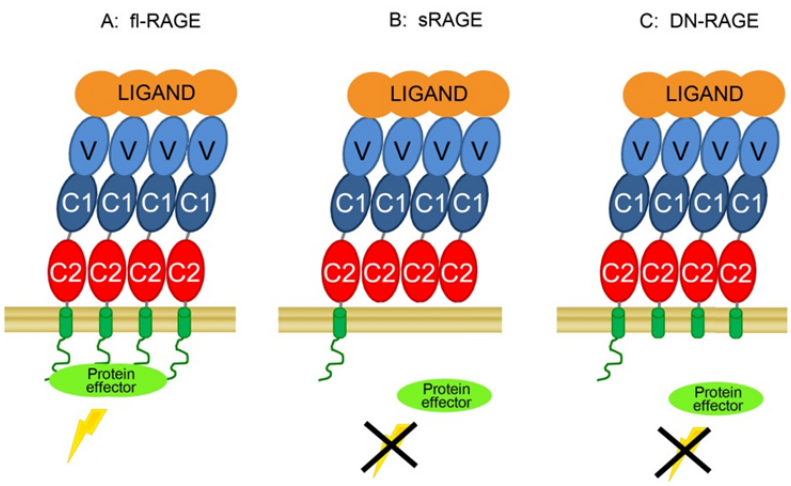

Figure 8. Models of RAGE inhibition by sRAGE and DN-RAGE. A. homodimerization of molecule of fl-RAGE, upon ligand binding, can activate signaling pathway. B and C. sRAGE and DN-RAGE can form heterocomplexes with fl-RAGE, but even if ligand binding can occur, the signaling pathway is not activated.

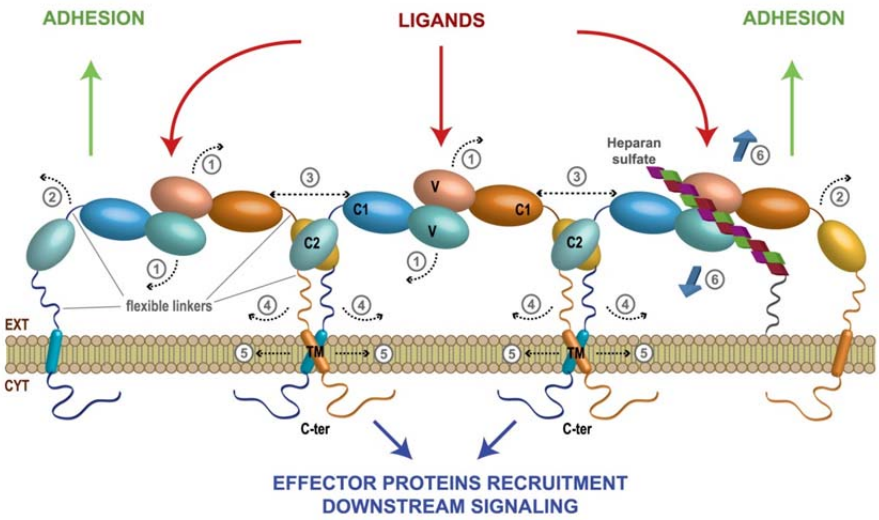

Figure 9. Schematic representation of multimodal oligomerization strategy of RAGE. In this scheme are reported the different oligomerization modes, undelaying the domains that are involved in different oligomerization: V-V contacts, C1-C1 contacts, C2-C2 contacts, TMD dimerization and hexamerization in the presence of heparan sulphate (out of plane oligomerization) [22].

RAGE ligands

The first identified RAGE ligands were AGEs, Advanced Glycation End products, but in a short time it became evident that a number of other ligands also interact with the receptor. **Table 1** summarizes a list of ligands with their related disease once they activate RAGE. It is still not clear the reason why RAGE binds so many different ligands and which common features they share. In order to provide an overview of the different ligands, a brief description of the different groups is reported below.

Table 1. RAGE ligands

Ligand	Description	Related disease	References
AGEs	Advanced glycation end products are present in high levels of diabetes	Diabetes	[34, 35]
HMGB1	Involved in cell stress mechanism. It also induces cellular migration	Tumor outgrowth, arthritis, sepsis	[9]
S100 calgranulins	Family of calcium binding protein	Alzheimer's disease	[1, 7]
Aβ	Insoluble extracellular aggregates of the amyloid β peptide	Alzheimer's disease	[8]
Mac-1	Involved with leukocyte recruitment relevant in inflammatory disorders	Diabetes	[36]
LPS	A component of bacterial cell walls	LPS-induced septic shock	[37, 38]
Transthyretin	Associated with extracellular amyloid deposits that lead to degeneration of neurons in the pheripheral nerve	Alzheimer's disease	[39, 40]
Phosphatidylserine	Assists in the clearance of apoptotic cells	Diabetes and atherosclerosis	[41]
DNA/RNA	Small nucleic acids	Sepsis	[42]
AOPPs	Advanced Oxidation Protein Products	Oxidative stress injury	[43]
Chondroitin sulphate	Sulphated glycosaminoglycan composed of a chain of alternating sugars	Tumor outgrowth	[44]
Heparan sulphate	Ubiquitous polysaccharide found covalently linked to membrane and matrix proteoglycans	Tumor outgrowth	[32, 45]
C1q and C3a	Complement components	Immune response	[46, 47]
LPA	Lysophosphatidic acid	Tumor outgrowth	[48]

Advanced Glycation End products

The Advanced Glycation End products (AGEs) are a heterogeneous group of covalently *in vivo* modified proteins, generated by the non-enzymatic reaction of sugars, or of their degradation products, with proteins [35]. The non-enzymatic reaction between the free amino groups of protein and the aldehyde groups of reducing sugars is known as Maillard reaction. The Maillard reaction comprises several steps, starting with the sugar that reacts with a free amino group of biological amines to form an unstable compound, the Schiff base. The Schiff base undergoes a rearrangement to a more stable Amadori product that is degraded to a variety of reactive dicarbonyl compounds (for example glyoxal and methylglyoxal) (**Figure 10**).

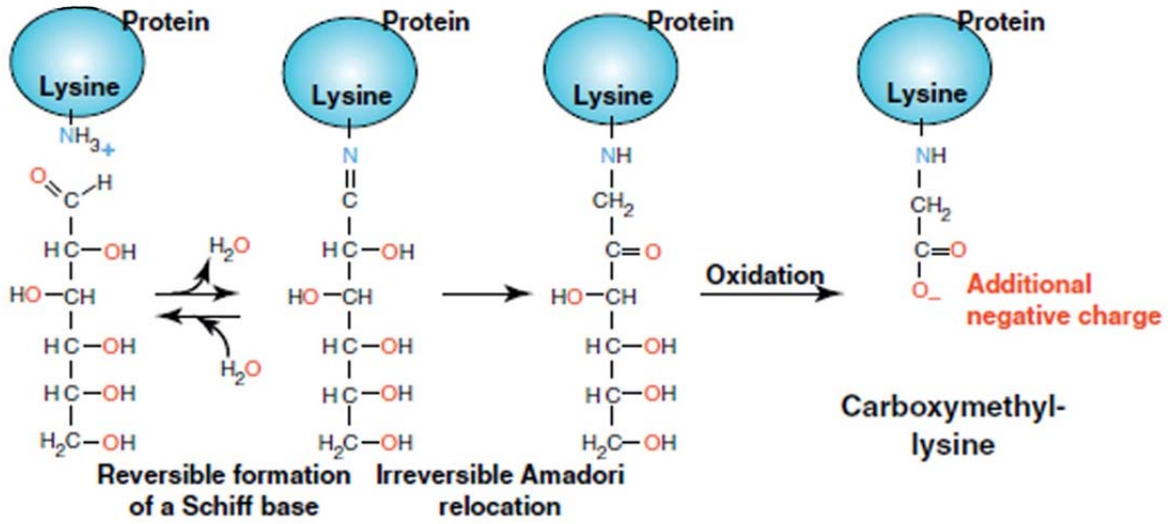

Figure 10. Schematic representation of the formation of Advanced Glycation End products [1].

Although the precise mechanism of AGE formation (also called glycation), is unclear, it involves reactions with compounds derived from the Amadori products [35, 49]. *In vivo*, these protein adducts occur during ageing and in conditions of hyperglycaemia contributing to the worsening of the symptoms of various diseases and also negatively affecting the functionality of hormones, cytokines, intracellular proteins and long-lived protein of the extracellular matrix. For example, the glycation of collagen induces vascular thickening with severe consequences including decreased vascular elasticity, hypertension and endothelial dysfunctions. Moreover, AGE formation accelerates the course of disorders such as atherosclerosis, nephropathy, and retinal pathologies. The glycation can also affect short-lived peptides causing changes in their biological functions as demonstrated by the accumulation of glycated insulin in the pancreatic β-cells of diabetic animal models [35]. Glycation results in modifications of the structure and function of proteins, it induces tissue stiffening by crosslinking of the modified proteins and it reduces their susceptibility to

catabolism. AGEs deposits were found in atherosclerotic plaques and myocardium of patients with diabetes [50-52].

AGEs can trigger a persisting inflammatory response by activating AGE receptors. The most important AGE receptor is RAGE, but other receptors were identified, such as P60/OST-48 protein (AGE-Rl), 80 K-H phosphoprotein (AGE-R2) and galectin (AGE-R3). AGEs-RAGE binding could result in fibrosis, impaired calcium metabolism, vasoconstriction in the cardiovascular system, an increase in oxidative stress (which is also associated to decline in organ function in aging) and aggravation in diabetic complications [34].

Despite the fact that the interaction of AGEs with RAGE has been studied for more than 20 years, the mechanism of AGE-RAGE complexes formation is unclear, prevalently due to the heterogeneity of AGEs: it is known that the negative charge of AGEs is critical for the binding to the positively charged V domain [53].

AGE-modified proteins are found under normal physiology, however, their concentration is low and individual proteins have at most only a single modified amino acid residue. The binding of a protein with a single modification to the V domain is weak, resulting in the impossibility to activate RAGE signaling. Under cellular stress caused by different pathologies, the concentration of modified-proteins increases and, in particular, the number of modification on a single protein increases [34]. This results in a stronger binding to the RAGE oligomer, triggering the RAGE-dependent response [53]. Therapeutic strategies are directed to inhibit AGE formation or accelerate their degradation or inhibit binding to the receptors [54].

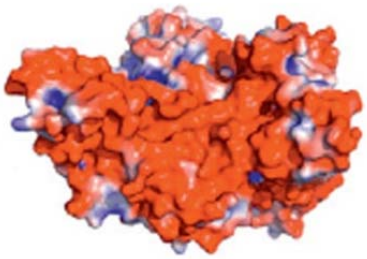

Figure 11 Human Serum Albumin (HSA) modified with sugar (glucose) is an example of AGE. The lysine after modification is carboxymethylated. The solvent accessible surface of AGE-modified HSA is depicted where the acidic residues are in red and the basic residues are in blue [1].

High mobility group protein B1

The High Mobility Group Box-1 protein (HMGB1 or Amphoterin) plays different roles depending on the type of cell and environment. It is an abundant non-histone DNA-binding protein that normally localizes to the nucleus. In inflammatory cells, such as monocytes and macrophages, it can be actively secreted through a vesicle-mediated secretory pathway. During tissue injury, necrotic cells (but not apoptotic cells) release HMGB1. Therefore HMGB1 is a damage-associated

molecular pattern protein (DAMP) [45]. The extracellular HMGB1 is associated with heparan sulphate-rich proteoglycans (HSPGs) in the extracellular matrix [55] and acts as proinflammatory activator in many types of cells, including monocytes, macrophages, neutrophils, dendritic cells, astrocytes and endothelial cells, and also induces cell migration [45]. When HMGB1 is released (via the secretory pathway or after necrosis, alone or associated with DNA) it can interact with RAGE [56]. The inflammatory response or migration of target cells mediated by the binding of HMGB1 to RAGE, involve activation of MAPKs, in particular Erk1/2 and p38, resulting in NF-κB nuclear translocation (see below, "RAGE dependent signaling pathways"). HMGB1 is composed of two positively charged N-terminal DNA binding domains and a C-terminal domain, rich of acidic amino acids, that is involved in RAGE binding (**Figure 12**). DNA-bound HMGB1 can bind to RAGE, to Toll-like Receptor 9 (TLR9) and form a complex with the two receptors. The complex HMGB1-RAGE-TLR9 activates autoreactive B cells [1].

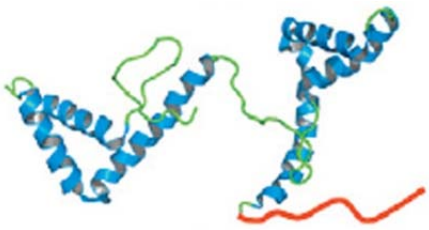

Figure 12. Schematic representation of HMGB1. In red is represented the acidic C-terminal portion [1].

S100 protein family

The S100 protein family comprises more than 25 acidic proteins characterized by two different calcium-binding EF-hand domains [1, 7]. Even if the S100 proteins constitute a young evolutionarily group present only in vertebrates, they may be divided into several sub-groups characterized by different functions, expression patterns and localization in the cell. S100 proteins are predominately intracellular calcium sensor proteins, however, some members of the family are found in the extracellular space where they exhibit cytokine-like properties. Moreover, some S100 proteins exhibit both intracellular calcium signaling functions and cytokine-like properties once they are secreted [1, 55]. The S100 proteins change their conformation upon calcium binding, resulting in different distribution of surface charges and accessibility of hydrophobic residues. In the extracellular space, where calcium concentrations are high, the S100 proteins are permanently loaded with calcium, which is a prerequisite for binding to RAGE [1].

Most S100 proteins form homodimers, but some are able to form also heterodimers and oligomers (from tetramers to octamers) and in particular the oligomeric complexes of extracellular S100 proteins are thought to be crucial for their cytokine function. Several members of the family have been shown to interact with RAGE *in vitro* or in cell-based assays: S100B, S100P, S100A1,

S100A2, S100A4, S100A5, S100A6, S100A7, S100A8/A9, S100A12 and S100A13 [7]. The S100 proteins are divided in sub-groups that bind to different domains of RAGE: S100B binds to the V domain, S100A6 can interact with the V and C2 domain while S100A12 bind to the V and C1 domain. S100B, S100A4, S100A8/A9 and S100A12 in the dimeric and oligomeric state, interact with RAGE. The interaction of several S100 proteins with RAGE was determined using different *in vitro* binding assays, in particular the Surface Plasmon Resonance (SPR). In **Figure 13** a summary of the interaction and the dissociation constant (*K*d) determined for different S100 protein and different version of RAGE is reported [7].

The S100 proteins can induce different cellular responses. S100B promotes neuronal survival and axon growth, S100A7, S100A8/A9 and S100A12 act as proinflammatory molecules, S100A2 and S100A4 are associated with differentiation and cell growth, S100A5, S100A6 and S100P can promote tumor growth [1].

S100	RAGE domain	Affinity
S100B	V	3.6 μM (62%) 2.2 nM (38%)
Dimers	VC1	11 nM (84%) 0.2 μM (16%)
	GST-RAGE	8.3 μM
	sRAGE	3.6 μM (62%) 2.2 nM (38%)
S100B Tetramers	GST-RAGE	1.1 μM (66%) 42 nM (34%)
S100A1	GST-RAGE	23 μM (85%) 6.8 nM (15%)
	V-domain	0.6 μM
S100A2	GST-RAGE	5.46 μM (70%) 56 nM (30%)
	V-domain	89.5 nM
S100A4	GST-RAGE	0.62 μM (79%) 1.7 μM (21%)
Dimers	sRAGE-Fc	0.138 μM
	sRAGE-Fc	0.138 μM
S100A4 Oligo.		
S100A5	V-domain	6.59 μM
S100A6	V	13.5 μM (97%) 0.5 μM (3%)
	VC1	5.8 μM (82%) 0.6 μM (18%)
	C2	1 μM (55%) 28 nM (45%)
	sRAGE	0.6 μM (51%) 0.5 μM (49%)
S100A12 Dimers	sRAGE-Fc	79 nM
S100A12 Tetramers	V-domain	167 nM

Figure 13. Interaction of S100 proteins with RAGE. The interactions were determined using SPR. The numbers indicated in parenthesis correspond to the S100 population that was calculated to bind to RAGE with a two independent binding sites model [7].

β-amyloid

Alzheimer's disease is characterized by extracellular deposition of insoluble aggregates of the amyloid β peptides that originate from the proteolytic cleavage of the amyloid precursor protein. The two major amyloid β peptides are composed of 40 or 42 amino acid residues and are called respectively Aβ (1-40) and Aβ (1-42). Both Aβ (1-40) and Aβ (1-42) contain acidic (**Figure 14**) as well hydrophobic residues and have the tendency to aggregate in amyloid fibrils, resulting in amyloid plaques in the brain of AD patients [1].

The finding that RAGE binds amyloid β peptides, provides a link between RAGE and degenerative disorders like Alzheimer's disease (AD) and amyloidosis [8, 57]. RAGE binds free Aβ peptides and triggers cellular responses that include transport of circulating plasma Aβ across the blood-brain barrier (BBB) into the central nervous system, oxidative stress, reduction in the cerebral blood flow and increases level of proinflammatory cytokines [8].

Recently an inhibitor (FPS-ZM1) that blocked Aβ binding to the V domain of RAGE has been identified. FPS-ZM1 interacts with high affinity with RAGE and blocks the binding of Aβ-40 and Aβ-42 in RAGE-expressing cells *in vitro* and in the mouse brain *in vivo*. FPS-ZM1 is non-toxic to mice and can cross the BBB [58]. FPS-ZM1 bound exclusively to RAGE in brain, resulting in the inhibition of β-secretase activity and Aβ production. Moreover, it suppresses microglia activation and the neuroinflammatory response. The results in using this inhibitor are the reduction of Aβ-40 and Aβ-42 levels in brain and the normalization of cognitive performance and cerebral blood flow responses in aged model mice for Alzheimer's disease [58].

It has been demonstrated that RAGE is able to bind also amyloid fibrils [59].

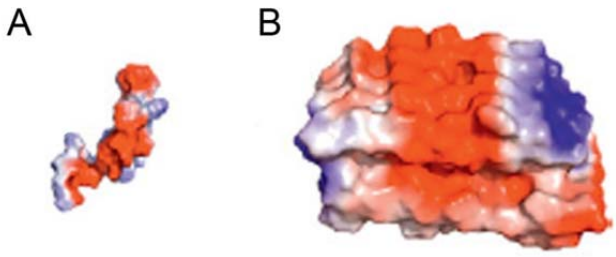

Figure 14. Surface representation of Amyloid β peptide (1-40) (A) and Amyloid β fibrils (B). The peptide displays a net negative charge (red), whereas the fibril displays a pattern of negative charge (red) [1].

Mac-1

Macrophage-1 antigen (Mac-1 or integrin $\alpha_M\beta_2$) is a heterodimeric Complement Receptor of type 3 (CR3) composed by the subunit CD11b (integrin αM) and the subunit CD18 (integrin β2). Mac-1 is present primarily on the surface of leukocytes and involved in leukocyte adhesion and migration.

RAGE has been identified as a counter-receptor of Mac-1. RAGE present on the surface of endothelial cell attracts leukocytes by interaction with Mac-1. The RAGE-Mac-1 interaction is amplified by S100-proteins (S100B, S100A9) and HMGB1 [60]. The interaction of RAGE with Mac-1 defines a novel pathway for the leukocyte recruitment that is relevant in inflammatory disorders associated with increased RAGE expression, such as diabetes complications [60].

LPS

Septic shock is a response, involving all the systems, to severe bacterial infection. LPS is the major component of the cell surface of Gram-negative bacteria. The septic shock caused by LPS is often associated with high mortality. LPS can induce massive production of cytokines by immune and non-immune cells, resulting in inflammatory tissue injuries and multi-organ failure. Several receptors were identified as LPS receptor, such as the Toll Like Receptor 4 (TLR4 member of pathogen recognition receptors PRRs), Toll Like Receptor 2 (TLR2), heat shock proteins 70 and 90, CXCR4 and growth differentiation factor 5 cluster, RP105-MD-1 complex, CD11c, CD55, L-selectin (CD62L), P-selectin and scavenger receptor class A. Recently, it has been reported that also RAGE recognizes LPS (in a LPS shock model), resulting in NF-κB activation and TNF-α (Tumor Necrosis Factor α) secretion [37]. RAGE signaling activated by LPS accelerates acute inflammatory reactions resulting in tissue damage. This leads to the release of HMGB1, resulting in RAGE-dependent lethality in septic shock.

In a recent report [38] where an infection model with alive *E. coli* was used instead of the LPS shock model, RAGE signaling was demonstrated to contribute to an effective antibacterial defence such as inhibition of bacterial outgrowth and dissemination. RAGE deficiency results in enhanced organ injuries such as liver necrosis. In general, the innate immune response to severe bacterial infection can act in a double way, protecting the host against invading pathogens or potentially destroying cells and tissues. Even though the LPS shock model is an extreme exaggerated inflammation model, RAGE can participate in sensing pathogens and controlling a delicate balance between clearance of invading pathogens and exaggerated inflammation [37].

Transthyretin

Transthyretin (TTR) is a plasma homotetrameric protein of 55 kDa that functions as a transporter for thyroxine (T4) and retinol (vitamin A) by formation of a 1:1 molar complex with retinol-binding protein (RBP) [39]. The name Transthyretin is derived by its function (*trans*ports *thy*roxine *retin*ol). A number of studies have shown that glycation induces the formation of the β-sheet structures in protein such as Transthyretin. Transthyretin fibrils are associated with the pathology of familial amyloidotic polyneuropathy (FAP), in which extracellular amyloid deposits lead to degeneration of

cells and tissues, in particular neurons of the peripheral nerve [39]. RAGE acts as a selective cell surface receptor for both soluble and fibrillar Transthyretin, leading the activation of the transcription factor NF-κB and the progression of neurodegenerative diseases [40].

Phosphatidylserine

Rapid removal of apoptotic cells by phagocytes is crucial for preventing inflammation and autoimmune responses against intracellular antigens released from the dying cells. Phosphatidylserine (PS) acts as a particular signal (called "eat me-signal") since it is recognized by phagocytes via specific receptors. Several classes of receptors have been implicated in the recognition of apoptotic cells, via direct binding to PS, such as brain-specific angiogenesis inhibitor 1 (BAI1), T-cell immunoglobulin and mucin domains-containing protein 4 (Tim4) and stabilin-2, or indirect binding through bridging molecules as milk fat globule-EGF factor 8 protein (MFG-E8) and growth arrest-specific 6 (Gas6) [41].

RAGE is included in the class of receptors that recognise apoptotic cell via direct binding with PS. RAGE binds to PS and activates signalling cascades in phagocytes that lead cytoskeletal reorganization to allow corpse internalization. Deficiencies of the receptors that participate in the recognition of PS on the surface of apoptotic cells lead to a failure to maintain self-tolerance and the development of autoimmunity [41].

Nucleic acids

Recognition of DNA and RNA derived from pathogens or self-antigen is a way mammalian immune system senses infection and tissue damages. Activation of immune signaling receptors by nucleic acids is controlled by limiting the access of DNA and RNA to intracellular receptors. RAGE binds directly to DNA and RNA and promotes their uptake into the cells, lowering the immune recognition threshold for the activation of Toll like receptor 9 (TLR9), the principal DNA-recognizing transmembrane signaling receptor [42]. RAGE binds the charged sugar phosphate backbones of nucleic acids in a sequence-independent manner. RAGE binds various forms of nucleic acids, such as ds or ss DNA and RNA of about 15 nucleotides in length. Structural analysis of RAGE-DNA complexes indicate that DNA interacts with VC1 domain of RAGE and could induce formation of higher-order receptor complexes (**Figure 15**) [42]. No conformational changes were observed in the VC1 domain between the DNA-bound structures and those of the non-DNA bound forms. This is consistent with the observation that the linkage between the V and C1 domains is rigid and is not modified by the binding to DNA [42].

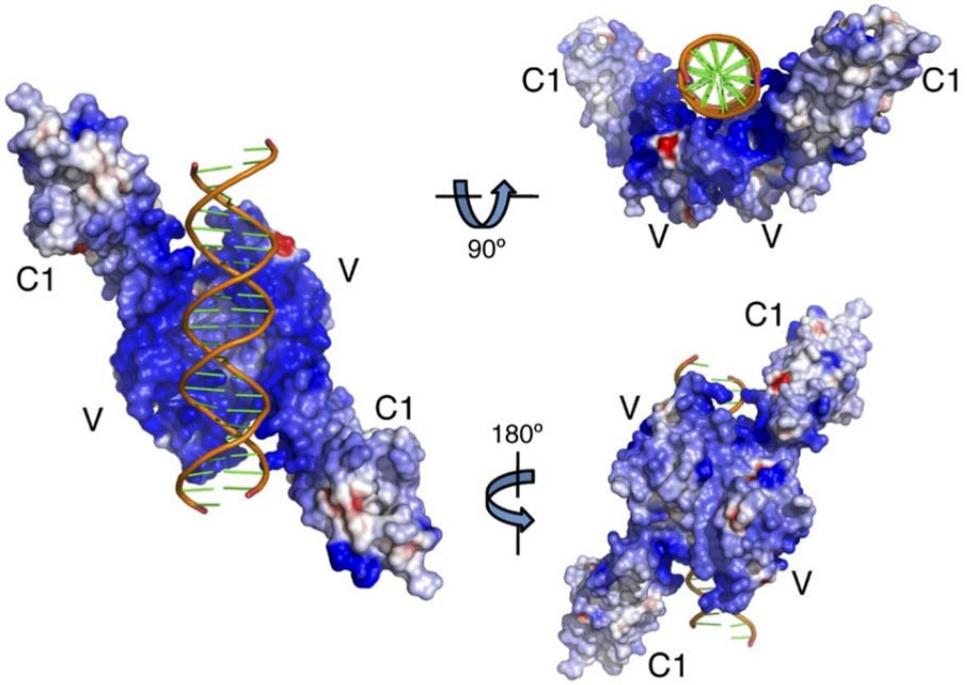

Figure 15. Electrostatic charge surface of VC1 (blue +10 kT/e, red -10 kT/e) in different orientation. The bound dsDNA is represented in orange. DNA interacts with a region of positive charges at the VC1 dimer interface [42].

AOPPs

Advanced oxidation protein products (AOPPs) are a family of oxidized di-tyrosine-containing and crosslinked protein products formed during oxidative stress by reaction of plasma protein with chlorinated oxidants. AOPPs are often carried by albumin *in vivo*. Accumulation of plasma AOPPs was first found in patients undergoing dialysis and subsequently demonstrated in patients with diabetes and metabolic syndrome. The accumulation of AOPPs results in a cascade of signaling events coupled with intracellular oxidative stress. AOPPs were found to be colocalized and interact with RAGE, which was the first receptor identified to transduce AOPPs signal [43].

Chondrointin Sulphate and Heparan Sulphate

Chondroitin Sulphate (CS) and Heparan Sulphate (HS) are sulphated glycosaminoglycans (GAGs) that are covalently attached to extracellular matrix proteins to form proteoglycans (CS- and HS-PGs, respectively). They are ubiquitous in the extracellular matrix and at cell surface in various tissues. CS/HS-PGs regulate various physiological events such as cytokinesis, morphogenesis, viral and bacterial infections, tumor growth, and tumor metastasis [44]. CS-PGs facilitate tumor invasion at the tumor cell surface and in the extracellular matrix by enhancing integrin-mediated cell adhesion, motility and intracellular signaling. HS-PGs play an important role in tumor proliferation, metastasis, invasion, adhesion and angiogenesis. During proteomic searches for CS and HS ligands, RAGE was identified as a receptor for these sulphated glycosaminoglycans [44, 45]. It was shown that HS binds HMGB1 and RAGE. HMGB1 is a HS dependent signaling factor, but for the

activation of signaling pathway the requirement for HS is manifested at the level of the receptor RAGE rather than HMGB1. RAGE and HS form a complex [45]. *In vitro*, the binding between RAGE and a dodecasaccharide derived from a highly sulphate form of HS, induces hexamerization of the receptor extracellular domain (VC1). The hexamers consist of a trimer of dimers, with a stoichiometry of 2:1 RAGE:dodecasaccharide [32]. This result was not seen, so far, for CS.

C1q and C3a

The complement protein C1q is a protein that binds and labels immune complexes or microbial surfaces to initiate complement activation. In addition to its role in the classical pathway of complement activation, C1q is involved in other immune functions, including the clearance of apoptotic cells and the modulation of adaptive immune response. This biological process is important both in homeostasis than during pathological process. For example in the nervous system the synapses and distal axons are selectively eliminated during development, but also during pathologic responses through mechanisms sharing features with apoptotic cell removal. Several C1q functions may be mediated by C1q receptors present on the effector cell surface. RAGE is a C1q receptor that enhances C1q mediated phagocytosis and the complex plays roles in adaptive immunity. RAGE-C1q complex can weakly activate the complement system, but RAGE activated by the binding with C1q-tagged material (as bacteria or apoptotic cellular debris) enhances phagocytic clearance. Moreover, Mac-1-RAGE complex may be formed to further enhance such phagocytic function [46].

Many complement components have been recently screened in searching for new RAGE ligands and among them, C3a was found to bind RAGE [47].

LPA

Endogenous phospholipids, as Lysophosphatidic Acid (LPA), regulate fundamental cellular processes such as proliferation, survival, motility and invasion, and are implicated in vascular signaling, tumorigenesis and neuropathic diseases. LPA regulates cellular signal transduction cascades implicated both in homeostatic and pathological conditions. LPA exerts homeostatic effects in development, but in adult organisms during pathological conditions in stressed tissues LPA signaling is activated resulting in neointimal expansion, tumor growth and metastasis. LPA exerts its effects through RAGE. LPA physically interacts with RAGE, in particular with V domain. *In vitro*, RAGE was required for LPA-mediated signal transduction in vascular smooth muscle cells and C6 glioma cells, as well as proliferation and migration. *In vivo*, the administration of sRAGE or the genetic deletion of RAGE mitigated the activation of Protein Kinase B (PKB, see below) by LPA [48].

Mediators for the activation of intracellular signaling

Since the cytoplasmic tail of RAGE (ctRAGE) is devoid of intrinsic tyrosine protein kinase activity typical of many receptors, intense studies have been carried out in order to understand how RAGE activates intracellular signalling. Its activation resembles that of integrin, a receptor also devoid of enzymatic activity and having a short cytoplasmic tail. The mammalian Diaphanous related formin 1 (mDia1) was identified as binding partner of ctRAGE and a key mediator of RAGE-dependent intracellular signalling events [61, 62]. mDia1 belongs to the formin protein family of actin and microtubule polymerization factors, which controls cell migration and division. It contains two proline-rich formin homology domains (named FH1 and FH2) that are essential for the association with ctRAGE. mDia1 protein levels are positively regulated by increased RAGE expression. It has been shown that mDia1 has a key role in mediating RAGE ligand stimulated signaling (see below) [61].

Other studies reported that ctRAGE may also bind to Src, MyD88 and to TIRAP. The activation of Src is responsible for many RAGE dependent downstream signal events, including the activation of MAPK signaling pathway (Erk1/2, p38 and JNK) and JAK/STAT signaling pathway [18]. TIRAP and MyD88 are adaptor proteins for Toll like receptors 2 and 4 [63, 64]. Their function was associated with RAGE signal events, but so far the direct interaction of MyD88 and TIRAP with ctRAGE was not demonstrated. Whether RAGE ligand binding recruits other adaptors proteins, in particular in a cell-specific manner, remains to be determined.

RAGE-dependent signaling pathways

RAGE signaling is influenced by a multitude of different factors. The cellular response induced upon ligand binding is not only dependent on the identity of the ligand, but also on the cell type, the concentration of the ligand, the presence of other ligands, the surface concentration of RAGE, the presence of coreceptors, different adaptor molecules mediating the signal and signaling pathways established in the cell. A brief description of the most important signaling pathways activated by RAGE is reported in **Figure 16**.

The stimulation of RAGE by ligands and subsequent induction of oxidative stress activates the mitogen-activated protein kinase (MAPK) signaling cascades, resulting in release and activation of NF-κB:

One of the first protein kinase involved in RAGE-dependent signalling is Src (proto-oncogene tyrosine protein kinase) that activates RAS. RAS activates the extracellular signal regulated kinases

(Erk1, also called p44 and Erk2 also called p42), and, in turn, Erk1/2 stimulate NK-*k*B [18]. Erk are also able to stimulate the transcription factor CREB (cAMP response element-binding protein). In addition, ctRAGE contains a putative Erk binding domain (Leu-362 to Ala-375) and may thereby promote directly Erk activation as effectors. Another MAPK, p38, is required for the induction of NF-κB activation. Different studies report that p38 is stimulated upon activation of cdc42-Rac-1 pathway [65], while others suggest that p38 is directly activated by Src-RAS [66]. The apparent discrepancy regarding the activation of p38-NF-κB cascade can be explained by the fact that different doses of RAGE ligands, duration of stimulation and cell type were used among these studies. This underlines that functional specificity of the cells and therefore distinct signaling pathways are operating in response to each of the RAGE ligands in different cell types [18]. Another well-characterized signaling mechanism by which RAGE induces inflammation is the third MAPK pathway, JNK. The activation of JNK leads to increases in the transcriptional activity of activator protein 1 (AP-1), which together with NF-κB, up-regulates the transcription of proinflammatory genes. The stimulation of JNK by RAGE ligands is dependent upon cdc42 and Rac-1 [67] and may also be activated by PKCβII (Protein Kinase c βII). PKCβII is also able to activate the pathway that leads to the activation of GSK3β (Glycogen Synthase Kinase 3β) resulting in microtubule stabilization [18]. Another signaling mechanism induced by RAGE ligands which activate NF-κB is the PI3K-PKB pathway (PI3K phosphatidylinositol 3-kinase, PKB Protein Kinase B, also known as Akt). There is no direct evidence of the activation of P13K-PKB pathway by RAGE, and also some RAGE ligands activate this pathway via other receptors (for example HMGB1 via Toll like receptors), but part of the increase in PKB activity induced by AGEs is mediated by RAGE [68].

Another pathway activated by RAGE is the JAK-STAT pathway (JAK Janus Kinase, STAT Signal Transducer and Activator of Transcription), whose activation leads to the activation of the transcription factor STAT3.

Other signaling pathways activated by RAGE culminate in the activation of the transcription factors CREB, miogenin, AP-1 and Egr-1, which mediate alterations in cell fate, migration and production of inflammatory and pro-fibrotic mediators.

RAGE is expressed on multiple cell types and, as reported above, specific signaling pathways activated by RAGE ligands are greatly dependent on the ligand, duration of ligand stimuli and the specific functions of each cell type. **Figure 17** reports a schematic description of the pathways activated by RAGE in different cell type and upon binding to specific ligands [29].

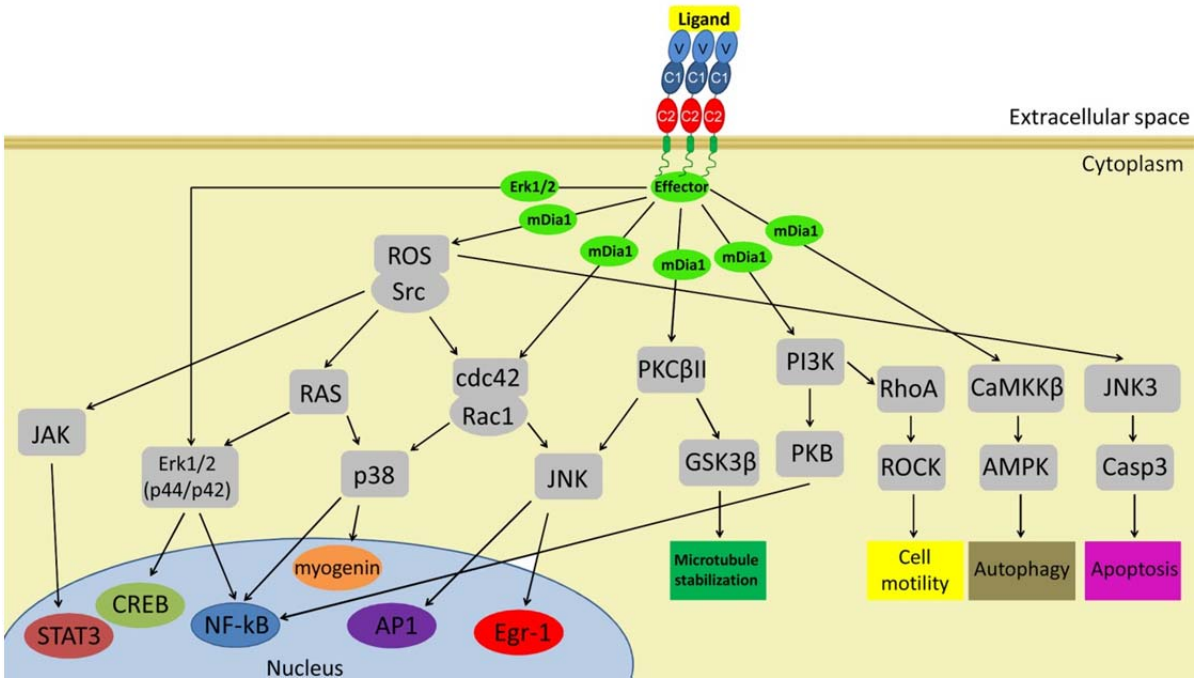

Figure 16. Schematic representation of cellular signaling pathways controlled by RAGE activation. RAGE controls different cellular process though many intracellular signaling pathway, such as MAPK pathway (involving Erk1/2, p38 and JNK), JAK/STAT pathway, PI3K/PKB pathway. The stimulation of these pathways leads to the activation of the signal transductions STAT3, CREB, NF-κB, myogenin, AP1 and Egr-1, and cellular process like microtubule stabilization, cell motility, autophagy and apoptosis.

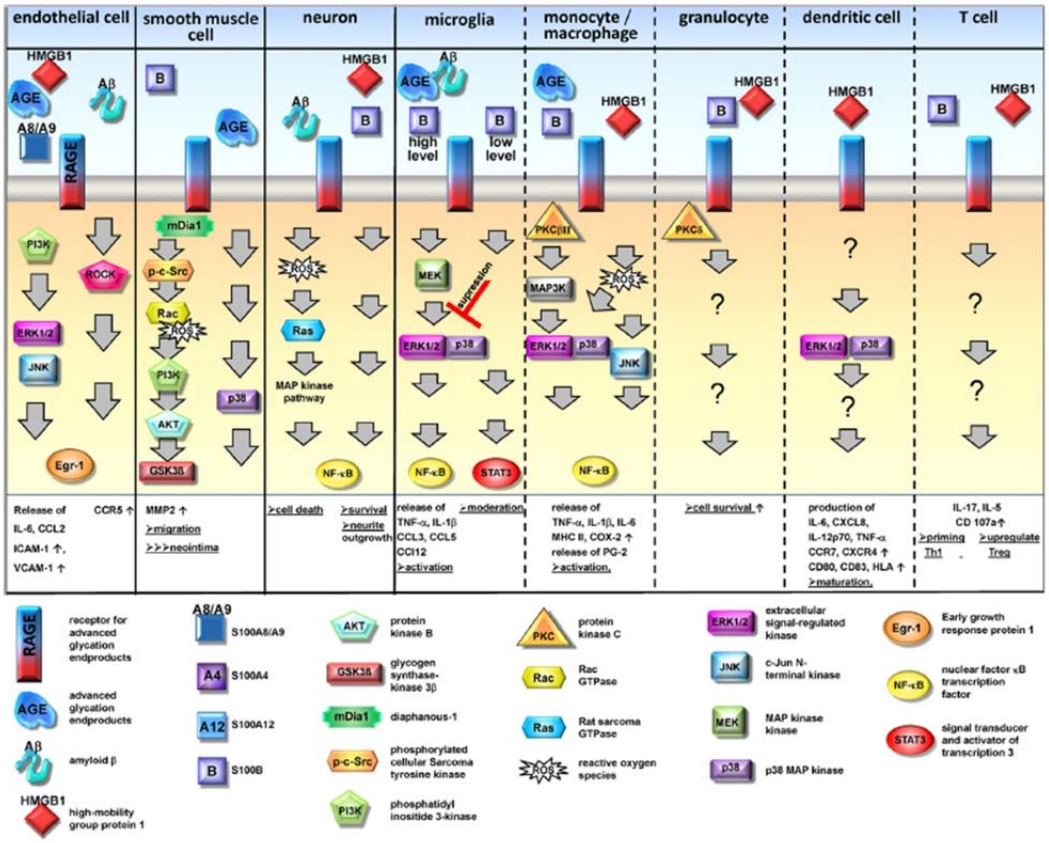

Figure 17. Schematic representation of the different signaling pathways activated by RAGE on different cell type upon binding with specific ligands [29].

Physiological role of RAGE

Despite extensive studies on RAGE signaling have associated this receptor with several diseases, RAGE also play beneficial roles for human biology. RAGE, that is currently described both as a receptor and as an adhesion molecule, is involved in the fine regulation of the delicate balance between pathological and physiological states [69]. As reported above, the signaling pathway activated by RAGE depends mostly on the identity and concentration of the ligands, the surface concentration of RAGE and the cell type. The widespread expression of RAGE during development, in contrast with the low expression of RAGE in the vast majority of cell types in the adult, reflects the important, but still undisclosed role of this receptor during embryonic life. Besides RAGE signaling has been proposed to contribute to the resolution of inflammation and to tissue regeneration, especially in injured tissues where re-expression of RAGE occurs [69]. Low concentrations of RAGE ligands activate a short-term RAGE dependent-signaling that may stimulate tissue homeostasis and repair by promoting cell proliferation and differentiation. Long-term RAGE signaling triggered by high concentrations of ligands may be deleterious, amplifying and perpetuating the inflammatory response, excessively stimulating cell survival, proliferation and migration or causing a lethal accumulation of ROS [64]. The different expression pattern of RAGE during development (from the embryonic to adult stages) and the ability of the ligands to up-regulate RAGE expression, are factors that appear to play a fundamental role in the equilibrium from pathological and physiological function of the receptor. The majority of the studies on the beneficial role of RAGE where performed using RAGE-knockout mice (KO). Here the major processes associated with a beneficial role of RAGE are reported [69].

Lung homeostasis

In adult cells in physiological conditions, RAGE is expressed at low level except in the lung, where its expression is high [29]. Even if the RAGE-KO mice do not exhibit severe pulmonary alterations, they manifest significant increase in dynamic lung compliance and a decrease in the maximal expiratory airflow [69]. Blockade of RAGE has been reported to result also in disturbed cell-matrix contacts in lung cells [70].

Bone metabolism

RAGE was proposed to have a role in osteoclast maturation and bone remodelling [71, 72]. Under physiological condition RAGE is expressed in both osteoclasts and osteoblasts. RAGE appears to be up-regulated in primary cultured bone marrow macrophages (BMM) during osteoclast differentiation. BMMs differentiated from RAGE-KO mice bone marrow cultures appear smaller in size compared with cells from WT mice cultures. This suggests a morphologic defect in *in vitro*

differentiated osteoclasts of RAGE-KO mice. Moreover in these mice both bone mineral density and bone biomechanical strength are increased and decreased number of osteoclasts and an osteoporosis-like phenotype was reported [72]. So, it was proposed that RAGE serves as a positive factor to regulate the osteoclast formation. Further, bone remodelling is altered in RAGE-KO mice due to decreased bone resorption by osteoclasts [69, 72].

Immune system

Different studies indicate a role for RAGE in immune and inflammatory responses, suggested by its ability to bind proinflammatory cytokines [73]. Blockage of RAGE causes a retarded inflammatory response by arresting signaling pathways involve in inflammation [11, 74]. As reported above, RAGE was found to be a counter-receptor for Mac-1, resulting directly involved in leukocyte recruitment. The interaction of RAGE with leukocytes results in activation of sustained NF-κB-dependent gene expression [75]. Recently, RAGE has been identified to form *in vitro* a complex with Toll-like receptor 9 (TLR9), the principal DNA-recognizing receptor. RAGE lowers the threshold of DNA concentration that is needed for the activation of TLR9 and promotes DNA uptake into endosomes. The RAGE-TLR9 complex is able to detect DNA from pathogens [42, 76]. This molecular mechanism is supported by *in vivo* experiments indicating that $RAGE^{-/-}$ mice are unable to support a typical inflammatory response to DNA in the lung [42].

Neuronal system

RAGE-KO mice exhibit hyperactivity and increased sensitivity to auditory stimuli suggesting that it is required in neuronal signaling in the brain [77]. In the peripheral nervous system, RAGE appears beneficial in neurite outgrowth required for regeneration after injury. The blockade of the receptor decreases regeneration after crush injury to the peripheral nerve (sciatic nerve) and the number of infiltrating phagocytes decreases [78, 79]. The equilibrium between physiological and pathological role of RAGE in the central nervous system seems mediated by ligands.

Ligands for RAGE in the central nervous system are HMGB1, S100B, AGEs, and amyloid-β fibrils. The interaction of RAGE with AGEs or amyloid-β fibrils leads to inflammation and oxidative stress and is involved in the pathogenesis of some neurological disorders (for example Alzheimer's disease), whereas HMGB1 and S100B are known to be involved in numerous neuronal functions, including neurite out growth, migration, differentiation and survival. Moreover, the concentration of ligands and the cell type seem to be important factors in predicting the effect of RAGE in the neuronal system. Low concentrations lead to more beneficial processes (neurite out growth), while high concentrations result in deleterious events (inflammatory signaling). Moreover, the binding of

HMGB1 results in neurite out growth in neurons, while in microglia HMGB1 induces potentially deleterious inflammatory signaling [69].

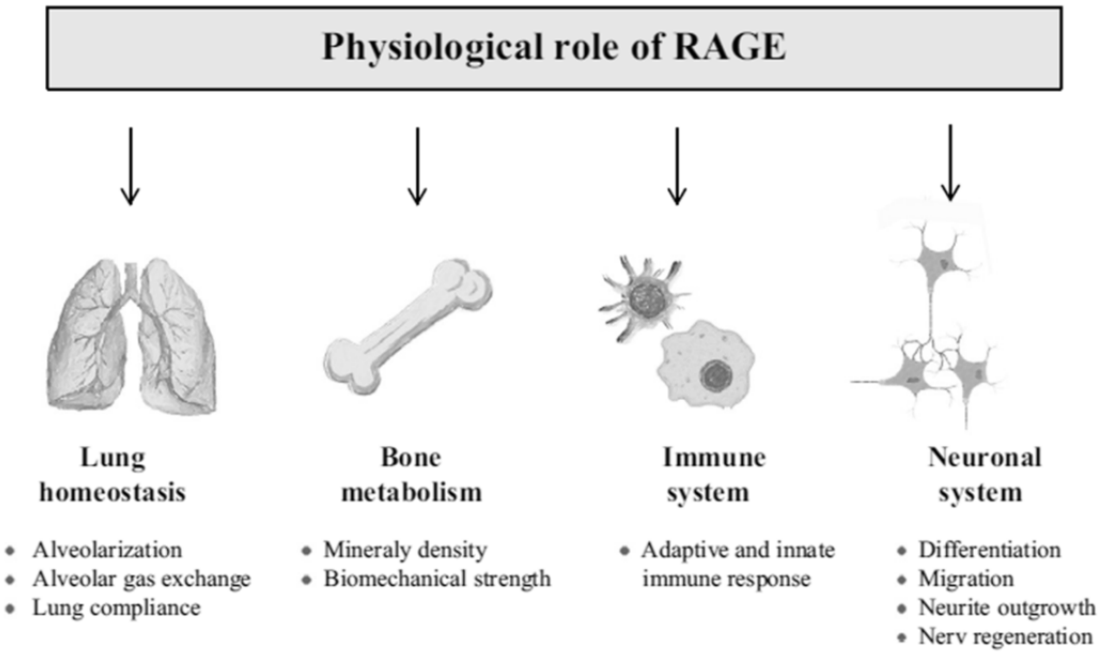

Figure 18. Physiological role of RAGE. RAGE-mediated changes in physiology of lung homeostasis, bone metabolism, immune system and neuronal system [69].

Aim of the Project

RAGE has been demonstrated to have a key role in the establishment and progression of oxidative and inflammatory based pathologies, like diabetic vascular complications, atherosclerosis, neurodegenerative disorders and cancer. Despite several ligands have been identified, a complete characterization of RAGE binding properties is still missing.

The aim of this project was the expression and purification of recombinant forms of human RAGE to set-up different biophysical methods to study the non-covalent interactions between RAGE and its ligands. We focused on the extracellular domains of RAGE that are responsible of ligand binding.

Since RAGE forms oligomers on the plasma membrane of mammalian cells, a version of VC1 suitable for immobilization on resin or matrix was designed in order to mimic the oligomeric state of the receptor.

Main Results

1. Expression and purification of His-tagged VC1 in *Escherichia coli*

The VC1 portion (amino acid 23-243) of the extracellular domain of human RAGE was produced in *E. coli* as an intracellular protein fused to an N-Terminal His-Tag and a Thrombin Cleavage site. The protein was purified using Nickel affinity chromatography and the His-Tag was removed through Thrombin digestion. During the purification VC1 showed a marked tendency to aggregate and precipitate resulting in low yield of soluble protein. Even if the protocol for the purification of VC1 was improved, only 10% of the purified His-tagged protein remained soluble after Thrombin digestion.

The identity of the purified VC1 was confirmed by trypsin digestion of the gel-purified protein, separation of the resulting peptides by reversed phase capillary column and identification of the sequence by MS/MS analyses. The primary structure of the protein corresponded to that deduced from the nucleotide sequence of VC1 with coverage higher than 85%.

2. Analysis of protein-ligand binding by native Mass Spectrometry (MS)

In order to better understand the ligand-binding properties of RAGE, a native MS method was used to study the non-covalent interactions between ligands and recombinant VC1 produced in *E. coli*. The advantages of native MS over other methods are (i) no labelling of the target or ligands, (ii) high sensitivity and low sample consumption, (iii) quick and automatable analysis and (iv) screening of the ligands as a mixture. The binding reactions consisted in maintaining constant the concentration of VC1 and increasing the ligand concentration. Even if we were able to detect binding between low molecular weight AGEs (peptide DEFKADE and FKDLGEE with the lysine residue modified as carboxymethyl lysine or carboxyethyl lysine) and VC1, the tendency of VC1 to adhere to the glass tubes of the spectrometer, even after silanization and conversion to microcapillary (static injection), resulted in poorly reproducible data. We concluded that this approach is not suitable for VC1.

3. VC1 expressed and purified from *Pichia pastoris* is glycosylated, functional and stable

We expressed secretory forms of the ligand binding domains of hRAGE in the lower eukaryote *Pichia pastoris.* The rational of this approach was that expression in a eukaryotic host and targeting to the secretory pathway could in principle improve the folding and solubility of the proteins, promote glycosylation and formation of disulphide bonds and reduce the stickiness of the proteins to the glass.

Since the fusion to a tag could facilitate protein purification, first the expression of His-tagged proteins was attempted but unsatisfactory results were obtained as described below (see paragraphs 4 and 5). Therefore untagged versions of the hRAGE domains were also attempted. We obtained *P. pastoris* strains expressing and secreting VC1 domain and we tested different growth conditions to optimize the expression whereas the V domain was expressed but retained intracellularly (see paragraph 5).

By Western Blotting analysis using a polyclonal anti-RAGE Ab, VC1 was detected in the medium as a doublet of two polypeptides of 34 and 36 kDa (called p34 and p36). The appearance of a unique band of about 29 kDa after treatment of VC1 with PNGase F (an amidase that catalyses the cleavage of *N*-linked oligosaccharides in glycoproteins) provided evidence that VC1 is heterogeneously *N*-glycosylated in *P. pastoris.* The degree of occupancy for Asn25 and partial for Asn81 that was also highly susceptible to spontaneous deamidation, in agreement with the data of the literature concerning hRAGE expressed in mammalian cells.

VC1 was then purified from the medium using a one-step elution cation-exchange chromatography as the capture step, exploiting the high charge of the protein (pI = 9.9) and a gel-filtration polishing step. We estimated a production of about 6 mg of VC1 per Liter of medium. We tested the functionality of VC1 (p34 + p36) by a filter binding assay using AGE-BSA, a well-known RAGE ligand and BSA as negative control. VC1 bound AGE-BSA, but not BSA, indicating that VC1 produced in *Pichia pastoris* is functional.

Furthermore, we developed a procedure for the optimization and scale-up purification of VC1, based on an ionic-strength linear gradient high resolution cation-exchange chromatography. With this improved procedure p34 and p36 separated in two partially overlapped peaks, allowing their isolation in homogeneous form.

We performed a thermal denaturation analysis (ThermoFluor) of p36, p34 and of the unmodified form produced in *E. coli* at different NaCl concentration. The two glycoforms of VC1produced in *P. pastoris* had similar melting temperatures (T_m) in 150 and 300 mM NaCl whereas in the absence of NaCl p36 appears to be more stable than p34. In addition, the T_m of the two glycoforms is higher than that of VC1 produced in *E. coli*. In particular in the absence of NaCl, this protein is highly unstable, its T_m being 22.6 °C. Thus, VC1 forms produced in *P. pastoris* displayed a remarkable improved stability in comparison with the unmodified VC1. These observations are consistent with the fact that VC1 glycoforms obtained from *P. pastoris* are highly soluble and display no tendency to aggregation.

4. Fusion of VC1 to a removable histidine tag reveals proteolytic activities in the medium

We expressed in *Pichia pastoris* also VC1 fused to a C- terminal His-Tag and a Thrombin cleavage site (VC1-His) in order to remove the tag if necessary. As for VC1, VC1-His was detected using Western blot analysis with anti-RAGE Ab in the medium as p34 and p36. Surprisingly, the two polypeptides were not recognized by anti-poly His mAb. In the cellular extracts the two polypeptides were recognized by both antibodies. This result indicates that VC1-His is expressed and glycosylated, but during secretion or in the culture medium the His-Tag is cleaved. The site of cleavage was identified by MS and corresponds to the cleavage site of Thrombin indicating that a secreted serine protease of *P. pastoris* could be responsible of the cleavage. A candidate was Sub2p, an endogenous subtilisin-like protease that is secreted in the medium in the presence of methanol (inducing condition). To verify if the His-tagged VC1 was a substrate of Sub2p, we transformed the deleted *sub2* strain and monitored the production of the tagged form of VC1. The cleavage occurred also in this strain, suggesting that another protease is secreted in *P. pastoris* medium.

5. Expression and purification of V module in *E. coli* and *P. pastoris*

It is still unclear the role of the V domain in the binding with AGEs, although a paper published in 2011 proposed that the only V domain is necessary to specifically bind AGEs. This prompted us to express this soluble truncated form in order to study the binding properties of V to low molecular weight AGEs.

The V domain was expressed in the *E. coli* strain as an intracellular recombinant protein with an N-Terminal His-Tag and a Thrombin Cleavage site. The protein was purified using Nickel affinity chromatography. The expression level of this recombinant protein was lower in comparison with the expression level of His-Tag-VC1 and most of the protein was found in the insoluble fraction. Furthermore, His-Tag-V aggregates and precipitates dramatically during the purification procedures, resulting in the impossibility to treat the protein with Thrombin in order to remove the His-Tag.

Therefore, we attempted to express the V domain in *P. pastoris*. We obtained *P. pastoris* cells expressing V and we tested different induction conditions. In all the conditions tested, no bands were detected in the media using Western Blotting analysis with polyclonal anti-RAGE Ab. In the cell extracts three bands were recognized by polyclonal anti-RAGE Ab. We observed that the V polypeptide was glycosylated, as the detected polypeptides were susceptible to PNGase F treatment. These results strongly indicate that V is expressed intracellularly and modified in the ER but it is not transported to the extracellular space probably as a consequence of protein folding. From the results of expression and purification obtained from *E. coli* and *Pichia pastoris*, the V module appeared to be unstable, probably due to the absence of C1 domain, indicating that VC1 is a single

folding unit. Our results, based on an *in vivo* approach, extend previous *in vitro* biochemical studies indicating that V and C1 constitute a single integrated unit of the ectodomain of RAGE.

6. Expression of VC1-StrepTag

To identify new RAGE ligands and enrich AGEs from biological samples (for example fluids from diabetic patients), we set up a pull down assay. This technique requires an immobilized form of RAGE. The rational was to purify a recombinant VC1 with a C-terminal StrepTag that binds with high affinity to streptavidin-resin. The tag was placed at the C-terminal and to let VC1 interact freely with the AGE ligands and to our knowledge this is the first construct of VC1 immobilized through the C-terminal end. The resin with VC1-Strep immobilized was named RAGE-column.

We developed different strategies: (i). VC1-StrepTag expressed in *E. coli* and directly immobilized on streptavidin resin from the soluble fraction of *E. coli*, (ii). HisTag-VC1-StrepTag expressed in *E. coli*, purified by Nickel affinity chromatography and then treated with thrombin to remove the His-Tag; immobilization the purified protein on the streptavidin resin, (iii). VC1-Strep expressed and secreted in *P. pastoris,* purified and immobilized on the streptavidin-resin.

Using the protein produced in *E. coli* (i, ii), the RAGE-column was able to capture ligands such as purified species of AGEs (BSA-ribose, BSA-glucose), S100B and S100A12. BSA-ribose was also specifically identified from a complex matrix like milk. With this pull down assay we also captured proteins from sera from diabetic patients. MS analyses are in progress to reveal the identity of the polypeptides identify.

VC1-Strep *Pichia pastoris* medium (iii) was successfully immobilized on streptavidin resin and the system was set for future experiments.

Conclusions and Future Prospects

The activation of RAGE upon ligand binding, modulates different signal transduction pathways, culminating in the expression of genes involved in the inflammatory response. Therefore, in the context of hyperglycaemia and/or oxidative stress-based diseases, RAGE activation can establish a sustained inflammation crucial for the progression of nephropathies or atherosclerosis. Moreover, inflammation increases oxidative stress, reinforcing the expression of RAGE and RAGE signaling pathway by a vicious cycle. The characterization of RAGE binding properties is crucial to develop antagonists able to reduce the effects of RAGE activation. For this purpose we focused in obtaining recombinant and soluble form of the receptor in order to perform ligand binding experiments.

During my PhD project, different recombinant forms of the human Receptor for the Advanced Glycation End products were produced in different heterologous expression systems.

V and VC1 were expressed as intracellular proteins in *E. coli*, but the tendency to aggregate and precipitate of the purified proteins resulted in low yield of VC1 and greater loss of V. A native MS method was used to study the non-covalent interactions between ligands and the recombinant VC1 produced in *E. coli*, but the tendency of VC1 to adhere to the glass tubes of the spectrometer, even after silanization, resulted in poorly reproducible data. We concluded that this approach is not suitable for VC1.

Since RAGE has disulphide bonds and is also glycosylated, we expressed V and VC1 as secreted protein in the methylotrophic yeast *Pichia pastoris*. VC1 produced in *Pichia pastoris* was purified from the culture supernatant with no relevant loss of the protein during the purification steps. VC1 was glycosylated and displayed to mimic the glycosylation pattern observed in human cells. Moreover the protein did not show tendency to aggregate and precipitate. By measuring the melting temperature of VC1 produced in *E. coli* and in *Pichia pastoris*, the protein from *P. pastoris* proved to be more thermal stable, indicating that the addition of N-linked glycans is important for proper folding, protein stability and solubility. Unfortunately, the presence of the oligosaccharide chains hampers the use of native MS to study the non-covalent interactions of RAGE with ligands, but other techniques, such as Microscale Thermophoresis or SPR, will be used.

In contrast with VC1, the V domain was retained intracellularly in *Pichia pastoris*, suggesting that it did not acquire the proper folding. This result obtained with an *in vivo* approach, indicates that V and C1 form a single folding unit and that V is not a domain but rather a module of RAGE and also reinforce the conclusion derived from previously published *in vitro* biophysical studies indicating that V and C1 form a single integrated domain

Another approach for the study of the binding properties of RAGE and the discovery of new ligands is currently under development. The method consists in the setup and implementation of an innovative approach that combines affinity chromatography and MS to capture and characterize RAGE ligands from biological samples, such as serum obtained from patients with hyperglycemia and oxidative stress (nephropathic diabetic patients). VC1 was expressed as a recombinant protein with a C-terminal StrepTag in *E. coli* and in *P. pastoris*. Then VC1-Strep was immobilized on a streptavidin resin to create the solid phase of a chromatography column (called RAGE-column). The RAGE-column was tested and proved to be able to capture well known RAGE ligands.

Using this RAGE-column, endogenous RAGE ligands will be captured from biological samples, such as serum obtained from patients in conditions that mimic the physiological ones.

Phr family of Candida albicans

Candida albicans

Candida albicans is a eukaryotic microorganism and is the most common human pathogen among the *Candida species*. *C. albicans* infections occur predominantly on mucosal surfaces, including oral mucosal, gut, vaginal mucosa and skin. The mucosal infections, that cause morbidity and reduce the quality of life for infected individuals, are extremely common and occur in healthy individuals. However, when the fungus penetrates through the epithelial barrier, enters the bloodstream and invades organs like kidney or liver, infections can become life threatening [80]. These types of infections are called systemic/invasive candidiasis and can be acute or chronic. Invasive candidiasis is reported to be the fourth most common cause of bloodstream infections in the United States [81].

Under normal circumstances, *C. albicans* is a commensal of the human mucosae and skin predominantly found in the gastrointestinal tract, where the microbial flora, epithelial barriers and the innate immune system control its invasiveness. Antibiotic treatments, surgery trauma, catheters and neutropenia are considered major risk factors for invasive candidiasis [82]. Even if the commensal stage is frequently described as "harmless" for the host, this stage is highly regulated and the fungus interacts continuously and transiently with the host immune system [82, 83]. *Candida albicans* is often classified as an opportunistic pathogen, but infections are not strictly limited to individuals with compromised immunity. In fact, *C. albicans* can cause superficial mucosal infections in healthy hosts that suffer of disturbances in normal flora due to antibiotic use or vaginal infection caused by hormonal changes [80].

The success of *C. albicans* as a pathogen depends on its morphological plasticity. *C. albicans* is a polymorphic fungus and the most frequently observed morphological forms are the yeast and the filamentous forms (pseudo-hyphae and hyphae) (**Figure 19**). *C. albicans* yeast cells resemble the budding yeast *Saccharomyces cerevisiae*. Filamentous growth results in the production of elongated cells that differ for their size shape: hyphal cells are narrower then pseudo-hyphae and have parallel walls with no constriction at the site of septation, while pseudo-hyphae are wider and form constriction between elongated buds [84]. Yeast form is the preferred morphology for dissemination within the blood flow while the switch to hyphal growth allows an efficient penetration of *C. albicans* through the tissues [85]. Complex and interconnected signaling cascades regulate morphogenesis in *C. albicans*, in particular elevated CO_2, serum, 37° C, nutrient and phosphate limitation and alkaline pH promote yeast-to-hyphae transition. These morphological states also enable the formation of biofilm (**Figure 19**), complex surface-associated (usually on medical devices) communities composed of a mixed population of yeast cells, pseudo-hyphae and hyphae. Biofilm is usually resistant to antifungal drugs [86].

The morphological plasticity of *C. albicans* is an important virulence factor, as mutants that are unable to undergo morphogenesis are usually attenuated in virulence [84].

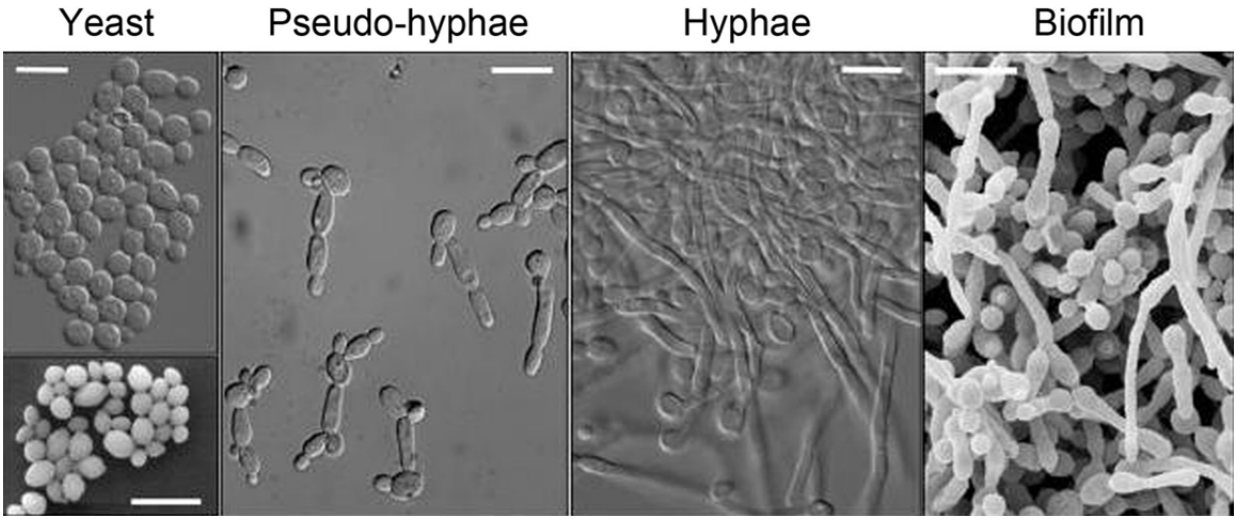

Figure 19. **Images of the different morphological states of *C. albicans* (Yeast, Pseudo-hyphae, hyphae and biofilm).** Yeast cells are shown under differential interference contrast (DIC) microscopy (upper panel) and scanning electron microscopy (SEM, lower panel). The filaments in this figure (DIC) were induced by different conditions: medium at pH 6 at 35°C (Pseudo-hyphae) and 10% serum at 37°C (Hyphae). The biofilm image is a SEM image of a mature 48 h-biofilm composed of yeast and filamentous cells. The bars indicate 10 μm [84].

Candida albicans cell wall

In the establishment and progression of pathogenesis, *C. albicans* cell wall plays an important role. The cell wall is the first structure that interacts with the host cells, it carries important antigens and it is responsible for the adherence of the pathogen [87]. As in fungi in general, the cell wall of *Candida albicans* is an articulate and ordered structure, made by arrangement of its different components. Some of these are linked by covalent bonds, whereas others are retained in the wall by hydrogen bonds, salt-type, hydrophilic or hydrophobic interactions. The cell wall provides protection to the cell against physical, chemical and biological aggression and is responsible for its morphogenesis [87].

C. albicans cell wall represents about 15-30% of the dry weight of the cell and is composed of polysaccharides and proteins, as major components, and lipids present as minor component [87]. The cell wall has a layer organization, where the structural polysaccharides accumulate in the inner layer while mannoproteins are enriched in the outer layer and are essential for adhesion, virulence and biofilm formation (**Figure 20**).

The polysaccharides are present in three major forms: β-glucans, chitin and mannans of mannoproteins. β-glucans are the unique and most abundant polysaccharide (*C. albicans* cell wall does not contain α-glucans) and are polymers of glucose joined by β-1,3 and/or β-1,6 glycosidic linkages (β-1,3 glucan and β-1,6 glucan) [82, 87]. Chitin is a linear polysaccharide made of more than 2000 units of N-acetylglucosamine joined by β-1,4 linkages. Chitin chains are associated in an antiparallel mode through hydrogen bonds to form microfibrils composed of about 20-400 chains. The linkages of chitin to β-1,3 glucan form a scaffold to which mannoproteins are covalently associated. The last types of polysaccharide present in *C. albicans* cell wall are mannans, O-linked and N-linked to the mannoproteins. Mannans are the post-translational modification of cell wall proteins [82, 87].

The cell wall proteins (CWPs), that are covalently attached to the scaffold of structural fibrillar polysaccharide, are divided in two classes. The first and the most abundant class of CWPs is linked to β-1,6-glucan through a glycosyl phosphatidyl inositol (GPI) remnant, and are called GPI-CWPs. The second class of proteins, termed Pir (proteins with internal repeats), are linked directly to the β-1,3-glucan. An additional class of CWPs does not utilize a covalent attachment for retention in the cell wall. These proteins have substrates in the cell wall and remain predominantly cell associated [88]. In conclusion, β-glucan and chitin are structural polysaccharides of the inner layer and ensure strength and shape to the cell wall. In contrast, mannoproteins form a fibrillar outer layer and the mannans, less structured and with low permeability and porosity, prevent the permeability of the host attacking molecules and antifungal drugs, but does not influence cells shape (**Figure 20**) [82].

The cell wall of *C. albicans* contributes to the activation of the immune response by the host. It contains pathogen-associated molecular patterns (PAMPs) that are recognized, via pattern recognition receptors, by the innate immune system as non-self-molecules, triggering a cascade of molecular events that will end with a protective response against the fungus [89]. In particular, the constituents of the cell wall are highly immunogenic and engage a variety of pattern recognition receptors (PRRs) as represented in **Figure 21**. For example, O-linked mannans are recognized by Toll like receptor 4 (TLR4), N-linked mannan by the Mannose Receptor (MR), Galectin-3 and DC-SIGN. β-1,3-glucan is the major pro-inflammatory mediator and its main PRR is C-type lectin Dectin-1, which can collaborate with TLR2. The damage of the mannan layer, with consequential exposure of β-1,3-glucan, enhances the strength of the proinflammatory signal [82]. Chitin also participates in immune recognition, but the chitin binding receptor was not identified so far [82, 89].

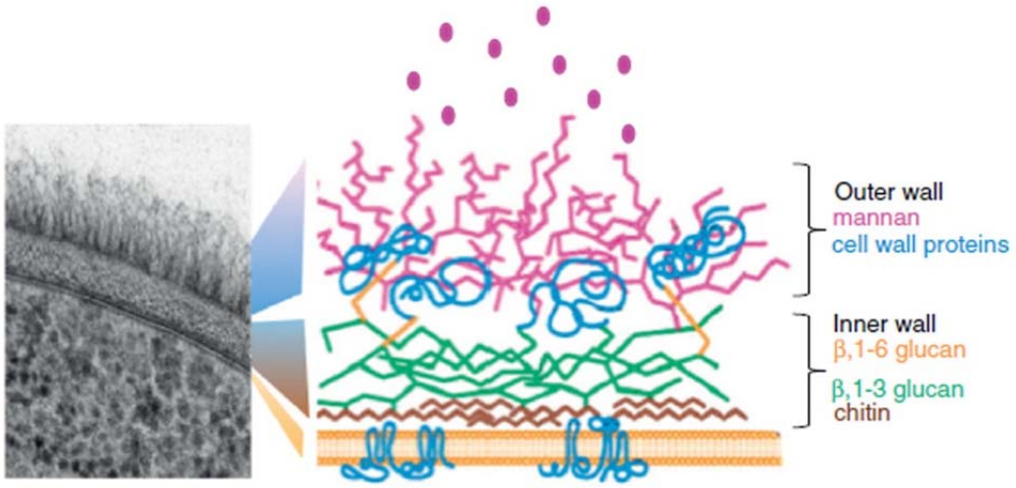

Figure 20. **Structure of *Candida albicans* cell wall.** On the left, section of the *C. albicans* cell wall (Transmission electron micrograph, TEM). On the right scheme showing the architecture of the major components of the cell wall [82].

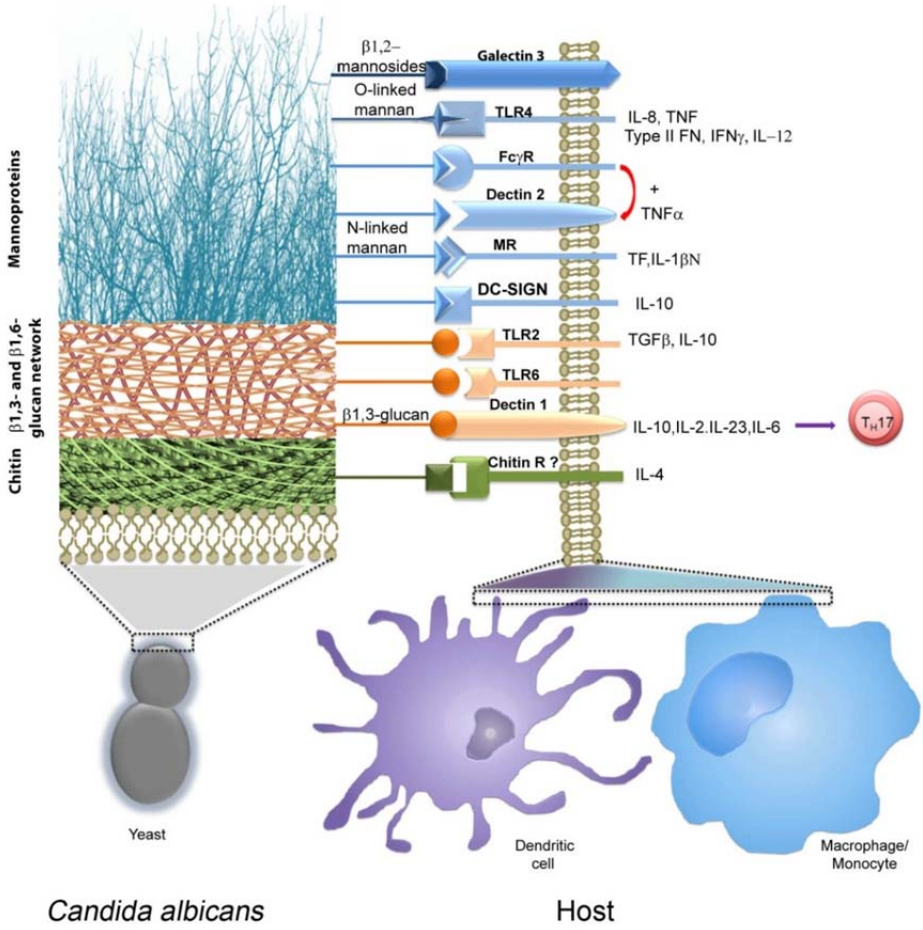

Figure 21. The cell wall of *C. albicans* plays a central role in the activation of host immune cells. Cell wall components are pathogen-associated molecular patterns (PAMPS) that interact with several pattern recognition receptors (PRRs) present on immune cells (for example monocytes, macrophages and dendritic cells). This results in the stimulation and production of anti- and pro-inflammatory cytokines [89].

The Phr family of glucan remodelling enzymes

Cell wall biogenesis of fungi requires three groups of enzymes involved in synthesis, assembly and remodelling, namely: synthases, transglycosidases and glycosylhydrolases. The PHR family of *C. albicans* encodes for β-1,3-glucanosyltransferases and is one of the best characterized families of glucan remodelling enzymes. The PHR family has high homology with the GEL and GAS families of *Aspergillus fumigatus* and *Saccharomyces cerevisiae* and together form the GH72 family of the Carbohydrate Active Enzyme database (http://www.cazy.org/ [90]). GH72 is a family of enzymes unique to fungi [91]. GH72 enzymes *in vitro* cleave internally a β-1,3-glucan and transfer the newly generated reducing end to the non-reducing end of another β-1,3-glucan molecule, forming a β-1,3-linkage. This results in the elongation of the β-1,3-glucan chains [92-94]. From *in vivo* analyses of several mutants with reduced GH72 activity, it has been proposed that these enzymes contribute to the formation of the long and branched β-1,3-glucan that constitutes the scaffold of the fungal wall [95]. The crucial role of β-1,3-glucanosyltransferases in the assembly of the cell wall core has been recently demonstrated *in vivo* in *S. cerevisiae* where the absence of this activity caused the conversion of the high molecular weight β-1,3-glucan into a highly polydisperse polymer [93, 96].

The GH72 enzymes have similar structural characteristics: (i) a signal peptide necessary for the targeting of the protein in the secretory pathway, (ii) an N-terminal domain (GH72) with two conserved glutamic acid residues essential for enzyme activity and cysteine residues essential for the formation of the disulphide bonds, (iii) a linker that connects GH72 domain with the other portion of the protein and contains a conserved cysteine in a region usually not conserved, (iv) a region with 8 cysteine residues, called Cys-box or X8, present only in a subfamily of GH72 enzymes, called $GH72^{+}$ (the subfamily without the Cys-box is called $GH72^{-}$) [97], (v) a disorder region with a cluster of serine residues (PolySer), site for *O*-mannosylation, (vi) a C-terminal signal sequence for GPI attachment.

In all fungal species so far analysed, the GH72 family of β-1,3-glucanosyltransferases consist of four to seven members [91]. The biological significance of this redundancy has been deeply investigated in *S. cerevisiae* that presents five GH72 members (*ScGAS1-5*). It has been shown that different paralogs are expressed at specific stages of the yeast cycle. *Sc*GAS1 and *Sc*GAS5 are expressed during vegetative growth and are required for cell wall assembly, whereas *Sc*GAS2 and *Sc*GAS4 are repressed during vegetative growth and transcribed in the middle of meiosis where they are essential for spore wall formation [93, 97, 98]. Among GH72 family some members have been demonstrated to be essential genes, for example *AfGEL4* of *Aspergillus fumigatus* and $Spgas1^{+}$ of *Schizosaccharomyces pombe* [99, 100].

C. albicans PHR family consists of five genes, *PHR1*, *PHR2*, *PHR3*, *PGA4* and *PGA5*. *PHR1* and *PHR2* were the first identified pH-responsive genes in *C. albicans* [101, 102]. *PHR1* expression is triggered at pH values higher than 6 whereas *PHR2* has the reverse expression pattern. Ambient pH is an important parameter that affects the ability of this major fungal pathogen to survive and grow within the human body where pH can be slightly alkaline, such as in the bloodstream (pH 7.3), close to neutrality such as in organs like kidney, liver and duodenum or acidic as in the stomach (pH 2) and vagina (pH 4.5) [93]. Loss of *PHR1* induces morphological defects at neutral-alkaline ambient pH, the mutant exhibits a round morphology and the inability to support hyphal growth, to adhere and invade human epithelia. Moreover, *PHR1* null mutants are avirulent in mouse models of systemic infection (pH 7.3) and in the model of experimental keratomycosis (pH 7.5) [103, 104]. At acidic pH, *PHR2* null mutant has the growth and morphological defects of *PHR1* mutant at its restrictive pH [101, 102] and it is avirulent in the rat model of vaginitis (pH 4.5) [103].

PGA4 mRNA was detected independently of ambient pH and was upregulated upon *in vitro* model of infection and transiently increased upon yeast-to-hyphal switch [105] *PGA4* null mutant does not exhibit a defective phenotype: growth rate and sensitivity of the strain to stress inducing and cell wall perturbing agents are not affected, indicating that the cell wall is not damaged. Moreover, the virulence of the mutant was unchanged with respect to the wild type strain [105]. *PHR3* and *PGA5* transcripts are absent or hardly detectable with microarray or Northern hybridization analysis. The null mutant of *PHR3* does not result in a distinct phenotype, while phenotype of *PGA5* null mutant was never published [105].

In **Figure 22** a scheme of the domain organization of Phr protein is reported.

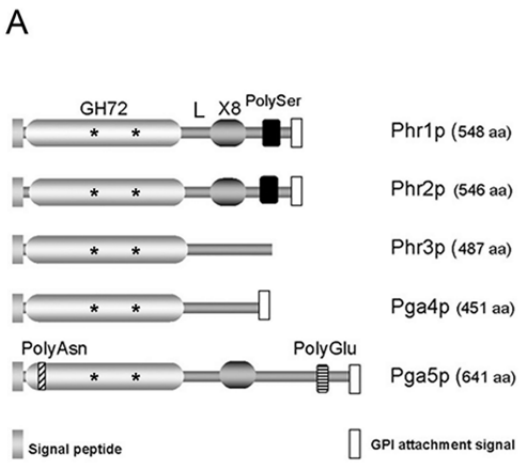

B

S. cerevisiae (stage of expression)

C. albicans orthologs	Veg		Spo		Veg/Spo
	Gas1 1-366 367-559	**Gas5** 1-366 367-484	**Gas2** 1-385 385-555	**Gas4** 1-371 372-471	**Gas3** 1-393 394-524
Phr1 1-377 378-548	**59** **47**	42 NS	49 25	38 NS	40 NS
Phr2 1-367 368-546	**64** **58**	44 NS	50 43	37 NS	38 NS
Pga4 1-357 358-451	42 NS	**60** NS	42 NS	47 NS	42 NS
Phr3 1-379 380-487	42 NS	43 NS	42 NS	**58** NS	45 NS
Pga5 1-420 421-641	46 44*	38 NS	**53** **38***	38 NS	38 NS

Figure 22. **A. domain organization of the Phr protein family of *Candida albicans*.** The asterisk indicates the conserved glutamic acid residues. B. Percentage of amino acid identity between the indicated portion of the N-terminal and C-terminal parts of the proteins. Blast2n was used with the filter option for LC region. The values in bold indicate the highest percentage of amino acid identity. NS: no similarity. The asterisk indicates the presence of PolyAsn and PolyGlu in Pga5p.

Aim of the Project

The Phr family of *Candida albicans* is a family of five GPI-anchored glycoproteins with glucanosyltransferase activity. They catalyse the elongation of β-1,3-glucan and of its branches in the fungal cell wall. These enzymes are essential for formation of the core glucan network, for the morphological plasticity and adaptability of this pathogen to different ambient pHs.

The first aim was the investigation of the biochemical properties of three GPI-anchored β-1,3-glucanosyltransferases of *C. albicans*, Phr1p, Phr2p and Pga4p. A fluorescent assay for β-1,3-glucanosyltransferases activity was used to study the catalytic properties of recombinant Phr proteins produced in *Pichia pastoris*.

The second part of this project was focused on the study of the transcriptional profile of *C. albicans* cells lacking β-1,3-glucanosyltransferase activity. The transcriptional profile of *phr1*Δ cells during induction of hyphal growth was analysed. Despite the defective phenotype of *phr1*Δ in these conditions, the cells maintain their integrity because a complex adaptive response.

These studies could provide useful information for the development of new therapeutic strategies aimed to combine the inhibition of cell wall target together with the compensatory pathways.

Main Results

1. Production of soluble and glycosylated forms of Phr proteins

In order to study the biochemical properties of Phr proteins of *C. albicans*, they were produced and purified as secreted proteins in *Pichia pastoris*. Since *PHR3* and *PGA5* genes are weakly or not expressed in *C. albicans* and their products were never detected, we focused only on the study of Phr1p, Phr2p and Pga4p. *P. pastoris* is a suitable host for the expression of proteins that are abundantly glycosylated and rich of disulfide bonds as Phr proteins. Moreover, this eukaryotic microorganism secretes very few proteins and at a very low level. Thus, the recombinant protein is the major product present in the medium and can be easily purified by affinity chromatography on Nickel resins, provided that a 6xHis tag is fused to the protein.

PHR1, *PHR2* and *PGA4* were cloned into the pHIL-S1 vector for *P. pastoris.* In order to obtain secreted proteins, in each gene the sequences encoding the original N-terminal signal peptide was replaced with a signal sequence from *P. pastoris*. Moreover, the C-terminal signal for GPI attachment was substituted by the His-Tag. After sequencing to check the absence of mutations in the nucleotide sequence and the proper gene fusion, the recombinant plasmids were used to transform *P. pastoris* strain GS115. The production and secretion of the soluble proteins were induced and major bands of 90, 96 and a doublet of 60-66 kDa were detected in the SDS-PAGE with the medium of the cells expressing Phr1p, Phr2p and Pga4 respectively. At 48 h of induction the protein production was 10 mg for Phr1p, 55 mg for Phr2p and 40 mg for Pga4p for Liter of culture. The recombinant proteins were purified from the culture supernatants by Nickel affinity chromatography.

The purified proteins were analysed on SDS-PAGE before and after treatment with PNGase F, an amidase that catalyses the cleavage of N-linked oligosaccharides chain. The apparent molecular mass of Phr1p, Phr2p and Pga4p upon treatment with PNGase F decreases from about 90, 96 and a doublet of 60-66 kDa respectively to about 70, 78 and a single band of about 46 kDa. This result indicates that the Phr proteins produced in *Pichia pastoris* are N-glycosylated. This is in agreement with the presence of 3 potential N-glycosylation sites in Phr1p, 4 in Phr2p and 3 in Pga4p. However, the predicted molecular weight for the His-tagged polypeptides is 54875 for Phr1p and 54359 for Phr2p suggesting that the serine-rich region present in these proteins might be target of O-mannosylation. On the contrary, the predicted molecular weight of Pga4p is 45164 that is very close to the apparent molecular weight of the deglycosylated band, suggesting that the protein is not heavily O-glycosylated, in agreement with the lack of a PolySer tract. Moreover, after PNGase F treatment, Pga4p doublet migrated as a single polypeptide suggesting that the heterogeneity in the apparent molecular weight is due to the N-glycan moiety.

2. Characterization of the catalytic properties of Phr1p, Phr2p and Pga4p

To analyse the catalytic properties of the recombinant Phr proteins, we used a new fluorescent method that is based on the β-1,3-glucanosyltarnsferasis activity of this protein. This activity consists of the (i) internal cleavage of the donor substrate, a linear and water-soluble β-1,3-glucan (laminarin), (ii) release of the reducing end product, and then (iii) transfer of the remaining portion to the non-reducing end of another β-1,3-glucan molecule that functions as an acceptor. In the absence of a suitable acceptor, the polysaccharide residue may be transferred to a water molecule (hydrolysis). The new fluorescent assay is based on the use of laminarin as substrate and linear laminarioligosaccharide of 5 or 6 glucose residues (L5 or L6) as acceptors. The acceptor is fluorescently labelled by conjugation of the reducing end to sulforhodamine (L5-SR or L6-SR).

The reaction mixture was in solution and contained the Phr enzyme, laminarin as donor and L5-SR or L6-SR as acceptors. The elongated products resulting from the transferase reaction are fluorescent and insoluble in 66% ethanol, whereas the L5-SR or L6-SR molecules are readily soluble. After the removal of unreacted L5-SR or L6-SR with 66% ethanol, the fluorescence of the elongated products is measured.

The fluorescent assay was used to test the effect of different pH on the transglycosylating activity of the Phr proteins in buffers of different pH but constant ionic strength. The pH-dependent activity curves showed their maximum at different pH values. Phr1p was most active at pH about 5.8 with a sharp decrease of activity at pH higher than 6.5, while the highest activity of Phr2p was at pH 3. The partial overlap of the two curves indicated that both enzymes have activity also between 4 and 5.5. Regarding the temperature optimum, Phr1p and Phr2p activity had similar curve and an optimum of temperature at 30°C. This assay was used to determine the acceptor and donor substrate specificity on a panel of polysaccharides and laminarioligosaccharides of increasing length. Phr1p and Phr2p used exclusively β-1,3-glucan or cell wall glucan as donor and laminarin-derived oligosaccharides as acceptor.

Unexpectedly, Pga4p was inactive in all the condition tested with the fluorescent assay, suggesting that Pga4p is an inactive member of the Phr family and it probably turned into a structural mannoprotein.

3. Stress response to Phr1p deficiency

PHR1 is expressed at neutral-alkaline pH in *C. albicans* in both yeast and hyphal forms. In the transition from yeast to hyphae at 37°C, pH 7.5, the wild type cells emit germ tubes that elongate and form thin hyphae whereas *phr1*Δ cells exhibit short and large germ tubes, aberrant septa and never elongate to form hyphae. These effects clearly indicate a defect in the polarized growth and cell wall formation. β-1,3-glucan decreases and chitin level increases indicating the presence of a

wall stress response. We exploited the pH-conditional nature of a *PHR1* null mutant to analyse the genome-wide transcriptional changes (DNA microarray analysis) in response to absence of β-1,3-glucan remodelling during the transition from yeast to hyphae.

Two classes of differentially modulated genes were identified: (i) Class 1: genes whose transcript levels were more abundant in the mutant in comparison with the wild type, (ii) Class 2: genes whose transcript levels were less abundant in the mutant in comparison with the wild type.

Among Class 1, the functional category of genes related to the cell wall was the largest. We found in *phr1*Δ cells increase of transcript level for 19 proteins included in the functional category cell wall/surfaces. Among this we can find a cross-linking enzyme (*CRH11*), two chitin synthases (*CHS2* and *CHS8*), a β-1,3-glucanase (*XOG1*) and several GPI anchored proteins (for example *PGA23*, *PGA13*, *PGA6* and *PGA54*). In the mutant the chitin level increased, as the level of transcript for *CHS2* and *CHS8*. To evaluate the role of chitin synthases in the adaptive response of the *phr1*Δ mutant, a *PHR1* homozygous null mutation was introduced into strains lacking *CHS2*, *CHS8*, *CHS2* and *CHS8* or *CHS3*. During the induction of hyphal growth, the double mutant *CHS3-PHR1* presented a defective phenotype, resulting in lethality in particular conditions. Thus, *CHS3*-mediated chitin synthesis is essential for *phr1*Δ viability.

PHR2 was repressed during induction of hyphal growth and none of the other three members of the *PHR* family was up-regulated indicating that no transcriptional-mediated cross compensatory mechanism exists for the paralogs.

Up-regulation of DNA replication genes was seen in *phr1*Δ mutant especially in the first time points during hyphal indication. We analyzed by flow cytometry the DNA distribution profile of wild type and *phr1*Δ mutant strains undergoing the transition from yeast to hyphae. These experiments confirmed that the mutant enters early in into S-phase in comparison with wild type and also the mutant presented an enrichment of cells at G_2/M.

β-1,3-glucan remodelling is important to sustain the hyphal development and its absence activates an adaptive response to preserve cell integrity. Phr1p and Chs3p are potential targets for combined treatments of *C. albicans* infections.

Conclusions and Future Prospects

The synthesis, assembly and hydrolysis of the fungal wall require three groups of enzymes: synthases, transglycosylases and glycosylhydrolases. The function of these enzymes is tightly regulated by the machinery controlling polarized growth and in turn affects the morphological development of fungi. Transglycosylases are responsible for the formation of a branched β-1,3-glucan structure on which other components are linked in a layered organization. The structure and architecture of the fungal wall undergo dynamic changes during the fungi life cycle, in response to environmental signals and damages that may affect cell integrity. Moreover, in fungal pathogens, the cell wall is the primary interface with the host. Surface properties are crucial for the establishment and progression of an infection and also for the interaction with the immune cells. Thus, the cell wall is rich of ideal targets for new antifungal agents, candidates for vaccines or immune modulators.

Phr family is a component of the family 72 of Glycosyl hydrolases (GH), which is unique to fungi. These enzymes, *in vitro,* catalyse the internal cleavage of a β-1,3-glucan, the transfer of the new reducing end to the non-reducing end of another β-1,3-glucan (acceptor) with the formation of a new β-1,3-glycosidic linkage. This reaction results in the elongation of the acceptor. *In vivo* this activity is required for morphogenesis and virulence and in some fungal species is essential for viability

This work was focused on the study of the catalytic properties of some members of the Phr family of *Candida albicans*, Phr1p, Phr2p and Pga4p. The three Phr proteins were expressed and purified as soluble proteins in the eukaryotic system *Pichia pastoris*. A sensitive fluorescent assay for β-1,3-glucanosyltransferase activity was applied on the recombinant proteins. A panel of different possible donor and acceptor were tested. The strict substrate specificity of Phr proteins indicates that they are typical homotransglycosylases specialized in cleaving and re-joining molecules of β-1,3-glucan. The optimal reaction temperature was 30°C for both enzymes, while the pH optimum was 5.8 for Phr1p and 3 for Phr2p. The overlap of the pH dependent curves shows that two enzymes have relevant activity also between 4 and 5.5, suggesting that they can buffer reciprocally their function during pH transition. The presence of different enzymes with same activity at different pH enable *Candida albicans* to growth over the whole spectrum of physiological pH of the host niches of the human body that vary from acidic (stomach, vagina) to neutral (kidney, duodenum) or slightly alkaline (blood).

Surprisingly, Pga4p showed no transglycosylases activity in all the conditions tested, consequently we proposed that Pga4p turned into a structural cell wall protein. The absence of any relevant

phenotype in *pga4*Δ null mutant suggests that the potential structural function of Pga4p in not fundamental for *Candida albicans*.

In the second part of the project, a transcriptional profile of *phr1*Δ mutant in the transition from yeast to hyphae was analysed, resulting in the identification of genes involved in the response of cell wall stress induced by the absence of β-1,3-glucanosyltransferase activity. We produced a series of double mutants for chitin synthases (*CHS*) genes and *PHR1,* finding the existence of synthetic lethality between *PHR1* and *CHS3.*

Since cell wall components are highly immunogenic, essential for fungi life and absent in humans, the cell wall represents a target of great scientific and biomedical interest for the development of new agents for therapy and prophylaxis. Therapies of candidiasis rely on the use of a still limited armamentarium of drugs that target ergosterol (amphotericin B and azoles) or the synthesis of β-1,3-glucan (echinocandins). However, a compensatory response can generates tolerance to these drugs.

The results from these two projects provide new insights in *C. albicans* glycobiology This knowledge can be used in the future for applications such as the search of β-1,3-glucanosyltransferase inhibitors to be used alone or in combination with inhibitors of the compensatory pathway activated by cell wall stress.

References

1. Fritz, G., *RAGE: a single receptor fits multiple ligands.* Trends in Biochemical Sciences, 2011. **36**(12): p. 625-632.
2. Roth, Z., G. Yehezkel, and I. Khalaila, *Identification and Quantification of Protein Glycosylation.* International Journal of Carbohydrate Chemistry, 2012. **2012**: p. 1-10.
3. Wormald, M.R., et al., *Conformational studies of oligosaccharides and glycopeptides: complementarity of NMR, X-ray crystallography, and molecular modelling.* Chem Rev, 2002. **102**(2): p. 371-86.
4. Spiro, R.G., *Protein glycosylation: nature, distribution, enzymatic formation, and disease implications of glycopeptide bonds.* Glycobiology, 2002. **12**(4): p. 43R-56R.
5. Neeper, M., et al., *Cloning and expression of a cell surface receptor for advanced glycosylation end products of proteins.* J Biol Chem, 1992. **267**(21): p. 14998-5004.
6. Li, J. and A.M. Schmidt, *Characterization and functional analysis of the promoter of RAGE, the receptor for advanced glycation end products.* J Biol Chem, 1997. **272**(26): p. 16498-506.
7. Leclerc, E., et al., *Binding of S100 proteins to RAGE: An update.* Biochimica et Biophysica Acta (BBA) - Molecular Cell Research, 2009. **1793**(6): p. 993-1007.
8. Deane, R.J., *Is RAGE still a therapeutic target for Alzheimer's disease?* Future Med Chem, 2012. **4**(7): p. 915-25.
9. Banerjee, S., et al., *The C-terminal acidic tail is responsible for the inhibitory effects of HMGB1 on efferocytosis.* J Leukoc Biol, 2010. **88**(5): p. 973-9.
10. Bierhaus, A., et al., *Understanding RAGE, the receptor for advanced glycation end products.* J Mol Med (Berl), 2005. **83**(11): p. 876-86.
11. Hofmann, M.A., et al., *RAGE mediates a novel proinflammatory axis: a central cell surface receptor for S100/calgranulin polypeptides.* Cell, 1999. **97**(7): p. 889-901.
12. Hudson, B.I., et al., *Identification, classification, and expression of RAGE gene splice variants.* FASEB J, 2008. **22**(5): p. 1572-80.
13. Kalea, Anastasia Z., Ann M. Schmidt, and Barry I. Hudson, *RAGE: a novel biological and genetic marker for vascular disease.* Clinical Science, 2009. **116**(8): p. 621.
14. Kang, P., C. Tian, and C. Jia, *Association of RAGE gene polymorphisms with type 2 diabetes mellitus, diabetic retinopathy and diabetic nephropathy.* Gene, 2012. **500**(1): p. 1-9.
15. Rouhiainen, A., et al., *RAGE-mediated cell signaling.* Methods Mol Biol, 2013. **963**: p. 239-63.
16. Dattilo, B.M., et al., *The extracellular region of the receptor for advanced glycation end products is composed of two independent structural units.* Biochemistry, 2007. **46**(23): p. 6957-70.
17. Chuah, Y.K., et al., *Receptor for Advanced Glycation End Products and Its Involvement in Inflammatory Diseases.* Int J Inflam, 2013. **2013**: p. 403460.
18. Xie, J., et al., *Cellular signalling of the receptor for advanced glycation end products (RAGE).* Cell Signal, 2013. **25**(11): p. 2185-97.
19. Falcone, C., et al., *Plasma levels of soluble receptor for advanced glycation end products and coronary atherosclerosis: possible correlation with clinical presentation.* Dis Markers, 2013. **35**(3): p. 135-40.
20. Koch, M., et al., *Structural Basis for Ligand Recognition and Activation of RAGE.* Structure, 2010. **18**(10): p. 1342-1352.
21. Park, H. and J.C. Boyington, *The 1.5 A Crystal Structure of Human Receptor for Advanced Glycation Endproducts (RAGE) Ectodomains Reveals Unique Features Determining Ligand Binding.* Journal of Biological Chemistry, 2010. **285**(52): p. 40762-40770.

22. Yatime, L. and G.R. Andersen, *Structural insights into the oligomerization mode of the human receptor for advanced glycation end-products.* FEBS J, 2013. **280**(24): p. 6556-68.

23. Park, S.J., T. Kleffmann, and P.A. Hessian, *The G82S polymorphism promotes glycosylation of the receptor for advanced glycation end products (RAGE) at asparagine 81: comparison of wild-type rage with the G82S polymorphic variant.* J Biol Chem, 2011. **286**(24): p. 21384-92.

24. Srikrishna, G., et al., *Carboxylated N-glycans on RAGE promote S100A12 binding and signaling.* J Cell Biochem, 2010. **110**(3): p. 645-59.

25. Yang, L., et al., *Association of the receptor for advanced glycation end products gene polymorphisms and circulating RAGE levels with diabetic retinopathy in the Chinese population.* J Diabetes Res, 2013. **2013**: p. 264579.

26. Xie, J., et al., *Hexameric calgranulin C (S100A12) binds to the receptor for advanced glycated end products (RAGE) using symmetric hydrophobic target-binding patches.* J Biol Chem, 2007. **282**(6): p. 4218-31.

27. Xie, J., et al., *Structural basis for pattern recognition by the receptor for advanced glycation end products (RAGE).* J Biol Chem, 2008. **283**(40): p. 27255-69.

28. Zong, H., et al., *Homodimerization is essential for the receptor for advanced glycation end products (RAGE)-mediated signal transduction.* J Biol Chem, 2010. **285**(30): p. 23137-46.

29. Kierdorf, K. and G. Fritz, *RAGE regulation and signaling in inflammation and beyond.* J Leukoc Biol, 2013. **94**(1): p. 55-68.

30. Sevillano, N., et al., *Internalization of the receptor for advanced glycation end products (RAGE) is required to mediate intracellular responses.* J Biochem, 2009. **145**(1): p. 21-30.

31. Haglund, K., T.E. Rusten, and H. Stenmark, *Aberrant receptor signaling and trafficking as mechanisms in oncogenesis.* Crit Rev Oncog, 2007. **13**(1): p. 39-74.

32. Xu, D., et al., *Stable RAGE-heparan sulfate complexes are essential for signal transduction.* ACS Chem Biol, 2013. **8**(7): p. 1611-20.

33. Wei, W., et al., *Disulfide bonds within the C2 domain of RAGE play key roles in its dimerization and biogenesis.* PLoS One, 2012. **7**(12): p. e50736.

34. Simm, A., *Protein glycation during aging and in cardiovascular disease.* J Proteomics, 2013. **92**: p. 248-59.

35. Vistoli, G., et al., *Advanced glycoxidation and lipoxidation end products (AGEs and ALEs): an overview of their mechanisms of formation.* Free Radic Res, 2013. **47 Suppl 1**: p. 3-27.

36. Pullerits, R., et al., *Soluble receptor for advanced glycation end products triggers a proinflammatory cytokine cascade via beta2 integrin Mac-1.* Arthritis Rheum, 2006. **54**(12): p. 3898-907.

37. Yamamoto, Y., et al., *Septic shock is associated with receptor for advanced glycation end products ligation of LPS.* J Immunol, 2011. **186**(5): p. 3248-57.

38. van Zoelen, M.A., et al., *Receptor for advanced glycation end products facilitates host defense during Escherichia coli-induced abdominal sepsis in mice.* J Infect Dis, 2009. **200**(5): p. 765-73.

39. Monteiro, F.A., et al., *In vitro inhibition of transthyretin aggregate-induced cytotoxicity by full and peptide derived forms of the soluble receptor for advanced glycation end products (RAGE).* FEBS Lett, 2006. **580**(14): p. 3451-6.

40. Sousa, M.M., et al., *Interaction of the receptor for advanced glycation end products (RAGE) with transthyretin triggers nuclear transcription factor kB (NF-kB) activation.* Lab Invest, 2000. **80**(7): p. 1101-10.

41. He, M., et al., *Receptor for advanced glycation end products binds to phosphatidylserine and assists in the clearance of apoptotic cells.* EMBO Rep, 2011. **12**(4): p. 358-64.

42. Sirois, C.M., et al., *RAGE is a nucleic acid receptor that promotes inflammatory responses to DNA.* J Exp Med, 2013. **210**(11): p. 2447-63.

43. Zhou, L.L., et al., *The receptor of advanced glycation end products plays a central role in advanced oxidation protein products-induced podocyte apoptosis.* Kidney Int, 2012. **82**(7): p. 759-70.

44. Mizumoto, S., J. Takahashi, and K. Sugahara, *Receptor for advanced glycation end products (RAGE) functions as receptor for specific sulfated glycosaminoglycans, and anti-RAGE antibody or sulfated glycosaminoglycans delivered in vivo inhibit pulmonary metastasis of tumor cells.* J Biol Chem, 2012. **287**(23): p. 18985-94.

45. Xu, D., et al., *Heparan sulfate is essential for high mobility group protein 1 (HMGB1) signaling by the receptor for advanced glycation end products (RAGE).* J Biol Chem, 2011. **286**(48): p. 41736-44.

46. Ma, W., et al., *RAGE binds C1q and enhances C1q-mediated phagocytosis.* Cell Immunol, 2012. **274**(1-2): p. 72-82.

47. Ruan, B.H., et al., *Complement C3a, CpG oligos, and DNA/C3a complex stimulate IFN-alpha production in a receptor for advanced glycation end product-dependent manner.* J Immunol, 2010. **185**(7): p. 4213-22.

48. Rai, V., et al., *Lysophosphatidic acid targets vascular and oncogenic pathways via RAGE signaling.* J Exp Med, 2012. **209**(13): p. 2339-50.

49. Singh, V.P., et al., *Advanced Glycation End Products and Diabetic Complications.* Korean J Physiol Pharmacol, 2014. **18**(1): p. 1-14.

50. Araki, N., et al., *Immunochemical evidence for the presence of advanced glycation end products in human lens proteins and its positive correlation with aging.* J Biol Chem, 1992. **267**(15): p. 10211-4.

51. Schleicher, E.D., E. Wagner, and A.G. Nerlich, *Increased accumulation of the glycoxidation product N(epsilon)-(carboxymethyl)lysine in human tissues in diabetes and aging.* J Clin Invest, 1997. **99**(3): p. 457-68.

52. Nakamura, Y., et al., *Immunohistochemical localization of advanced glycosylation end products in coronary atheroma and cardiac tissue in diabetes mellitus.* Am J Pathol, 1993. **143**(6): p. 1649-56.

53. Xue, J., et al., *Advanced Glycation End Product Recognition by the Receptor for AGEs.* Structure, 2011. **19**(5): p. 722-732.

54. Aldini, G., et al., *Molecular strategies to prevent, inhibit, and degrade advanced glycoxidation and advanced lipoxidation end products.* Free Radic Res, 2013. **47 Suppl 1**: p. 93-137.

55. Stern, D., et al., *Receptor for advanced glycation endproducts: a multiligand receptor magnifying cell stress in diverse pathologic settings.* Adv Drug Deliv Rev, 2002. **54**(12): p. 1615-25.

56. Yan, S.F., R. Ramasamy, and A.M. Schmidt, *Receptor for AGE (RAGE) and its ligands-cast into leading roles in diabetes and the inflammatory response.* J Mol Med (Berl), 2009. **87**(3): p. 235-47.

57. Yan, S.D., et al., *Receptor-dependent cell stress and amyloid accumulation in systemic amyloidosis.* Nat Med, 2000. **6**(6): p. 643-51.

58. Deane, R., et al., *A multimodal RAGE-specific inhibitor reduces amyloid beta-mediated brain disorder in a mouse model of Alzheimer disease.* J Clin Invest, 2012. **122**(4): p. 1377-92.

59. Haupt, C., et al., *Pattern recognition with a fibril-specific antibody fragment reveals the surface variability of natural amyloid fibrils.* J Mol Biol, 2011. **408**(3): p. 529-40.

60. Chavakis, T., et al., *The pattern recognition receptor (RAGE) is a counterreceptor for leukocyte integrins: a novel pathway for inflammatory cell recruitment.* J Exp Med, 2003. **198**(10): p. 1507-15.

61. Rai, V., et al., *Signal transduction in receptor for advanced glycation end products (RAGE): solution structure of C-terminal rage (ctRAGE) and its binding to mDia1.* J Biol Chem, 2012. **287**(7): p. 5133-44.

62. Ramasamy, R., S.F. Yan, and A.M. Schmidt, *Receptor for AGE (RAGE): signaling mechanisms in the pathogenesis of diabetes and its complications.* Ann N Y Acad Sci, 2011. **1243**: p. 88-102.

63. Sakaguchi, M., et al., *TIRAP, an adaptor protein for TLR2/4, transduces a signal from RAGE phosphorylated upon ligand binding.* PLoS One, 2011. **6**(8): p. e23132.

64. Sorci, G., et al., *RAGE in tissue homeostasis, repair and regeneration.* Biochim Biophys Acta, 2013. **1833**(1): p. 101-9.

65. Sorci, G., et al., *Amphoterin stimulates myogenesis and counteracts the antimyogenic factors basic fibroblast growth factor and S100B via RAGE binding.* Mol Cell Biol, 2004. **24**(11): p. 4880-94.

66. Huttunen, H.J., C. Fages, and H. Rauvala, *Receptor for advanced glycation end products (RAGE)-mediated neurite outgrowth and activation of NF-kappaB require the cytoplasmic domain of the receptor but different downstream signaling pathways.* J Biol Chem, 1999. **274**(28): p. 19919-24.

67. Harja, E., et al., *Vascular and inflammatory stresses mediate atherosclerosis via RAGE and its ligands in apoE-/- mice.* J Clin Invest, 2008. **118**(1): p. 183-94.

68. Qin, Q., et al., *Heparanase induced by advanced glycation end products (AGEs) promotes macrophage migration involving RAGE and PI3K/AKT pathway.* Cardiovasc Diabetol, 2013. **12**: p. 37.

69. Ott, C., et al., *Role of advanced glycation end products in cellular signaling.* Redox Biol, 2014. **2**: p. 411-429.

70. Queisser, M.A., et al., *Loss of RAGE in pulmonary fibrosis: molecular relations to functional changes in pulmonary cell types.* Am J Respir Cell Mol Biol, 2008. **39**(3): p. 337-45.

71. Ding, K.H., et al., *Disordered osteoclast formation in RAGE-deficient mouse establishes an essential role for RAGE in diabetes related bone loss.* Biochem Biophys Res Commun, 2006. **340**(4): p. 1091-7.

72. Zhou, Z., et al., *Regulation of osteoclast function and bone mass by RAGE.* J Exp Med, 2006. **203**(4): p. 1067-80.

73. Chavakis, T., A. Bierhaus, and P. Nawroth, *RAGE (receptor for advanced glycation end products): a central player in the inflammatory response.* Microbes and Infection, 2004. **6**(13): p. 1219-1225.

74. Padilla, L., S. Dakhel, and J.L. Hernandez, *S100 to Receptor for Advanced Glycation End-products binding assay: looking for Inhibitors.* Biochem Biophys Res Commun, 2014.

75. Pichiule, P., et al., *Hypoxia-inducible factor-1 mediates neuronal expression of the receptor for advanced glycation end products following hypoxia/ischemia.* J Biol Chem, 2007. **282**(50): p. 36330-40.

76. Tian, J., et al., *Toll-like receptor 9-dependent activation by DNA-containing immune complexes is mediated by HMGB1 and RAGE.* Nat Immunol, 2007. **8**(5): p. 487-96.

77. Nam, S.W., et al., *Molecular changes from dysplastic nodule to hepatocellular carcinoma through gene expression profiling.* Hepatology, 2005. **42**(4): p. 809-18.

78. Nerlich, A.G., E.D. Schleicher, and N. Boos, *1997 Volvo Award winner in basic science studies. Immunohistologic markers for age-related changes of human lumbar intervertebral discs.* Spine (Phila Pa 1976), 1997. **22**(24): p. 2781-95.

79. Nilsson, J., et al., *Affinity fusion strategies for detection, purification, and immobilization of recombinant proteins.* Protein Expr Purif, 1997. **11**(1): p. 1-16.

80. Moran, G., D. Coleman, and D. Sullivan, *An introduction to the medically important Candida species.* Candida and Candidiasis, 2012. **2**: p. 11-25.

81. Wisplinghoff, H., et al., *Nosocomial bloodstream infections in US hospitals: analysis of 24,179 cases from a prospective nationwide surveillance study.* Clin Infect Dis, 2004. **39**(3): p. 309-17.

82. Gow, N.A. and B. Hube, *Importance of the Candida albicans cell wall during commensalism and infection.* Curr Opin Microbiol, 2012. **15**(4): p. 406-12.

83. Mochon, A.B., et al., *Serological profiling of a Candida albicans protein microarray reveals permanent host-pathogen interplay and stage-specific responses during candidemia.* PLoS Pathog, 2010. **6**(3): p. e1000827.

84. Shapiro, R.S., N. Robbins, and L.E. Cowen, *Regulatory circuitry governing fungal development, drug resistance, and disease.* Microbiol Mol Biol Rev, 2011. **75**(2): p. 213-67.

85. Saville, S.P., et al., *Engineered control of cell morphology in vivo reveals distinct roles for yeast and filamentous forms of Candida albicans during infection.* Eukaryot Cell, 2003. **2**(5): p. 1053-60.

86. d'Enfert, C., *Biofilms and their role in the resistance of pathogenic Candida to antifungal agents.* Curr Drug Targets, 2006. **7**(4): p. 465-70.

87. Ruiz-Herrera, J., et al., *Molecular organization of the cell wall of Candida albicans and its relation to pathogenicity.* FEMS Yeast Res, 2006. **6**(1): p. 14-29.

88. Chaffin, W.L., *Candida albicans cell wall proteins.* Microbiol Mol Biol Rev, 2008. **72**(3): p. 495-544.

89. Perez-Garcia, L.A., et al., *Role of Cell Wall Polysaccharides during Recognition of Candida albicans by the Innate Immune System.* Glycobiology, 2011. **1**(1): p. 1-7.

90. Lombard, V., et al., *The carbohydrate-active enzymes database (CAZy) in 2013.* Nucleic Acids Res, 2014. **42**(Database issue): p. D490-5.

91. Sillo, F., et al., *Expression and phylogenetic analyses of the Gel/Gas proteins of Tuber melanosporum provide insights into the function and evolution of glucan remodeling enzymes in fungi.* Fungal Genet Biol, 2013. **53**: p. 10-21.

92. Hartland, R.P., et al., *A novel beta-(1-3)-glucanosyltransferase from the cell wall of Aspergillus fumigatus.* J Biol Chem, 1996. **271**(43): p. 26843-9.

93. Kovacova, K., et al., *Catalytic properties of Phr family members of cell wall glucan remodeling enzymes: implications for the adaptation of Candida albicans to ambient pH.* FEMS Yeast Res, 2015. **15**(2).

94. Mouyna, I., et al., *Glycosylphosphatidylinositol-anchored glucanosyltransferases play an active role in the biosynthesis of the fungal cell wall.* J Biol Chem, 2000. **275**(20): p. 14882-9.

95. Latge, J.P., *The cell wall: a carbohydrate armour for the fungal cell.* Mol Microbiol, 2007. **66**(2): p. 279-90.

96. Cabib, E., N. Blanco, and J. Arroyo, *Presence of a large beta(1-3)glucan linked to chitin at the Saccharomyces cerevisiae mother-bud neck suggests involvement in localized growth control.* Eukaryot Cell, 2012. **11**(4): p. 388-400.

97. Ragni, E., et al., *The Gas family of proteins of Saccharomyces cerevisiae: characterization and evolutionary analysis.* Yeast, 2007. **24**(4): p. 297-308.

98. Rolli, E., et al., *Expression, stability, and replacement of glucan-remodeling enzymes during developmental transitions in Saccharomyces cerevisiae.* Mol Biol Cell, 2011. **22**(9): p. 1585-98.

99. de Medina-Redondo, M., et al., *beta(1,3)-glucanosyl-transferase activity is essential for cell wall integrity and viability of Schizosaccharomyces pombe.* PLoS One, 2010. **5**(11): p. e14046.

100. Gastebois, A., et al., *beta(1-3)Glucanosyltransferase Gel4p is essential for Aspergillus fumigatus.* Eukaryot Cell, 2010. **9**(8): p. 1294-8.

101. Muhlschlegel, F.A. and W.A. Fonzi, *PHR2 of Candida albicans encodes a functional homolog of the pH-regulated gene PHR1 with an inverted pattern of pH-dependent expression.* Mol Cell Biol, 1997. **17**(10): p. 5960-7.

102. Saporito-Irwin, S.M., et al., *PHR1, a pH-regulated gene of Candida albicans, is required for morphogenesis.* Mol Cell Biol, 1995. **15**(2): p. 601-13.

103. De Bernardis, F., et al., *The pH of the host niche controls gene expression in and virulence of Candida albicans.* Infect Immun, 1998. **66**(7): p. 3317-25.

104. Yuan, X., et al., *The RIM101 signal transduction pathway regulates Candida albicans virulence during experimental keratomycosis.* Invest Ophthalmol Vis Sci, 2010. **51**(9): p. 4668-76.

105. Eckert, S.E., et al., *PGA4, a GAS homologue from Candida albicans, is up-regulated early in infection processes.* Fungal Genet Biol, 2007. **44**(5): p. 368-77.

PART II

List of papers

Project hRAGE

Manuscript submitted and currently under revision

The ligand binding domain VC1 but not the V fragment of the receptor for the advanced glycation end products (RAGE) is expressed and secreted in *P. pastoris*

Genny Degani, Mara Colzani, Alberto Tettamanzi, Luca Sorrentino, Alessandro Aliverti, Guenter Fritz, Giancarlo Aldini and Laura Popolo

Protein expression and purification

Patent request under deposition

Sistema di espressione migliorato del recettore per gli Advanced Glycation End Products (AGE) e gli Advanced Lipid Glycation End Products (ALE) e sue applicazioni

Richiedente: EUROCLONE S.p.A.; Università degli Studi di Milano

Italian patent

Project Phr proteins

Published article

Catalytic properties of Phr family members of cell wall glucan remodeling enzymes: implications for the adaptation of *Candida albicans* to ambient pH

Kristína Kováčová, Genny Degani, Eva Stratilová, Vladimír Farkaš and Laura Popolo

FEMS Yeast Res, 2015. 15(2)

Project hRAGE

Manuscript submitted and currently under revision (revised version)

The ligand binding domain VC1 but not the V fragment of the receptor for the advanced glycation end products (RAGE) is expressed and secreted in *P. pastoris*

Genny Degani, Mara Colzani, Alberto Tettamanzi, Luca Sorrentino, Alessandro Aliverti, Guenter Fritz, Giancarlo Aldini and Laura Popolo

Protein expression and purification

The ligand binding domain VC1 but not the V fragment of the receptor for the advanced glycation end products (RAGE) is expressed and secreted in *P. pastoris*

Genny Degani [a], Mara Colzani [b], Alberto Tettamanzi [a], Luca Sorrentino [a], Alessandro Aliverti [a], Guenter Fritz [c], Giancarlo Aldini [b] and Laura Popolo [a,]*

[a] Department of Biosciences, Via Celoria 26 and [b] Department of Pharmaceutical Sciences, Via Mangiagalli 25, University of Milan, 20133 Milano, Italy, [c] Institute for Neuropathology, University of Freiburg, Breisacher Str. 64, 79106 Freiburg, Germany

*Corresponding author

Laura Popolo
University of Milano
Department of Biosciences
Via Celoria 26
20133 Milano
Italy
Tel: +39-02-50314919

E-mail: Laura.Popolo@unimi.it

Abstract

The receptor for the advanced glycation end products (RAGE) is a type I transmembrane glycoprotein belonging to the immunoglobulin superfamily and binds a variety of unrelated ligands sharing a negative charge. Most ligands bind to the extracellular V or VC1 domains of the receptor. In this work, V and VC1 of human RAGE were produced in the methylotrophic yeast *Pichia pastoris* and directed to the secretory pathway. Fusions to a removable C-terminal His-tag evidenced proteolytic processing of the tag by extracellular proteases and also intracellular degradation of the N-terminal portion of V-His. Expression of untagged forms was attempted. While native VC1 was secreted into the culture medium and was functionally active in binding AGEs, the V domain was retained intracellularly. The glycosylation state of VC1 was analyzed by mass spectrometry and peptide-*N*-glycosidase F digestion. Like RAGE isolated from mammalian sources, the degree of occupancy of the *N*-glycosylation sites in VC1 was full at Asn25 and partial at Asn81 which was also subjected to non-enzymatic deamidation. A simple procedure for the purification to homogeneity of VC1 from the medium was developed. The folded state of the purified protein was assessed by thermal shift assays. Recombinant VC1 showed a remarkably high thermal stability as compared to the protein expressed in bacteria. Our *in vivo* approach indicates that the V and C1 domains constitute a single folding unit. The stability and solubility of glycosylated VC1 may be beneficial for future *in vitro* studies aimed to identify new ligands or inhibitors of RAGE.

Keywords: Receptors - RAGE - Immunoglobulin superfamily – *Pichia pastoris* – protein *N*-glycosylation – deamidation

Introduction

The receptor for the advanced glycation end products (RAGE) is a protein unique to mammals. In humans, it is expressed at low levels in many cell types, in particular leukocytes, dendritic cells, endothelial cells, smooth muscle cells, neurons and microglia and is abundant in the lung [1]. This receptor is important for human biology. It promotes neurite outgrowth, differentiation and migration in the nervous system, and is involved in bone metabolism and lung homeostasis [1]. It contributes to the inflammatory response [2] and participates to innate and adaptive immunity, where the activation of human RAGE (hRAGE) leads to the production of reactive oxygen species (ROS). Furthermore, hRAGE is involved in the pathogenesis of several diseases. Thus, hRAGE plays two opposing roles, one beneficial for human biology and one that promotes the disease establishment and progression.

High levels of hRAGE and its ligands lead to several dysfunctions through the sustained activation of different signal transduction pathways depending on cell type, context and ligand. The signaling pathways include (i) the p21ras/mitogen-activated cascade of protein kinases (MAPKs) such as ERK1/2 and the stress-activated kinases (JNK and p38) and (ii) the JAK/STAT pathway, resulting in the nuclear translocation of NF-κB and activation of transcription of inflammatory genes, of RAGE gene itself and of the interferon-stimulated response, (iii) the cdc42/rac pathway that is involved in cell growth and migration, and (iv) the NADPH oxidase pathway that leads to ROS formation [1, 2]. Sustained activation of RAGE signaling can result in cell damage as in complications of diabetes such as cardiovascular disorders, atherosclerosis, nephropathies and chronic inflammation. For these reasons, various studies indicate that antagonizing RAGE activation, by use of inhibitors or through binding to soluble ectodomain (sRAGE), has potential therapeutic effects in several inflammatory-based diseases including Alzheimer disease [3, 4]. Small molecules acting as RAGE antagonists have been recently reported and a Pfizer compound (PF-04494700) has reached a phase II clinical trial [3-5].

hRAGE is a type I transmembrane glycoprotein of 404 amino acids, a member of the immunoglobulin (Ig) superfamily and functionally and structurally similar to cell adhesion molecules [6, 7]. hRAGE contains a 22 residue signal peptide and an extracellular portion that comprises a variable (V) and two constant (C1 and C2) Ig-like domains. A single transmembrane domain connects the V-C1-C2 segment to a short C-terminal tail that is responsible for intracellular signaling. hRAGE binds a wide spectrum of ligands [8], the majority of which are: AGEs, *i.e.* products generated by the non-enzymatic glycation and subsequent oxidation of proteins, amyloid-β-peptide and β-sheet fibrils and members of the S100/calgranulin protein family [9]. Additional ligands include: extracellular matrix proteins, such as collagens I and IV, Mac-1 (member of the β2-

integrin family), the High Mobility Group protein Box-1 (HMGB-1 or amphoterin) which is a prototypic Damaged-Associated Molecular Pattern (DAMP) [6], the lipopolysaccharide of bacterial walls (LPS), the complement component C1q [10], chondroitin sulfate and heparan sulfate [11, 12] and nucleic acids [13]. hRAGE ligands do not share sequence or structural similarity but all display a highly negative charge at neutral pH and the tendency to oligomerize [14]. The 3D-structure of the RAGE extracellular portion (V-C1-C2), of VC1 and V, has been determined, providing an insight into the molecular mechanism of RAGE activation [14]. Most hRAGE ligands bind to the highly basic V domain through electrostatic and hydrophobic interactions. Due to its peculiar binding properties, RAGE is also defined as a pattern-recognition receptor. A model of RAGE activation proposes that RAGE molecules preassemble in the plane of the membrane and this potentiates signaling after the binding of the ligand to the V domain [2]. Moreover, two RAGE molecules are also able to associate in head-to-head fashion possibly mediating the interaction between cells similarly to adhesion proteins (homophilic adhesion).

We are interested in studying the binding of hRAGE to AGEs, since the RAGE-AGE axis is crucial in the etiology of many diseases. Indeed, the formation of AGEs is accelerated in the presence of hyperglycemia and oxidative stress (for a review, see [15]). In this work, we probed the expression of V and VC1 in the lower eukaryote *Pichia pastoris.* This microorganism has an efficient apparatus of protein glycosylation, folding and secretion that may be beneficial for the expression of naturally secreted glycoproteins. In addition, glycosylation, together with the formation of disulfide bonds, confers stability to proteins and also improves their solubility, properties that may favor *in vitro* studies on the protein biophysical properties. To our knowledge, the expression of the isolated V and VC1 domains in a eukaryotic system has not been attempted to date, although *P. pastoris* proved to be an appropriate host for the expression of the full ectodomain [16]. Here, we report the expression/secretion of VC1 and V domains of hRAGE in *P. pastoris*. A protocol for VC1 purification to homogeneity from the culture medium, the analysis of its glycosylation profile, the improved quality of the protein in comparison to the form produced in bacteria and the proof of its functionality are presented.

Materials and methods

Strains and growth conditions

The *E. coli* DH5α strain was used for DNA manipulation. *P. pastoris* GS115 strain (*his*4) (Invitrogen) was used for the heterologous expression of hRAGE domains. The GS115-*sub2* strain,

inactivated in the gene encoding the major secreted subtilisin-like protease, was kindly provided by Dr. Michel Monod (Centre Hospitalier Universitaire Vaudois, Lausanne, Switzerland). *P. pastoris* cells were routinely propagated on plates of YPDA (1% yeast extract, 2% peptone, 2% glucose and 2% agar) at 30 °C. To induce the expression of recombinant proteins, His^+ Mut^s cells were shifted from Buffered Glycerol-complex Medium (BMGY) (1% yeast extract, 2% peptone, 1% glycerol, 1.34% YNB, $4x10^{-5}$% biotin, 0.1 M potassium phosphate, pH 6.0) to Buffered Methanol-complex Medium (BMMY) (1% yeast extract, 2% peptone, 0.5% methanol, 1.34% YNB, $4x10^{-5}$% biotin, 0.1 M potassium phosphate, pH 6.0) according to the manufacturer's instructions. Alternatively, MGY and MMY media, having the same composition as above but without potassium phosphate buffer, were used. Cells were routinely grown in flasks at 28 °C under strong agitation and growth was monitored through the increase in optical density at 600 nm (OD_{600}).

Construction of the expression plasmids

Recombinant plasmids for integrative recombination in *P. pastoris* were obtained by cloning *Xho*I - digested PCR fragments into the *Xho*I site of pHIL-S1 (Invitrogen), to generate in-frame fusions with the secretion signal of *P. pastoris PHO1,* encoding an extracellular acid phosphatase. PCR was carried out using as a template pET-15b-$VC1^{243}$ [17], harboring the cDNA encoding a portion of hRAGE (residues 23-243), high-fidelity Fusion DNA polymerase (NEB) and appropriate primers (**Table 1).** The DNA fragments encoding $VC1^{233}$ and $VC1^{233}$-His were obtained using VC-For/VC233-Rev and VC-For /VC233His-Rev oligonucleotide pairs, respectively. Similarly, the DNA encoding V^{121} and V^{121}-His were obtained using the primer pairs VC-For/V121-Rev and VC-For/ V121His-Rev. Both PCR products and the digested vector were gel-purified before ligation. Screening of the transformants was performed by colony PCR using 5'-AOX1/VC233-Rev and VC-For/3'AOX1 for $VC1^{233}$, 5'-AOX1/VC233His-Rev and VC-For/3'AOX1 for $VC1^{233}$-His, 5'-AOX1/V121-Rev and VC-For/3'AOX1 for V^{121}, 5'-AOX1/V121HIS-Rev and VC-For/3'AOX1 for V^{121}-His (**Table 1**). Recombinant plasmid DNA, named pHIL-S1- $VC1^{233}$, pHIL-S1- $VC1^{233}$-His, pHIL-S1-V^{121} and pHIL-S1-V^{121}-His, were purified from positive clones. The correct orientation, the in-frame fusion, and the absence of random mutations in the inserts were verified by DNA sequencing (BMR Genomics, Padova, Italy).

Transformation of P. pastoris and expression of recombinant forms

Plasmids, linearized with *Bgl*II, were transformed into *P. pastoris* cells using the "EasyComp" chemical transformation method (Invitrogen). Selection of His^+ transformants and screening for Mut^s phenotype were performed as previously described [18]. To induce the expression of the recombinant proteins, the positive clones were grown overnight at 28 °C in 10 ml of glycerol-containing medium (BMGY or MGY) under strong agitation and at a ratio between volume of culture and capacity of the flask of 1:10. Then, appropriate amount of cells were collected and transferred in methanol-containing medium (BMMY or MMY) in order to obtain an initial OD_{600} of 1. Growth was monitored by increase of OD_{600}. Fresh methanol was added daily to 0.5% (v/v) final concentration. To monitor protein expression, supernatants from 1ml-aliquots of culture, withdrawn at intervals after induction, were obtained by centrifugation, flash-frozen and stored at –20 °C until analysis by SDS-PAGE. Total protein extracts from flash-frozen cell pellets were prepared as previously described [19]. At least three clones were analyzed per construct.

Purification of recombinant VC1

For protein small-scale purification, 80 ml-culture of induced *P. pastoris* cells was centrifuged at 4,000 × g for 10 min and the supernatant was filtered through cellulose nitrate filters (1.2 μm pore size, Sartorius) to remove residual cells and debris. After dialysis (Spectra/Por membranes, cut-off 6-8,000) at 4 °C for 16 h against 10 mM Na-acetate pH 5.0, the sample was applied to a cation-exchange RESOURCE S column (1.6 x 15 cm; GE Healthcare) connected to an ÄKTA-FPLC system (GE Healthcare) and equilibrated with 10 mM Na-acetate pH 5.0. The column was washed with the same buffer until the A_{280} reached the baseline. The protein was then eluted with 10 mM Na-acetate pH 5.0 containing 1M NaCl. The fractions containing the recombinant protein, as judged by SDS-PAGE, were pooled and chromatographed on a Superdex 75 (10/30) gel filtration column (GE Healthcare) equilibrated with 10 mM Na-acetate, pH 5.0, 1M NaCl. Fractions were added with trichloroacetic acid and precipitated proteins were analysed by SDS-PAGE. To estimate the molecular weight of VC1, standard proteins (BSA dimer, 132 kDa; BSA monomer, 66 kDa; carbonic anhydrase, 29 kDa; cytochrome *c*, 12.3 kDa) were separated under the same conditions.
For a large-scale purification, the supernatant from 400 ml-culture was obtained as described above. After concentration to ~ 30 ml by ultrafiltration using a 30,000 cut-off membrane and dialysis against 10 mM Na-acetate, pH 5.0, for 16 hours at 4°C, the solution was applied to a cation-exchange Mono S HR5/5 column (GE Healthcare) equilibrated with 10 mM Na-acetate, pH 5.0 and connected to an ÄKTA-FPLC system (GE Healthcare). After column washing with the same buffer,

elution was performed with a 0 -1 M NaCl gradient in the same buffer. Fractions were analyzed by SDS-PAGE.

Electrophoresis and immunoblotting procedures

P. pastoris culture supernatants and chromatographic fractions were denatured by boiling for 3 min in SDS sample buffer [0.0625 M Tris-HCl, pH 6.8, 2.3% (w/v) SDS, 5% (v/v) β-mercaptoethanol, 10% (w/v) glycerol and 0.01% Bromophenol blue]. SDS-PAGE was performed on 13% or 16% polyacrylamide gels (14 ×16 cm or 8 × 10 cm). Proteins bands were stained by Coomassie Blue Biosafe (Bio-Rad, USA). After Western blotting, immunodecoration was carried out using a 1:1,000 dilution of an affinity-purified goat polyclonal antibody raised against an N-terminal peptide of hRAGE (N-16, Santa Cruz Biotechnology) or a 1:10,000 dilution of a monoclonal anti-poly(His) antibody (mAb) (Novagen) in combination with the appropriate peroxidase-conjugated anti-goat (Sigma) or anti-mouse secondary antibodies (Jackson Laboratories). Bound antibodies were revealed by the LiteAblot®PLUS Western blotting detection reagent (Euroclone, Italy). Quantification of the intensity of VC1 bands on immunoblot was performed using a ChemiDoc MP system (Bio-Rad). The level of VC1 accumulated in the medium was determined by comparison to a calibration curve obtained using known amounts of VC1 overproduced in *E. coli* (60-240 ng/lane). VC1 purification from *E. coli* was previously described [20].

Treatment with peptide N-glycosidase F

N-peptide glycosidase F (PNGase F) treatment was performed on either concentrated culture supernatant or purified proteins. In order to remove the *N*-linked oligosaccharide chains, 0.5-1 µg of protein (5 µl) were denatured at 95 °C for 3 min in the presence of 0.2% SDS. Then, samples were diluted to 50 µl and their composition was adjusted to 0.02 % SDS, 1% Triton X-100, 10 mM EDTA, 1 mM phenylmethansufonyl fluoride (PMSF), 50 mM Na-acetate, pH 5.5. Each sample was halved and one aliquot was used as a control while the other was added with 0.3 U of PNGase F (Roche). The samples were incubated at 37 °C under gentle agitation for 16 h before SDS-PAGE analysis.

VC1 digestion

Bands excised from gels were digested accordingly to an established procedure [21]. Briefly, after destaining with 50% acetonitrile, 25 mM ammonium bicarbonate, gel pieces were incubated at 56 °C for 60 min with 10 mM dithiothreitol in 50 mM ammonium bicarbonate for reduction of disulfide bonds and then treated with 55 mM iodoacetamide in 50 mM ammonium bicarbonate at room temperature for 45 min, in the dark, to alkylate cysteine residues. Gel pieces were then rinsed with 50 mM ammonium bicarbonate and incubated in 100% acetonitrile for dehydration. About 1 µg sequencing-grade trypsin (Roche Diagnostics S.p.A, Monza, Italy) dissolved in 50 mM ammonium bicarbonate was added to each gel fragment. After overnight digestion at 37 °C, the liquid phase was withdrawn and gel pieces were washed first with 30% acetonitrile, 3% trifluoroacetic acid for 10 min, and then with 100% acetonitrile for 10 min. The three solutions were pooled and dried on a vacuum concentrator. Tryptic peptide mixtures were then suspended in 15 µl 0.1% formic acid for mass spectrometry analysis.

Mass spectrometry analyses

Peptides (5 µl) were injected on a reverse phase C18 HALO PicoFrit column (75 µm × 10 cm, 2.7 µm particle size, 100 Å pore size, New Objective, USA) using an UltiMate 3000 RSLCnano liquid chromatographic system online with an LTQ-Orbitrap mass spectrometer (Thermo Scientific, USA). Peptide separation was performed by a 35% acetonitrile linear gradient in 0.1% formic acid over 40 min, at flow rate of 300 nl/min. Eluting peptides were electrosprayed using a nanoESI source (Thermo Scientific, USA). The instrument operated in data-dependent mode to acquire both full MS and MS/MS spectra. Full MS spectra were acquired in profile mode by the FT analyzer in a scan range 300–1500 *m/z*, using capillary temperature of 220 °C, AGC 5×10^5 and resolution 100,000 FWHM at *m/z* 400. Tandem mass spectra were acquired by the linear ion trap (LTQ) for the 3 most intense ions. MS/MS spectra acquisition was set as follows: centroid mode, resolution 15,000, precursorions isolation width of 2.5 *m/z*, AGC target 1×10^4 and normalized collision energy 30 eV. Dynamic exclusion was enabled to reduce redundant spectra acquisition: two repeat counts, 30 s repeat duration, 45 s exclusion duration. Monoisotopic precursor selection was enabled; singly and unassigned charged ions were not fragmented. Instrument control and spectra analysis were operated by the software Xcalibur 2.0.7 and Chromeleon Xpress 6.80.

Peptide identification

The software Proteome Discoverer (v 1.3, Thermo Scientific) was used to extract peaks from spectra and to match them to a dedicate protein database containing: (i) the sequences of VC1 and VC1-His preproteins obtained from the translation of the cDNA cloned in *P. pastoris* (**Supplementary file 1)** and (ii) *P. pastoris* proteome (8073 entries downloaded from UniProt database on 27.06.2014). Trypsin was selected as the cleaving protease, admitting a maximum of two missed cleavage sites. Peptide and fragment ions tolerance were set to 5 ppm and 0.3 Da, respectively. Cysteine carbamidomethylation was set as fixed modification and methionine oxidation was allowed as variable modifications. In PNGase F-treated samples, Asn-Asp conversion was also allowed as additional variable modification (monoisotopic delta mass equal to 0.984 Da). Low-confidence identifications were filtered out by selecting peptide confidence < 0.05 and at least 2 peptides/protein. Regarding the analysis of glycosylated peptides, the extracted ion chromatograms (XICs) of selected *m/z* values, corresponding to peptides of interest, were manually obtained from Quan Browser (Xcalibur software version 2.0.7) using tolerance 5 ppm and mass precision 5 decimals.

Filter binding assay

AGE-bovine serum albumin (AGE-BSA) was produced as described previously [22]. Serial dilutions of solutions of BSA, and AGE-BSA (BSA modified with ribose, also named BSA-R) were spotted on a nitrocellulose membrane. After saturation with 5% (w/v) dried milk powder in TBS-T (10 mM Tris-HCl, pH 7.4, 166 mM NaCl, 0.05 % Tween-20), the membrane was incubated over night at 4 °C with purified VC1 (5 µg/ml) in 20 mM HEPES, pH 7.1, 100 mM NaCl. The membrane was then washed twice with TBS-T for 10 min. To identify bound VC1, the membrane was incubated with a 1:1000 dilution of anti-RAGE antibody in TBS-T-BSA (5% BSA in TBS-T). After washing the membrane four times with TBS-T for 10 min and incubation with a 1: 80,000 dilution of secondary peroxidase-conjugated anti-goat IgG in TBS-T, immunocomplexes were detected as described above.

Thermal stability analysis

0.5 mg/ml purified proteins were added with the fluorescent dye SYPRO Orange (Sigma-Aldrich), according to the manufacturer's instructions in 10 mM Na-acetate, pH 5.0 containing no salt, 150 or 300 mM NaCl. 25 µl-aliquots were loaded in a multi-well plate (MJ white, Bio-Rad) and subjected to a 15 °-99 °C temperature ramp at a rate of 2 °C/min using the real time PCR apparatus

MiniOpticon MJ Mini (Bio-Rad). The intensity of fluorescence emission in the range 540-700 nm was recorded after each 0.2 °C increment. Each protein under each ionic strength condition was analyzed in triplicate. Melting temperature of the proteins (T_m) was identified as the inflection point of the plot of the fluorescence emission as a function of temperature and was determined as the maximum of the first derivative of such a function.

Results

Expression of His-tagged VC1 fragment of hRAGE reveals proteolytic activities in the medium and inside P. pastoris cells

To produce and secrete the VC1 and V domains in *P. pastoris*, the human N-terminal signal peptide was replaced by the signal sequence of *P. pastoris PHO1* encoding the extracellular acid phosphatase Pho1p (see scheme in **Fig. 1)**. Expression was driven by the strong methanol-inducible promoter *AOX1*. VC1 and V domains were tagged with a thrombin cleavable hexa-His sequence at the C-terminus to facilitate purification and allow the removal of the tag to avoid interference in binding studies (see **Fig. 1**). Two bands of about 34 and 36 kDa were detected by immunoblot with anti-RAGE antibody in the medium of *P. pastoris* cells expressing VC1-His, but these polypeptides did not react with anti-poly(His) mAb, indicating that the tag was removed (**Fig. 2A)**. To ascertain whether the tag was cleaved inside the cell or after secretion, we analyzed cell extracts. Both anti-RAGE antibody and anti-poly(His) mAb recognized the two bands, indicating that the tag was removed outside the cell (**Fig. 2A**). Interestingly, in the cell extracts an additional band of about 30 kDa was detected exclusively by anti-poly(His) antibody suggesting that this protein is devoid of the N-terminal epitope recognized by the anti-RAGE antibody (**Fig. 2A**). This N-terminal truncated form likely represents an intermediate of VC1 degradation that probably occurs at the level of the ER.

MS analysis of the secreted VC1 protein did not detect the C-terminal His-tag (data not shown) (**Supplementary file 1**). These results are consistent with the hypothesis that the His-tag is proteolytically cleaved by an extracellular protease. To verify if the tagged VC1 forms were substrates of Sub2p, the major secreted subtilisin-like protease of *P. pastoris* [23], we analyzed the production of the tagged VC1 in a *sub2*-deficient strain (**Fig. 2B**). VC1-His forms were detected in cell extracts but only the forms devoid of the tag were present in the medium suggesting that a secreted protease other than Sub2p is responsible of the proteolytic cleavage of the tag.

The histidine tagged V domain of hRAGE does not properly fold when expressed in P. pastoris

Fusion of the V domain to the His-tag (*see* **Fig. 1**), resulted in the accumulation in *P. pastoris* cells of polypeptides of about 20, 21 and 16 kDa recognized by the anti-poly(His) mAb (**Fig. 3**, *left panel*). Treatment with PNGase F indicated that such recombinant products represent different glycosylated forms of the V protein (data not shown). These proteins reached a maximal level after 48 h induction (**Fig. 3**, *left panel*). None of these polypeptides reacted with the anti-RAGE antibody (**Fig. 3**, *right panel*), indicating that the N-terminal epitope was removed, as described above for the 30 kDa form of VC1. Moreover, no V-His forms were detected in the culture supernatant (data not shown). Despite several attempts to overcome the block of secretion by employing a mixed induction regimen or lowering the growth temperature, no secretion of V-His was observed.
These results strongly indicate that the isolated V-His domain is incorrectly folded in *P. pastoris* and likely undergoes degradation in the ER and/or in the vacuole.

Expression and secretion of the VC1 domain of hRAGE in P. pastoris

VC1 and V domains were subsequently expressed in *P. pastoris* without a tag (see scheme in **Fig. 1**). No specific bands of the V domain were detected in the culture supernatant even after 30-fold medium concentration, by SDS-PAGE and Coomassie staining or by immunoblotting (data not shown). No further attempts to secrete this protein were performed and the focus was placed on untagged VC1. The growth kinetics of cells expressing VC1 is shown in **Fig 4A**. After the shift to methanol containing medium (time zero), cells grew exponentially for about 24 h and then the growth rate progressively decreased. Two bands of ~34 and ~36 kDa were detected by SDS-PAGE analysis in the culture medium at 24, 48 and 72 h after induction but not in the medium of non-induced cells (**Fig. 4B**) and cross-reacted with anti-RAGE antibody (**Fig. 4C**). The two recombinant VC1 forms were named p34 and p36. Mass spectrometry (MS) analysis confirmed the identity of the two bands as proteins forms with the expected human VC1 sequence, as reported in **Supplementary File 1,** with coverage of 77.36% for p36 and 81.60% for p34. Moreover, the identification of the RAQNITAR peptide as the N-terminal end indicated that the cleavage of the Pho1p signal peptide occurs at the expected site.
VC1 levels in the medium were quantified, as described in the Materials and Methods**.** The highest level, about 6 mg of total VC1 per liter culture medium, was reached after 72 h of induction, a time concomitant with the growth arrest (**Fig. 4A**). Protein production was highly reproducible among different recombinant clones. No substantial improvement in protein production was obtained by

lowering the growth temperature to 23 °C or using unbuffered media (MMY instead of BMMY). Therefore, buffered rich medium (BMMY) and 28 °C were chosen as standard growth conditions.

VC1 is N-glycosylated in P. pastoris and the site occupancy mimics the human one

p34 and p36 polypeptides displayed a lower electrophoretic mobility compared to VC1expressed in *E. coli* ($p32^{Ec}$), a sign of the presence of post-translational modifications. Since two potential *N*-glycosylation sites are located in the V domain, VC1 was subjected to treatment with PNGase F, an enzyme that removes the *N*-linked oligosaccharide chains and concomitantly converts the asparagine residue (Asn) into an aspartic acid (Asp). Upon deglycosylation, p36 and p34 were no longer detected and a polypeptide of ~32 kDa appeared. This indicates that VC1 is *N*-glycosylated in *P. pastoris* and that the observed mobility differences are due to heterogeneity of the glycan moiety (**Fig. 5**). These results are compatible with the presence of 1 and 2 "core" type N-linked oligosaccharide chains in p34 and p36, respectively.

hRAGE contains two potential *N*-glycosylation sites, or "sequons" [consensus sequence: NX(S/T) where X≠P], namely Asn25 (NIT) and Asn81 (NGS) where the numbering refers to the precursor protein. Asn25 is reported to be fully occupied in native hRAGE whereas Asn81 is only partially *N*-glycosylated and is susceptible to deamidation that converts it into an aspartic acid [24]. The two sites correspond to Asn26 and Asn82 in the recombinant precursor forms *s* but for the sake of clarity here they will be referred to the numbers adopted for the human pre-protein.

To address the question whether such sites are *N*-glycosylated in *P. pastoris*, we mapped the Asp residues generated by the enzymatic removal of *N*-linked chains by MS analysis. Tryptic digests of gel-purified VC1 were analyzed by nano LC-MS/MS. Peptides were identified by database matching and the intensity of the peaks corresponding to the tryptic peptides containing the deamidated Asn25 and Asn81 were quantified relative to their unmodified form. The extent of p34 and p36 glycosylation was evaluated on the tryptic peptides $RAQN^{25}ITAR$ and $VLPN^{81}GSLFLPAVGIQDEGIFR$. Their natural, non-glycosylated forms were expected to appear in MS spectra at theoretical *m*/*z* values of 465.26740 and 1121.61512, respectively, for the double charged ions. In the presence of Asn to Asp conversion, $RAQD^{25}ITAR$ and $VLPD^{81}GSLFLPAVGIQDEGIFR$ were expected to display the increased *m*/*z* values of 465.75940 and 1122.10712. The high resolution of LTQ-Orbitrap XL and fragmentation spectra unambiguously discriminated the natural peptides from their deamidated variants.

The peptide $RAQN^{25}ITAR$ was not identified in the untreated VC1 sample (p34 and p36 bands), suggesting that this peptide is fully glycosylated in *P. pastoris*. Consistently with this hypothesis, its

variant RAQD[25]ITAR was identified in the deglycosylated p32. This observation was confirmed by the manual extraction of the chromatogram for the peaks corresponding to the two peptide variants; peaks at *m*/*z* 465.26740 were barely visible in p34 and p36, while an intense peak at *m*/*z* 465.75940 was indeed visible in the deglycosylated sample (about 3 orders of magnitude). This indicates that chemical deamidation is negligible and thus Asn25 is fully occupied in VC1. **Supplementary Fig. 1A** reports the extracted ion chromatograms. In contrast with RAQN[25]ITAR, the peptide VLPN[81]GSLFLPAVGIQDEGIFR was detected in the untreated VC1 sample, indicating that Asn81 is present both in glycosylated and unglycosylated state (**Supplementary Fig. 1B**).Consistently, its deamidated variant was identified upon enzymatic deglycosylation (p32 band). Moreover, the peptide VLPD[81]GSLFLPAVGIQDEGIFR was also detected in the untreated VC1 sample indicating that chemical deamidation occurs at Asn81 as already reported for hRAGE expressed in human cell lines [24]. Following PNGase F treatment, the ratio of peak intensities of deamidated *versus* unmodified peptide increased, confirming that a subpopulation of Asn81 is glycosylated, as reported also by Srikrishna G. *et al*. [25].

Overall, our analyses suggest that Asn25 is fully occupied whereas only a subpopulation of Asn81 is glycosylated as occurs in human cells.

Finally, the difference between p34 and p36 electrophoretic mobilities suggests that the *N*-linked chains are of the “core” type, consistently with the notion that hypermannosylation of the *N*-linked oligosaccharide chains is rare in *P. pastoris* in contrast to *Saccharomyces cerevisiae*.

VC1 is a monomer and is functional

VC1 was purified from the culture supernatant by cation-exchange chromatography as the capture step, exploiting the high charge of the protein (pI = 9.9) and a final gel filtration polishing step. As shown in the SDS-PAGE of **Fig. 6A**, the one-step elution from the cation-exchange column yielded highly enriched p34 and p36 forms contaminated by a small amount of a lower mobility protein and abundant heterogeneous low M_r components of the growth medium. Gel filtration studies yielded pure VC1 that eluted in a single sharp peak corresponding to monomeric VC1 forms. The low M_r contaminants eluted as a broad peak at higher elution volume (**Fig. 6B**). It was well expected that glycosylated VC1 is monomeric under the chosen acidic and high salt buffer conditions, as previously observed for un-glycosylated VC1 expressed in *E. coli* [14].

The functionality of purified VC1 was tested by nitrocellulose filter-binding assay (**Fig. 6D**). Different amounts of BSA and AGE-BSA were absorbed onto nitrocellulose in dot-blot format. Following incubation of the membrane with purified VC1, bound protein was detected by anti-

RAGE antibody as described under Materials and Methods. VC1 binding to AGE-BSA but not to BSA indicated that the protein is functional (**Fig. 6D**).

Analysis of the thermal stability of VC1 glycosylated forms

During the optimization and scale-up of the VC1 purification protocol, we developed a procedure based on an ionic-strength linear gradient for the fractionation of the concentrated culture supernatant by high resolution cation-exchange chromatography. Such an improved procedure yielded the two individual glycosylated species of VC1 in homogeneous form. Indeed, p34 and p36 separated in two partially overlapped peaks, allowing their isolation in homogeneous form at the expenses of a loss in recovery (**Fig. 7**). Since the p*I* of the two glycoforms is expected to be the same, the separation likely reflects the different steric hindrance caused by the presence of one or two glycans which affects the affinity of the glycoprotein for the resin. Indeed, p36 with two glycans eluted before p34, which contains just one glycan. As shown in **Fig. 7**, VC1 glycoforms were well separated from low M_r components of the growth medium that eluted during the first part of the salt gradient. The immunoblot shown in **Fig. 7** also indicates that no relevant protein degradation occurred during purification. Overall, this procedure of purification provided pure VC1 with a minimum loss of the target protein. **Table 2** summarizes the progress of the purification attained from 1 l-culture.

Recently, ThermoFluor emerged as a powerful technique to evaluate the conformational stability of recombinant proteins [26]. Therefore, thermal denaturation analysis of p36, p34 and of the unmodified form produced in bacteria ($p32^{Ec}$) was performed at different ionic strengths. Melting temperatures (T_m) obtained for the various proteins are reported in **Table 3**. The two glycoforms of VC1produced in *P. pastoris* are equally stable in 150 or 300 mM NaCl whereas, in the absence of NaCl, p36 appears to be more stable than p34. In addition, the two glycoforms are more stable than $p32^{Ec}$. In particular, in the absence of NaCl, $p32^{Ec}$ is highly unstable (T_m = 22.6 °C). Thus, VC1 forms produced in *P. pastoris* displayed a remarkable improved stability in comparison with the unmodified $p32^{Ec}$. These observations are consistent with the fact that VC1 glycoforms obtained from *P. pastoris* are highly soluble and display no tendency to aggregation that is, in contrast, a typical feature of $p32^{Ec}$ (data not shown).

Discussion

We here demonstrated that the VC1 tandem domain of hRAGE can be produced in secretory form in *P. pastoris*. Recombinant VC1 forms can be purified to homogeneity from the concentrated culture supernatant by cation-exchange chromatography with no relevant protein loss during the purification step. Moreover, no other highly basic proteins appear to be secreted by *P. pastoris*. The level of VC1 forms produced by flask cultivation reached about 6 mg/l after 72 h of induction but by using fermentation-based technologies this level is expected to increase as higher cell density can be reached.

The VC1 protein forms are of good quality since they show no tendency to aggregate/precipitate. Compared to VC1 produced intracellularly in *E. coli* ($p32^{Ec}$), the secreted proteins are remarkably more thermally stable as demonstrated by thermal shift assays. Most importantly, the VC1 forms produced in *P. pastoris* proved to be functional, as verified by binding to AGE-BSA.

In contrast with these findings, the V module of hRAGE was retained intracellularly in *P. pastoris*. The ER harbors an ER protein quality control (ERQC) that ensures only properly folded and assembled proteins traffic to the Golgi apparatus. Proteins that do not pass ERQC are diverted by retro-translocation back to the cytosol for degradation by the 26S proteasome in a process termed ER-associated degradation (ERAD). Moreover, a previous work in *P. pastoris* suggested that misfolded proteins can also be transported from the Golgi to the vacuole for degradation [27].

Previous studies indicated that the isolated V, and to a lower extent also VC1 domain, produced in *E. coli* possess a highly dynamic conformation and that V requires C1 association to fold properly [17, 28]. Thus, our finding that V does not acquire the proper folding in *P. pastoris* is consistent with, and also extends, previous biophysical *in vitro* studies [17]. Molecular models based on X-ray crystallography and NMR, support the notion that V and C1 domains physically interact through surfaces exposing hydrophobic amino acids [14]. Our results obtained using an *in vivo* approach, support such observations and strongly indicate that V and C1 domains form a single folding unit. Consequently, the V unit should be described as a protein module rather than a domain. Our study also provides evidence of a cellular protease that removes the N-terminal portion of the V module. This protease likely is a component of the ERQC of *P. pastoris*.

This work also showed the full occupancy of Asn25 and the partial occupancy of Asn81 in the VC1 forms produced in *P. pastoris*. This glycosylation pattern mimics that observed in human cells [24] indicating that it is driven by intrinsic features of VC1, such as the target sequences, its location in the three-dimensional structure of the protein and the microenvironment. Moreover, we have shown here that Asn81 undergoes partial deamidation. Interestingly, as previously reported for Asn81 of hRAGE from mammalian sources and also for different types of antibodies, specific asparagine residues can undergo non-enzymatic deamidation [16, 24]. The susceptibility to deamidation

markedly increases if a glycine residue is immediately after the asparagine [29]. In this case, deamidation occurs via cyclization of asparagine by the β-aspartyl shift mechanism in which the main chain peptide nitrogen of the glycine residue acts as a nucleophile on the Asn side chain amide group forming a succinimide intermediate that breaks down in α- or β-isomeric aspartate products [29]. Interestingly, Asn81 is located in the sequon N-Gly-S providing an explanation of the marked propensity to deamidation of this site in hRAGE.

In fact, a polymorphism, consisting in a single nucleotide change, occurs at the Asn81 sequon in humans and results in a Gly to Ser replacement that leads G/S or S/S genotypes, often associated with diseases. G/S (heterozygous) individuals are more prone to undergo diabetic retinopathy with respect to G/G (homozygous) patients in the Chinese population [30, 31]. An association of the S allele with microvascular complications in diabetic patients has been reported and theS/S genotype has been correlated to low levels of circulating sRAGE [30]. Notably, the G82S replacement increases the occupancy of Asn81 and this could affect AGE-RAGE binding [24].

Finally, glycosylation was proposed to affect RAGE ligand binding specificity. For example, the lack of glycans in bacterial recombinant proteins is accompanied by increased affinity for some ligands, while others have been shown to bind more tightly to glycosylated RAGE [25, 32]. Thus, the availability of glycosylated VC1 forms from a eukaryotic microorganism can prove useful in future studies. It is important to note that *P. pastoris* was also engineered to produce humanized *N*-glycan chains, an important accomplishment in the perspective to produce biotherapeutic products in this yeast [33]. However, irrespective of the role of specific glycan requirements for ligand binding, the VC1 forms produced in *P.pastoris* proved to be more stable and soluble than the non-glycosylated VC1 produced in bacteria, suggesting that the oligosaccharide chains promote the proper folding and are important for protein stabilization and solubility. These features are expected to be beneficial for the *in vitro* studies of the properties of RAGE ligand binding domain and for the set-up of high throughput screening methods for the identification of RAGE antagonists.

Acknowledgements

The authors wish to thank the Consorzio Italiano Biotecnologie (CIB) for the financial contribution to the research training of G.D. and Louise Gourlay for English revision. L.S. and G.D. are recipients of PhD fellowships from the University of Milan. G.F. is supported by a grant and a Heisenberg fellowship of the Deutsche Forschungsgemeinschaft (FR1488/5-2 and FR1488/3-2).

References

[1] C. Ott, K. Jacobs, E. Haucke, A. Navarrete Santos, T. Grune, A. Simm, Role of advanced glycation end products in cellular signaling. Redox Biol 2 (2014) 411-429.

[2] K. Kierdorf, G. Fritz, RAGE regulation and signaling in inflammation and beyond. J Leukoc Biol 94 (2013) 55-68.

[3] R. Deane, I. Singh, A.P. Sagare, R.D. Bell, N.T. Ross, B. LaRue, R. Love, S. Perry, N. Paquette, R.J. Deane, M. Thiyagarajan, T. Zarcone, G. Fritz, A.E. Friedman, B.L. Miller, B.V. Zlokovic, A multimodal RAGE-specific inhibitor reduces amyloid beta-mediated brain disorder in a mouse model of Alzheimer disease. J Clin Invest 122 (2012) 1377-1392.

[4] M.N. Sabbagh, A. Agro, J. Bell, P.S. Aisen, E. Schweizer, D. Galasko, PF-04494700, an oral inhibitor of receptor for advanced glycation end products (RAGE), in Alzheimer disease. Alzheimer disease and associated disorders 25 (2011) 206-212.

[5] Y.T. Han, G.I. Choi, D. Son, N.J. Kim, H. Yun, S. Lee, D.J. Chang, H.S. Hong, H. Kim, H.J. Ha, Y.H. Kim, H.J. Park, J. Lee, Y.G. Suh, Ligand-based design, synthesis, and biological evaluation of 2-aminopyrimidines, a novel series of receptor for advanced glycation end products (RAGE) inhibitors. J Med Chem 55 (2012) 9120-9135.

[6] L. Sessa, E. Gatti, F. Zeni, A. Antonelli, A. Catucci, M. Koch, G. Pompilio, G. Fritz, A. Raucci, M.E. Bianchi, The receptor for advanced glycation end-products (RAGE) is only present in mammals, and belongs to a family of cell adhesion molecules (CAMs). PLoS One 9 (2014) e86903.

[7] G. Fritz, RAGE: a single receptor fits multiple ligands. Trends in Biochemical Sciences 36 (2011) 625-632.

[8] R.J. Deane, Is RAGE still a therapeutic target for Alzheimer's disease? Future Med Chem 4 (2012) 915-925.

[9] E. Leclerc, G. Fritz, S.W. Vetter, C.W. Heizmann, Binding of S100 proteins to RAGE: An update. Biochimica et Biophysica Acta (BBA) - Molecular Cell Research 1793 (2009) 993-1007.

[10] W. Ma, V. Rai, B.I. Hudson, F. Song, A.M. Schmidt, G.R. Barile, RAGE binds C1q and enhances C1q-mediated phagocytosis. Cellular immunology 274 (2012) 72-82.

[11] S. Mizumoto, J. Takahashi, K. Sugahara, Receptor for advanced glycation end products (RAGE) functions as receptor for specific sulfated glycosaminoglycans, and anti-RAGE antibody or sulfated glycosaminoglycans delivered in vivo inhibit pulmonary metastasis of tumor cells. J Biol Chem 287 (2012) 18985-18994.

[12] D. Xu, J. Young, D. Song, J.D. Esko, Heparan sulfate is essential for high mobility group protein 1 (HMGB1) signaling by the receptor for advanced glycation end products (RAGE). J Biol Chem 286 (2011) 41736-41744.

[13] C.M. Sirois, T. Jin, A.L. Miller, D. Bertheloot, H. Nakamura, G.L. Horvath, A. Mian, J. Jiang, J. Schrum, L. Bossaller, K. Pelka, N. Garbi, Y. Brewah, J. Tian, C. Chang, P.S. Chowdhury, G.P. Sims, R. Kolbeck, A.J. Coyle, A.A. Humbles, T.S. Xiao, E. Latz, RAGE is a nucleic acid receptor that promotes inflammatory responses to DNA. J Exp Med 210 (2013) 2447-2463.

[14] M. Koch, S. Chitayat, B.M. Dattilo, A. Schiefner, J. Diez, W.J. Chazin, G. Fritz, Structural Basis for Ligand Recognition and Activation of RAGE. Structure 18 (2010) 1342-1352.

[15] G. Aldini, T. Grune, G. Bartosz, Special issue on "AGEs and ALEs: chemistry, physiopathology and molecular strategies for their inhibition". Free Radic Res 47 Suppl 1 (2013) 1-2.

[16] T. Ostendorp, M. Weibel, E. Leclerc, P. Kleinert, P.M.H. Kroneck, C.W. Heizmann, G. Fritz, Expression and purification of the soluble isoform of human receptor for advanced glycation end products (sRAGE) from Pichia pastoris. Biochemical and Biophysical Research Communications 347 (2006) 4-11.

[17] B.M. Dattilo, G. Fritz, E. Leclerc, C.W. Kooi, C.W. Heizmann, W.J. Chazin, The extracellular region of the receptor for advanced glycation end products is composed of two independent structural units. Biochemistry 46 (2007) 6957-6970.
[18] C. Carotti, E. Ragni, O. Palomares, T. Fontaine, G. Tedeschi, R. Rodriguez, J.P. Latge, M. Vai, L. Popolo, Characterization of recombinant forms of the yeast Gas1 protein and identification of residues essential for glucanosyltransferase activity and folding. European journal of biochemistry / FEBS 271 (2004) 3635-3645.
[19] E. Rolli, E. Ragni, J.M. Rodriguez-Pena, J. Arroyo, L. Popolo, GAS3, a developmentally regulated gene, encodes a highly mannosylated and inactive protein of the Gas family of Saccharomyces cerevisiae. Yeast 27 (2010) 597-610.
[20] M. Koch, S. Chitayat, B.M. Dattilo, A. Schiefner, J. Diez, W.J. Chazin, G. Fritz, Structural basis for ligand recognition and activation of RAGE. Structure 18 (2010) 1342-1352.
[21] M. Wilm, A. Shevchenko, T. Houthaeve, S. Breit, L. Schweigerer, T. Fotsis, M. Mann, Femtomole sequencing of proteins from polyacrylamide gels by nano-electrospray mass spectrometry. Nature 379 (1996) 466-469.
[22] J.V. Valencia, S.C. Weldon, D. Quinn, G.H. Kiers, J. DeGroot, J.M. TeKoppele, T.E. Hughes, Advanced glycation end product ligands for the receptor for advanced glycation end products: biochemical characterization and formation kinetics. Analytical biochemistry 324 (2004) 68-78.
[23] K. Salamin, D. Sriranganadane, B. Lechenne, O. Jousson, M. Monod, Secretion of an endogenous subtilisin by Pichia pastoris strains GS115 and KM71. Applied and environmental microbiology 76 (2010) 4269-4276.
[24] S.J. Park, T. Kleffmann, P.A. Hessian, The G82S polymorphism promotes glycosylation of the receptor for advanced glycation end products (RAGE) at asparagine 81: comparison of wild-type rage with the G82S polymorphic variant. J Biol Chem 286 (2011) 21384-21392.
[25] G. Srikrishna, H.J. Huttunen, L. Johansson, B. Weigle, Y. Yamaguchi, H. Rauvala, H.H. Freeze, N -Glycans on the receptor for advanced glycation end products influence amphoterin binding and neurite outgrowth. J Neurochem 80 (2002) 998-1008.
[26] K. Huynh, C.L. Partch, Analysis of protein stability and ligand interactions by thermal shift assay. Current protocols in protein science / editorial board, John E Coligan [et al, #422] 79 (2015) 28 29 21-28 29 14.
[27] M. Pfeffer, M. Maurer, J. Stadlmann, J. Grass, M. Delic, F. Altmann, D. Mattanovich, Intracellular interactome of secreted antibody Fab fragment in Pichia pastoris reveals its routes of secretion and degradation. Applied microbiology and biotechnology 93 (2012) 2503-2512.
[28] J. Xie, S. Reverdatto, A. Frolov, R. Hoffmann, D.S. Burz, A. Shekhtman, Structural basis for pattern recognition by the receptor for advanced glycation end products (RAGE). J Biol Chem 283 (2008) 27255-27269.
[29] H.T. Wright, Nonenzymatic deamidation of asparaginyl and glutaminyl residues in proteins. Critical reviews in biochemistry and molecular biology 26 (1991) 1-52.
[30] L. Yang, Q. Wu, Y. Li, X. Fan, Y. Hao, H. Sun, Y. Cui, L. Han, Association of the receptor for advanced glycation end products gene polymorphisms and circulating RAGE levels with diabetic retinopathy in the Chinese population. Journal of diabetes research 2013 (2013) 264579.
[31] H.M. Zhang, L.L. Chen, L. Wang, Y.F. Liao, Z.H. Wu, F. Ye, S. Xu, L.L. Yi, Association of 1704G/T and G82S polymorphisms in the receptor for advanced glycation end products gene with diabetic retinopathy in Chinese population. J Endocrinol Invest 32 (2009) 258-262.
[32] G. Srikrishna, J. Nayak, B. Weigle, A. Temme, D. Foell, L. Hazelwood, A. Olsson, N. Volkmann, D. Hanein, H.H. Freeze, Carboxylated N-glycans on RAGE promote S100A12 binding and signaling. J Cell Biochem 110 (2010) 645-659.
[33] S.R. Hamilton, R.C. Davidson, N. Sethuraman, J.H. Nett, Y. Jiang, S. Rios, P. Bobrowicz, T.A. Stadheim, H. Li, B.K. Choi, D. Hopkins, H. Wischnewski, J. Roser, T. Mitchell, R.R.

630 Strawbridge, J. Hoopes, S. Wildt, T.U. Gerngross, Humanization of yeast to produce complex
631 terminally sialylated glycoproteins. Science 313 (2006) 1441-1443.
632
633
634 **Legends**
635
636 **Figure 1. Schematic representation of the constructs used in this work.** The upper scheme shows the
637 domain structure and the *N*-glycosylation sites of the full-length hRAGE. After the N-terminal signal
638 peptide, three immunoglobulin-like domains (V, C1 and C2) are present, followed by the trans-membrane
639 domain and a short cytoplasmic tail. The numbers indicate the amino acid sequence positions at the domain
640 borders. The truncated proteins are shown in the lower part. The sequence of the thrombin recognition site
641 (T), present in the constructs carrying a C-terminal 6 x His Tag (H), is LVPRGS (with cleavage between R
642 and G).
643
644 **Figure2. Immunoblot analysis of culture supernatant and extracts of cell expressing VC1-His.** Culture
645 medium and cell extracts of GS115 (A) and GS115-*sub2* (B) expressing VC1-His were analyzed by
646 immunoblotting using anti-poly(His) mAb or anti-RAGE antibody as indicated. VC1-His expressed in *E.*
647 *coli* was used as positive control. Culture supernatants (110 µl) of the indicated time points were denatured
648 and loaded on SDS-slab gels. Cell extracts were obtained as described in Material and methods. Cell extracts
649 immunostained with anti-Poly(His) mAb contain an extra band of ~ 33 kDa ascribable to a VC1 proteolytic
650 product lacking the N-terminal RAGE epitope.
651
652 **Figure 3. Immunoblot analysis of cell extracts of cells expressing V-His.** Total extracts of GS115 cells
653 expressing V-His harvested after the indicated induction times were analyzed by immunoblotting using anti-
654 poly(His) mAb or anti-RAGE antibody as indicated. V-His expressed in *E. coli* was used as positive control.
655 The cell extracts were obtained as described in Material and methods. The lack of reactivity with the anti-
656 RAGE antibody is ascribable to a proteolytic cleavage occurred intracellularly at the N-terminus as shown in
657 Fig. 2 for VC1.
658
659 **Figure 4. Kinetics of accumulation of recombinant VC1 in *P. pastoris* culture medium**. **A**. Growth
660 kinetics at 28 °C of a representative culture of *P. pastoris* cells transformed with pHIL-S1-VC1^{233} plasmid
661 (solid line). Time zero indicates the moment of the shift from BMGY to the inducing medium, BMMY. The
662 arrows indicate the time points of the withdrawal of culture aliquots for analysis. The recombinant protein
663 level (dashed line) in the culture supernatant was estimated by densitometry as reported in Material and
664 methods using immunoblot with anti-RAGE antibody and recombinant VC1 isolated from *E. coli* as a
665 calibrator. **B**. SDS-PAGE of culture supernatant (160 µl) collected at the indicated induction times. Protein
666 bands were stained by Coomassie blue. **C**. Immunoblot analysis of the same samples of panel B. Culture

supernatant volumes loaded on the gel were 112 µl for 0 and 24 h, and100 µl for 48 and 72 h. Recombinant VC1 produced in *E. coli* was used as a control.

Figure 5. Analysis of the recombinant VC1 glycosylation.

Immunoblot analysis using anti-RAGE antibody of culture supernatant harvested after 72 h of induction and incubated in the absence (-) or presence (+) of PNGase F. Purified recombinant VC1 produced in *E. coli* was used as a control.

Figure 6. Purification of VC1 from the culture supernatant and filter binding assay.

A. Result of separation by cation-exchange chromatography and one-step elution of the culture supernatant at 72 h of induction. The Coomassie stained gel is shown. The arrows indicate p36 and p34; * indicates low M_r components of the medium. **B**. Profile of gel filtration chromatography on a Superdex 75 column of the partially purified VC1 forms. The peak eluted at 10 ml corresponds to VC1 forms, while those eluted between 13 and 18 ml correspond to the low Mr components of the medium (predominantly peptones *). Standard proteins were chromatographed under the same conditions to obtain the calibration curve shown in the inset (inset). **C.** SDS-PAGE and Coomassie staining of the fractions corresponding to the VC1 peak. Proteins were precipitated by 10% TCA. **D**. Filter binding assay. 2 µl of a concentrated solution of BSA or BSA-R (2mg/ml) (1) and 1:2 serial dilutions (from 2 to 6) were spotted on nitrocellulose filter that was incubated with purified VC1 as described in Materials and methods. VC1 specifically recognizes BSA-R indicating that the protein expressed and purified from *P. pastoris* is functional.

Figure 7. Large-scale purification and separation of p34 and p36 glycoforms of VC1 by cation-exchange chromatography. A. Cation-exchange chromatography on a Mono S column of 400-ml culture supernatant collected after 72 h of induction and 13 × concentrated by ultrafiltration (membrane cut-off 30,000). The fractions eluted using a linear ionic-strength gradient were analyzed by SDS-PAGE and proteins were stained by Coomassie blue **B**. Immunoblot with anti-RAGE antibody indicates that fractions 5 to 6 contain only p36, fractions 7 and 8 contain both forms and 9-10 contain only p34. The 66-kDa polypeptide visible in panel A (lane 1) is a contaminating endogenous protein. VC1 purified from *E. coli* ($p32^{Ec}$) was used as a control (C).

Figure 1

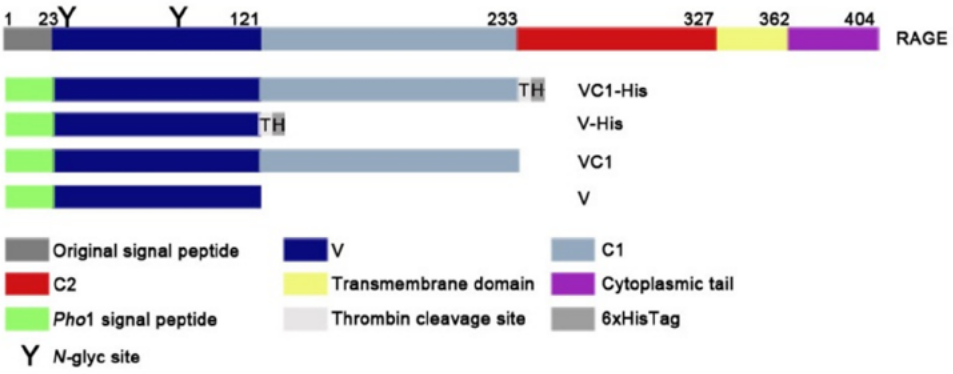

Figure 2

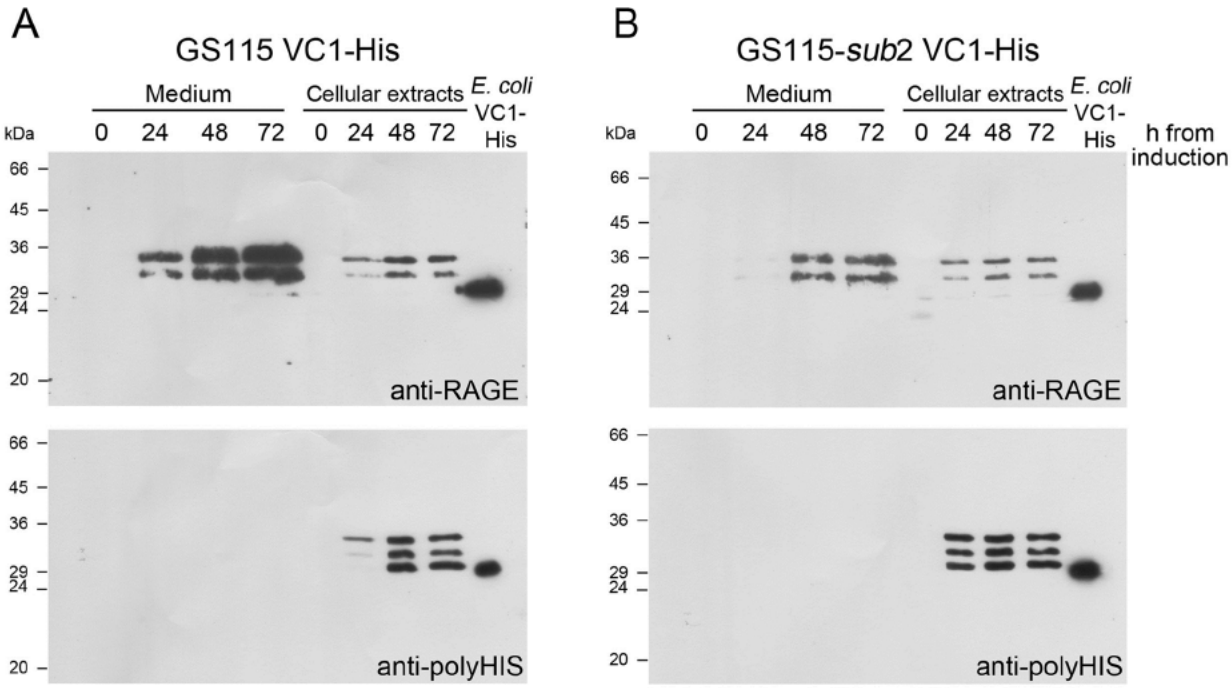

Figure 3

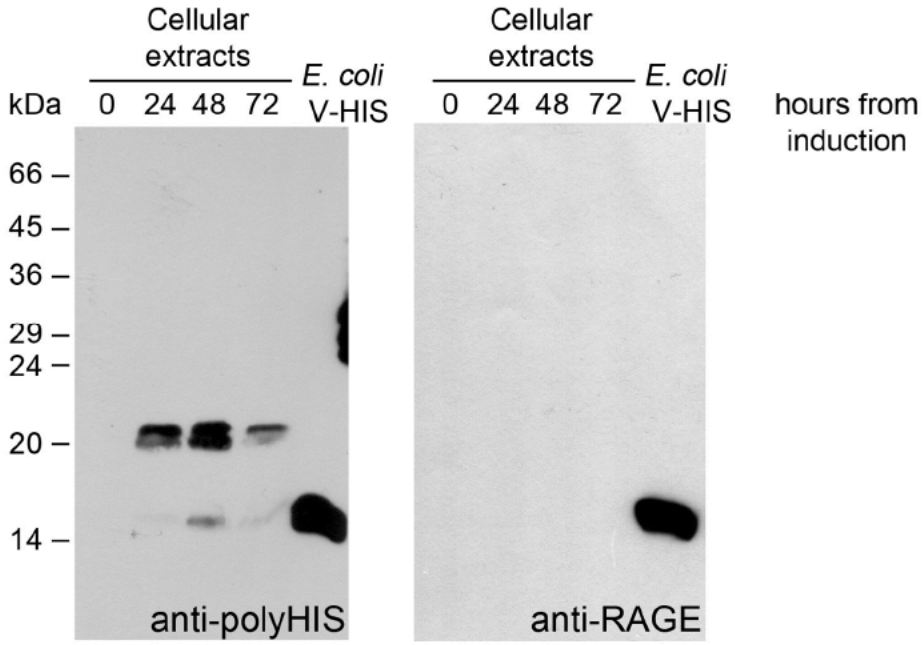

Figure 4

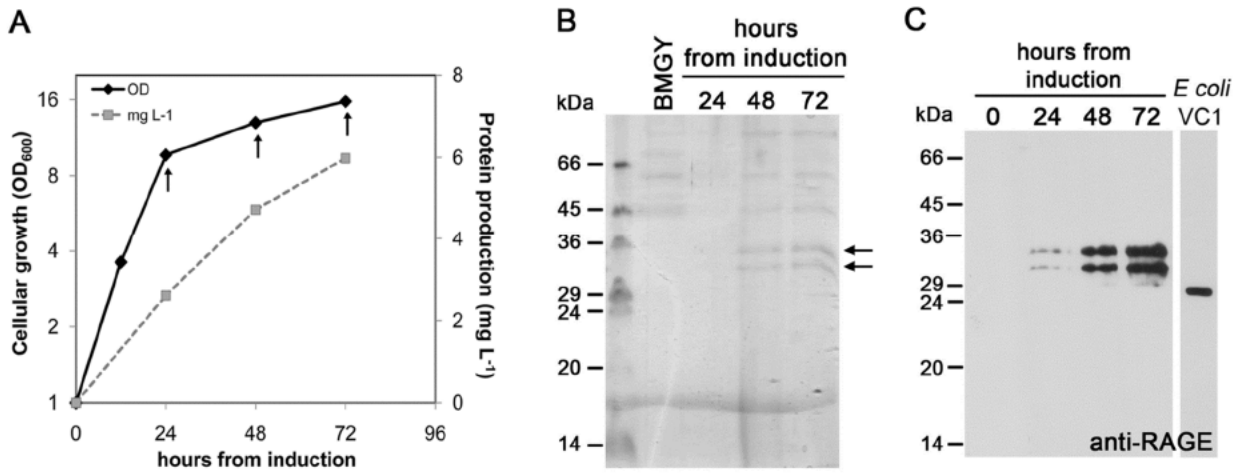

Figure 5

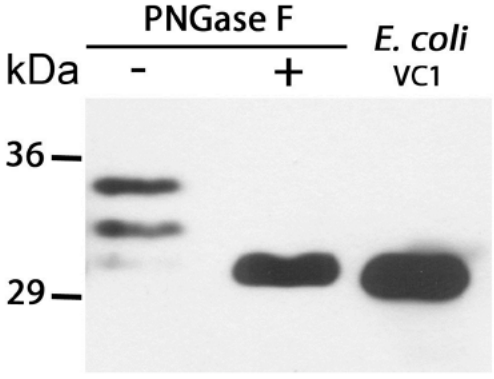

Figure 6

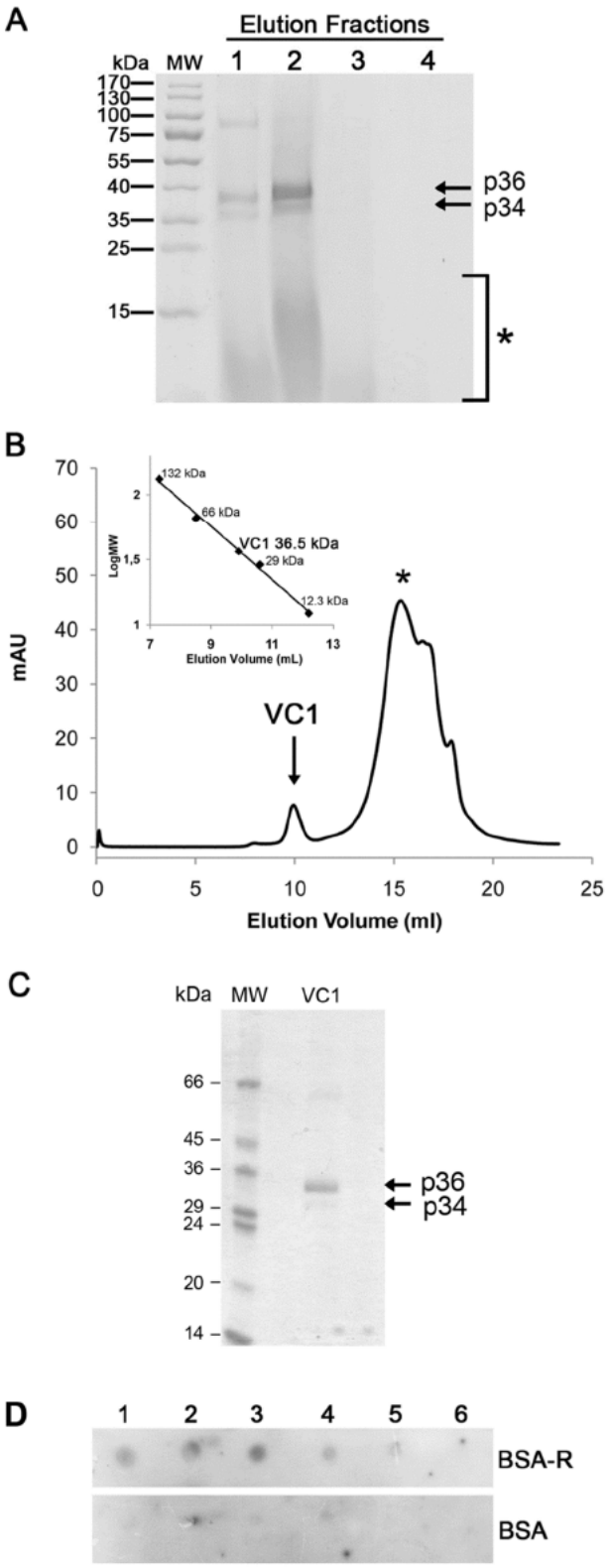
A
Elution Fractions
kDa MW 1 2 3 4
170
130
100
75
55
40
35
25
15
p36
p34
*
B
mAU
Elution Volume (ml)
VC1
*
132 kDa
66 kDa
VC1 36.5 kDa
29 kDa
12.3 kDa
LogMW
Elution Volume (mL)
C
kDa MW VC1
66
45
36
29
24
20
14
p36
p34
D
1 2 3 4 5 6
BSA-R
BSA

Figure 7

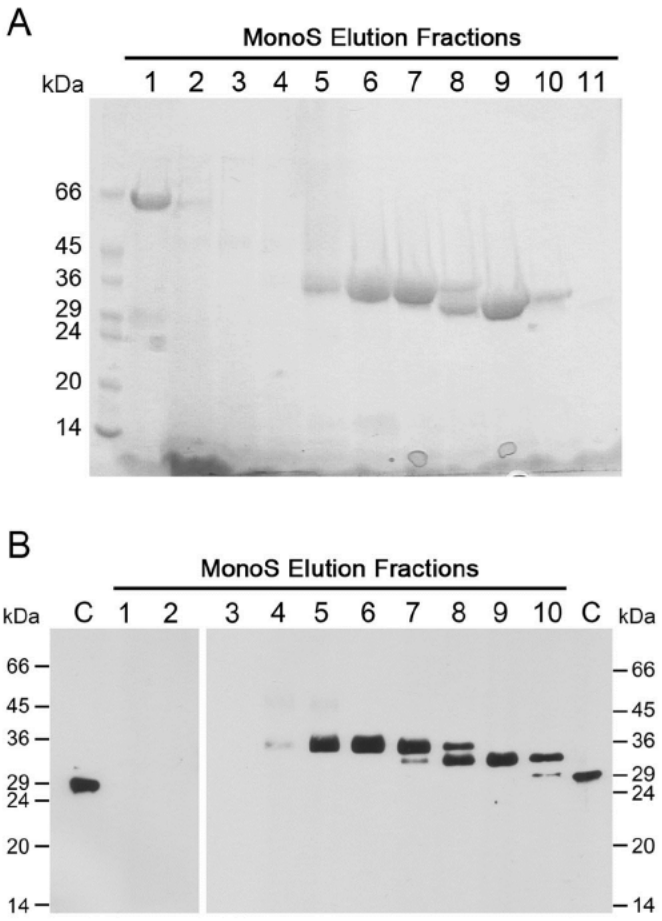
A
MonoS Elution Fractions
kDa
1 2 3 4 5 6 7 8 9 10 11
66
45
36
29
24
20
14
B
MonoS Elution Fractions
kDa
C 1 2 3 4 5 6 7 8 9 10 C
kDa
66
45
36
29
24
20
14

Table 1

Oligonucleotides used in this work[a]

Primer	**Sequence 5'-3'**
VC-For	AGCATATTCGACTGACTCGAG**CTCAAAACATCACAGCCCG**
VC233-Rev	ATCGTCGGGCTCACTCGAG*CTA***CACAGGCTCCCAGACACG**
VC233His-Rev	ATCGTCGGGCTCACTCGAG*CTA*GTGATGGTGATGGTGATGGCTGCTGCCGCTGCCGCG CGGCACCAGATGGCTGCTGCCGCTGCCGCGCGGCACCAGATG**CACAGGCTCCCAGA CACG**
V121-Rev	ATCGTCGGGCTCACTCGAG*CTA***AGGAATCTGGTAGACACGGA**
V121His-Rev	ATCGTCGGGCTCACTCGAG*CTA*GTGATGGTGATGGTGATGGCTGCTGCCGCTGCCGCG CGGCACCAGATGGCTGCTGCCGCTGCCGCGCGGCACCAGATG**AGGAATCTGGTAGA CACGGA**
5'-AOX1	GACTGGTTCCAATTGACAAGC
3'-AOX1	GCAAATGGCATTCTGACATCC

[a] *XhoI* site is underlined and CDS of VC1 or V is in bold. Stop codon is in italic

Table 2

Large-scale purification of VC1 from *P. pastoris* medium[a]

Purification step	VC1 protein (mg)	Yield (%)
Culture supernatant[b]	6.00[c]	100%
Concentration[b]	5.88	98%
Cation exchange chromatography[b]	5.21	86%
p36 form	1.45	24%
p34 form	1.52	25%
Cross-contaminated p34 p36 forms[d]	2.24	37%

[a]The starting material was the supernatant from a yeast 1-liter culture harvested after 72 h induction at the OD_{600} of 13.
[b]Data refer to total VC1, i.e. the sum of the two p36 p34 glycoforms.
[c]Determined by densitometry, since the high concentration of peptides in the medium precluded the determination of the actual total protein concentration.
[d]Purified VC1 not separated into its individual glycoforms.

Table 3

Melting temperatures of glycosylated and unglycosylated recombinant VC1 forms

	NaCl (mM)		
Protein	0	150	300
p36	35.0 ± 0.3	43.8 ± 0.1	48.2 ± 0.01
p34	31.6 ± 0.8	43.8 ± 0.2	47.2 ± 0.1
$p32^{Ec}$	22.6 ± 0.1	37.0 ± 0.2	42.0 ± 0.02

The values indicate the T_m (°C) ± S.D. (standard deviation) from triplicate samples. VC1 produced in *P. pastoris* (p36 and p34) and in *E. coli* ($p32^{Ec}$) were analyzed in 10 mM Na-acetate, pH 5.0, in the presence of the indicated saline concentration.

Supplementary file 1

Predicted VC1 sequence:

MFSPILSLEIILALATLQSVF▼ARAQNITARIGEPLVLKCKGAPKKPPQRLEWKLNTGRTEAW
KVLSPQGGGPWDSVARVLPNGSLFLPAVGIQDEGIFRCQAMNRNGKETKSNYRVRVYQIP
GKPEIVDSASELTAGVPNKVGTCVSEGSYPAGTLSWHLDGKPLVPNEKGVSVKEQTRRHP
ETGLFTLQSELMVTPARGGDPRPTFSCSFSPGLPRHRALRTAPIQPRVWEPV

Predicted VC1-His sequence:

MFSPILSLEIILALATLQSVF▼ARAQNITARIGEPLVLKCKGAPKKPPQRLEWKLNTGRTEAW
KVLSPQGGGPWDSVARVLPNGSLFLPAVGIQDEGIFRCQAMNRNGKETKSNYRVRVYQIP
GKPEIVDSASELTAGVPNKVGTCVSEGSYPAGTLSWHLDGKPLVPNEKGVSVKEQTRRHP
ETGLFTLQSELMVTPARGGDPRPTFSCSFSPGLPRHRALRTAPIQPRVWEPVHLVPRGSGSS
HHHHHH

▼ Pho1p signal peptide cleavage site

Supplementary figure 1

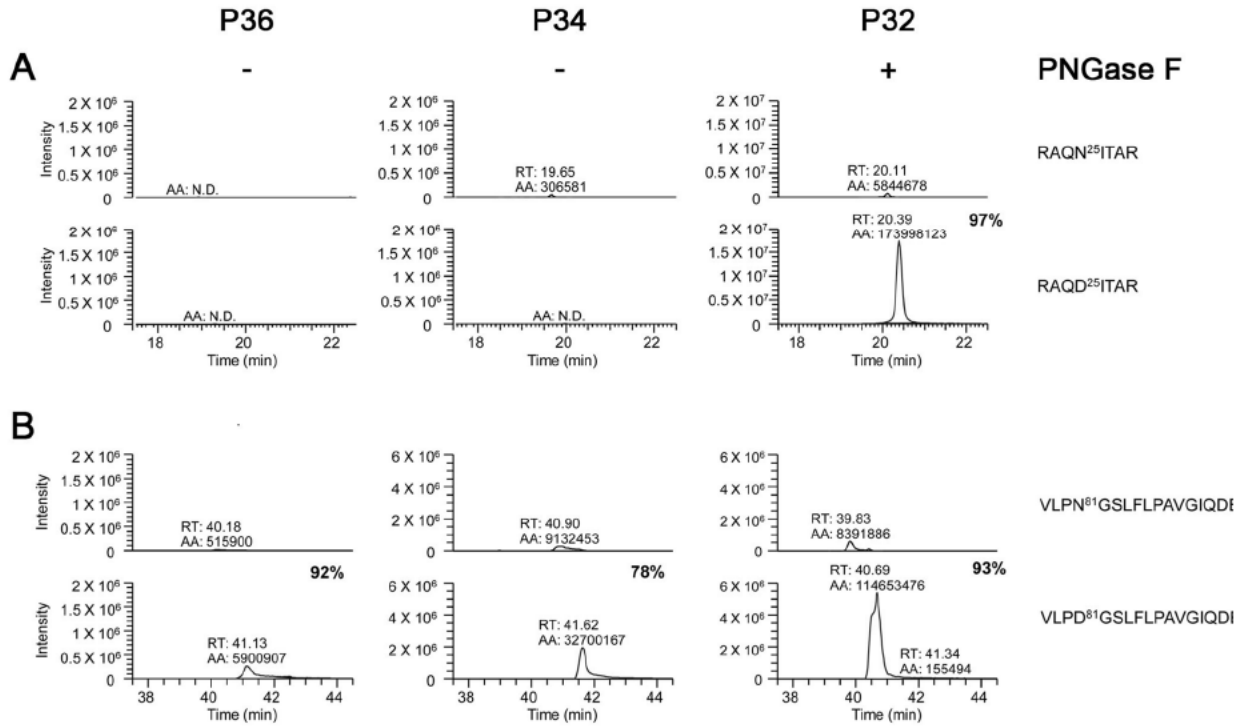

Figure S1. Peptide deamidation upon enzymatic deglycosylation by PNGase F confirms Asn25 and Ans81 as glycosylation sites. Gel bands containing the VC1 variants p36, p34 and p32 were excised, digested and analysed by LC-MS/MS. A) Extracted chromatograms for the *m/z* values 465.26740 and 465.75940, corresponding to the $[M+H]^+$ ions of the peptides RAQNITAR in its natural and deamidated forms. B) Extracted chromatograms for the *m/z* values 1121.61512 and 1122.10712, corresponding to the $[M+H]^+$ ions of the peptides VLPNGSLFLPAVGIQDEGIFR in its natural and deamidated forms. For each sample, the percentage of deamidated peptide vs. its natural form was quantified by estimating the area under the curve (AA) of the chromatographic peaks. The chromatograms for *m/z* values corresponding to the glycosylated peptides could not be extracted, because their mass is unknown.

Project hRAGE

Patent request under deposition

Sistema di espressione migliorato del recettore per gli Advanced Glycation End Products (AGE) e gli Advanced Lipid Glycation End Products (ALE) e sue applicazioni

Richiedente: EUROCLONE S.p.A.; Università degli Studi di Milano

Italian patent

Project Phr proteins

Published article

Catalytic properties of Phr family members of cell wall glucan remodeling enzymes: implications for the adaptation of *Candida albicans* to ambient pH

Kristína Kováčová, Genny Degani, Eva Stratilová, Vladimír Farkaš and Laura Popolo

FEMS Yeast Res, 2015. 15(2)

http://femsyr.oxfordjournals.org/content/15/2/fou011.long

FEMS Yeast Research, 15, 2015, fou011

doi: 10.1093/femsyr/fou011
Research Article

RESEARCH ARTICLE

Catalytic properties of Phr family members of cell wall glucan remodeling enzymes: implications for the adaptation of *Candida albicans* to ambient pH

Kristína Kováčová[1,#], Genny Degani[2,#], Eva Stratilová[1], Vladimír Farkaš[1] and Laura Popolo[2,*]

[1]Institute of Chemistry, Center for Glycomics, Department of Glycobiology, Slovak Academy of Sciences, 84538 Bratislava, Slovakia and [2]Università degli Studi di Milano, Dipartimento di Bioscienze, Via Celoria 26, 20133 Milano, Italy

*Corresponding author. Università degli Studi di Milano, Dipartimento di Bioscienze, Via Celoria 26, 20133 Milano, Italy. Tel: +39-02-50314919; Fax: +39-02-50314895; E-mail: Laura.Popolo@unimi.it
#These authors equally contributed to the work

One sentence summary: Phr1p and Phr2p are isoenzymes of the C. *albicans* Phr family of beta-1,3-glucanosyltransferases with different pH optimum. Pga4p is an inactive member. Only Phr1p-Phr2p are involved in the pH adaptation of cell wall glucan remodeling and are regulated at different levels.
Editor: Richard Calderone

ABSTRACT

Fungal wall formation is a dynamic process involving several categories of enzymes. The GH72 family of β(1,3)-glucanosyltransferases is essential for the determination of cell shape, for cell integrity and for virulence in pathogenic fungi. *Candida albicans* has five GH72 genes: *PHR1* and *PHR2* are pH dependent, the first being expressed at pH $\geq$ 6 and repressed at lower pH and the second regulated in the opposite manner, *PGA4* is transcribed independently of pH whereas *PHR3* and *PGA5* have low expression levels. To characterize the catalytic properties of Phr1p–2p and probe the activity of Pga4p, we heterologously expressed these proteins and used a fluorescent assay based on the transfer of oligosaccharyl units from a donor to a sulforhodamine-labeled acceptor. Phr1p–2p used exclusively β-1,3-glucan or cell wall glucan as donor and laminarin-derived oligosaccharides as acceptor. The acceptor efficiency increased with the length of the oligosaccharide. The temperature optimum was 30°C. The pH optimum was 5.8 for Phr1p and 3 for Phr2p. Overall, adaptation to pH of *C. albicans* appears to involve a fine interplay among the pH-dependent activity of Phr1p and Phr2p, the pH-regulated expression of their genes and protein stability. Unexpectedly, Pga4p was inactive suggesting that it turned into a structural mannoprotein.

Key words: fungal pathogens; *Pichia pastoris* expression; morphogenesis; glucanosyltransferases; family GH72; pH adaptation

Received: 11 October 2014; **Accepted:** 14 December 2014

PART III

Project Phr proteins

Manuscript in preparation

Genomic and functional analyses unveil the adaptive response to defective β-1,3-glucan remodeling during hyphal formation in *Candida albicans*

Genny Degani, Enrico Ragni, Pedro Botias, Davide Ravasio, Julia Calderon, Elena Pianezzola, Jose Manuel Rodriguez-Peña, Maria Antonietta Vanoni, Javier Arroyo, William A. Fonzi and Laura Popolo

MANUSCRIPT IN PREPARATION

Genomic and functional analyses unveil the adaptive response to defective β(1,3)-glucan remodeling during hyphal formation in *Candida albicans*

Genny Degani[1], Enrico Ragni[1¶], Pedro Botias[2] , Davide Ravasio[1§], Julia Calderon[1†] , Elena Pianezzola[1], Jose Manuel Rodriguez-Peña[3], Maria Antonietta Vanoni[1], Javier Arroyo[3], William A. Fonzi [4] and Laura Popolo[1*]

[1] Dipartimento di Bioscienze, Università degli Studi di Milano, Milano (Italy), [2] Unidad de Genómica, Campus Moncloa UCM/PCM, Madrid (Spain), [3] Departamento de Microbiologia II, Facultad de Farmacia, Universidad Complutense de Madrid, Madrid (Spain) and [4] Department of Microbiology and Immunology, Georgetown University, Washington, D.C. (U.S.A.)

Genny Degani: genny.degani@unimi.it
Enrico Ragni: enrico.ragni@policlinico.mi.it
Pedro Botias: pbotias@bio.ucm.es
Davide Ravasio: davide.ravasio@carlsberglab.dk
Julia Calderon: jcblanco@usal.es
Elena Pianezzola: elena.pianezzola@studenti.unimi.it
Jose Manuel Rodriguez-Peña: josemanu@farm.ucm.es
Maria Antonietta Vanoni: maria.vanoni@unimi.it
William Fonzi: fonziw@georgetown.edu
Javier Arroyo: jarroyo@farm.ucm.es

* Corresponding author: Laura Popolo
Università degli Studi di Milano
Dipartimento di Bioscienze
Via Celoria 26
20133 Milano (Italy)
E-mail: Laura.Popolo@unimi.it
Tel N. (0039)-(0)2-50314919
FAX: (0039)-(0)2-50314895

Footnotes present address: ¶ Enrico Ragni, Department of Regenerative Medicine, Fondazione IRCCS Cà Granda ,Ospedale Maggiore Policlinico, Milano, (Italy); § Davide Ravasio,Carlsberg Laboratory, Yeast Biology, Copenhagen (Denmark) and † Julia Calderon, Instituto de Biología Funcional y Genómica, (IBFG),Salamanca (Spain)

Summary

During the yeast to hypha (Y-H) transition, *Candida albicans* acquires attributes essential for adhesion and penetration into the tissues, two important processes for the establishment of invasive infections in immunocompromised patients. Cell wall β(1,3)-glucan remodeling catalyzed by Phr1p is required for hypha elongation, adhesion and virulence. We exploited the pH-conditional nature of a *PHR1* null mutant to analyze the genome-wide transcriptional response to the absence of β(1,3)-glucan remodeling during the Y-H transition. The changes include increase of transcript levels for 10 mannoproteins, a cell wall cross-linking enzyme (*CRH11*), two chitin synthases (*CHS2* and *CHS8*), a chaperone of ER-export of Chs3p (*CHS7*) and reduction of adhesins, indicating adjustments in hyphal wall structure. Additionally, up-regulation of DNA replication and cell-cycle control genes was associated with premature entry into S-phase. Chitin level increased in the mutant and the deletion of *CHS3* was synthetically lethal with deletion of *PHR1* whereas *CHS2* and *CHS8* were dispensable in M199 pH 7.5. Interestingly, the synthetic lethal phenotype of the *chs3 phr1* mutant on solid medium is affected by the filamentation conditions and a physiological adaptation of the double mutant occurred at pH 7.5 on the less demanding Spider medium.

Introduction

C. albicans is a medically important fungal pathogen that exhibits various morphological forms: yeast, hypha, pseudohypha and chlamydospore. The transition from yeast cell to hyphal form (Y-H) is one of the best-studied developmental pathways in fungi and also represents a major virulence attribute of this microorganism.

As a commensal, *C. albicans* grows on human mucosae and is a component of the oral fungal microbiome (Ghannoum *et al.*, 2010). Its extraordinary ability to inhabit diverse niches of the human body is reflected in its adaptability to a wide range of external pH values and to a range of oxygen pressures, ion concentrations, and carbon sources (Ene *et al.*, 2012, Davis, 2009). As an external envelope endowed with mechanical strength, the cell wall plays a primary role in determining cell shape and in maintaining cell integrity during morphological changes or osmotic shock. Additionally, the surface of the cell wall is positioned at the interface between the pathogen and the host cells, with which dynamic interactions crucial for adhesion or the immune response are established. Whereas the yeast form is suitable for dissemination through the blood stream, the thin filamentous shape of hyphae is specialized for adhesion to epithelial and endothelial barriers, and penetration and invasion of the tissues

below. Genomic scale expression studies of the Y-H morphological transition have identified a number of signature genes induced by this transition (Lane *et al.*, 2001, Nantel *et al.*, 2002, Wilson *et al.*, 2009).

Hypha formation requires a coupling between the polarity machinery of the cell and the components involved in the biogenesis of the wall in order to drive growth at the tip of the germ tube. The wall results from the synthesis and assembly of two glucose polymers, β(1,3)-glucan, the most abundant, and β(1,6)-glucan. Other major constituents are mannoproteins, many of which are modified by attachment to glycosylphosphatidylinositol (GPI) and are localized both in the plasma membrane and cell wall (reviewed in (Klis *et al.*, 2009). Chitin, a β(1,4)-linked polymer of *N*-acetylglucosamine (GlcNac), is a minor constituent but it is crucial for the formation of the septum and enhancement of the structural integrity of the wall. Fks1p, the catalytic subunit of β(1,3)-glucan synthase, polymerizes linear β(1,3)-glucan from UDP-glucose in a vectorial manner at the cell membrane, whereas mannoproteins and probably β(1,6)-glucan are processed through the secretory pathway. In the extracellular compartment, a branched β(1,3)glucan-chitin structure that forms the "core" of the wall is created (Latge, 2007). This core structure is decorated by links between chitin and β(1,6)-glucan or trimmed GPI-mannoproteins, the latter forming the "brush-like" surface layer of the wall which functions as a permeability barrier and adhesive surface.

Among the extracellular transglycosidases crucial for cell wall assembly, β(1,3)-glucan transglycosidases of family GH72 play a primary role. These enzymes internally cleave a donor glucan chain and attach a portion of the donor to an acceptor glucan in β(1,3)-linkage, thus lengthening one chain at the expense of the other (Mouyna *et al.*, 2000). Multigene families of redundant enzymes are present in all fungal species so far analyzed (Sillo *et al.*, 2013). These genes are essential for viability in many fungal species, such as in the pathogens *Aspergillus fumigatus (AfGEL4)* or *C. glabrata* (*CgGAS*), and in nonpathogenic species such as the fission yeast *Schizosaccharomyces pombe* (*Spgas1*$^{+}$) (Gastebois *et al.*, Weig *et al.*, 2001, de Medina-Redondo *et al.*, 2010).

C. albicans has a family of five GH72-encoding genes: *PHR1, PHR2, PHR3*, *PGA4* and *PGA5*. Phr1p and Phr2p are highly similar to *Sc*Gas1 and play the same glucanosyltransferase activity *in vitro*. Pga4p is most similar to *ScGas5* but recent evidence from our laboratory indicate that it is an inactive enzyme (Kovacova *et al.*, 2015). Phr3p and Pga5p are homologous to the sporulation-specific gene products *Sc*Gas4p and *Sc*Gas2p, respectively. The significance and the role of *PHR3* and *PGA5* are still unknown but the transcript level of both is very low or undetectable (Eckert *et al.*, 2007). Taking into account that *PGA4* deletion

does not bring any phenotype and Pga4p likely turned into a structural mannoprotein, Phr1p and Phr2p appear to be the major players among the *C. albicans PHR* family.

C. albicans PHR1 and *PHR2* are pH-regulated genes. *PHR1* is expressed when the external pH is higher than 6 both in yeast and hyphal growth. It is repressed in acidic conditions where it is replaced by *PHR2* which exhibits the opposite expression pattern (Muhlschlegel & Fonzi, 1997, Saporito-Irwin *et al.*, 1995b). Moreover, both *PHR1* and *PHR2* are repressed in stationary phase. *PHR1* is also induced at a transcriptional level in response to heat stress, to treatments with the antifungal drug caspofungin (CS) and during infection (Meyer *et al.*, 2007, Heilmann *et al.*, 2013, Liu *et al.*, 2005, Brown *et al.*, 2007).

Consistent with it enzymatic activity, the Phr1 protein localizes to sites of new wall formation such the periphery of the bud, the septum, the tip of the germ tube, the hyphal apex and it also concentrates at the hyphal septa (Ragni *et al.*, 2011a). Loss of Phr1p affects cell wall composition, with a reduction of β(1,3)-glucan content and an increase of chitin, and results in aberrant cell morphology (Fonzi, 1999, Popolo & Vai, 1998). At the restrictive pH of 7.5 at 25°C, *phr1* cells are round and multi-budded. At 37°C they are unable to form filaments and arrest with short and enlarged germ tubes. A delocalized actin cytoskeleton is apparent under both conditions (Saporito-Irwin *et al.*, 1995b). The phenotype is more severe if the pH is raised from 7.5 to 8, where greatly enlarged vacuoles and a swollen aspect are present (Saporito-Irwin *et al.*, 1995b). Moreover, *PHR1* null mutants are avirulent in an animal model of systemic infection (De Bernardis *et al.*, 1998) and in a model of experimental keratomycosis (Yuan *et al.*). The *PHR1* null mutant is unable to invade *in vitro* reconstituted epithelia and has a reduction in adhesion, two fundamental processes for the establishment of fungal infections (Calderon *et al.*, 2010).

By exploiting the pH-conditional nature of the *PHR1* null mutant, which manifests its defects in wall assembly only upon a shift to neutral-alkaline pH, we investigated the impact of defective glucan remodeling on the transcription profile during the induction of hyphal growth. Our results show that the activity of Phr1p is important to fully execute the genetic program of hyphal development. Among the different classes of functions that are involved in the adaptive response are genes involved in the reorganization of the cell wall but also in cell cycle control and morphogenesis and in DNA replication/repair and chromatin formation. Classes of genes involved in the cell cycle control and in morphogenesis indicate that the inability to accomplish the yeast-hypha transition in the *phr1 mutant*. Genetic analysis indicated that during hyphal growth *CHS3* is essential for viability but on mild solid filamentation media it its presence is dispensable and physiological adaptation occurs.

Results

Global transcriptional response to the lack of β(1,3)-glucan remodeling upon induction of hyphal growth in Candida albicans

To induce hyphal growth, a pH/temperature regimen was used. Blastospores of the wild type strain (CAI10) and *phr1*Δ mutant (CAS10) were transferred to buffered M199, pH 7.5 at 37° C. Despite the phenotype of the mutant was stronger at pH 8, the percentage of dead cells at 5 h after the pH shift, measured by methylene blue staining, was about 15% compared to only 5% at pH 7.5 and therefore the latter was the preferred condition for microarray analysis.
The Phr1p accumulation, the kinetics of germ tube induction and the changes in morphology were monitored after the shift to pH 7.5. Phr1p was recognized by anti-Gas1p antibodies and detected in CAI10 extracts as a glycosylated 88 kDa-polypeptide (Fig. 1A). Phr1p was absent at time zero but upon induction of hyphal growth, was already detected at 1, and was further accumulated at 3 and 5h and was still present 24 h after the shift (Fig. 1B) whereas was absent in CAS10 at all time points as expected (data not shown). At time zero, the morphology of CAI10 and CAS10 (*PHR1*$^{-/-}$) was indistinguishable (**Fig. 1C**) and the two strains had the same chitin content [8.8 ± 0.66 and 8.5 ± 0.88 μg *N*-acetylglucosamine (GlcNac)/mg d.w. (dry weight) of cells, for CAI10 and CAS10, respectively] supporting the notion that *PHR1* null deletion does not confer a detectable phenotype in non-inducing conditions. At 45 min, CAI10 cells started to form germ tubes and the percentage of cells with germ tubes steadily increased with time reaching 50% at 1 h after the shift and 80-90% by 3 h. CAI10 produced elongated hyphae whereas CAS10 cells produced germ tubes that remained short, enlarged and sometime curved culminating in a yeast-like aspect with large septa at 5 h from the shift (**Fig.1C**). These morphological defects were consistent with those described in previous reports (Saporito-Irwin *et al.*, 1995b). After 5 hours, chitin level increased to 11.7 ± 1.07 GlcNac/mg d.w. of cells in CAI10, in agreement with stimulation of chitin accumulation in hyphae, and to 16.4 ± 1.5 GlcNac/mg d.w. of cells in CAS10 and this ~ 40% extra chitin is ascribable to the presence of cell wall stress.

We characterized the pattern of gene expression at 1, 3 and 5 h after the pH shift. Principal component analysis showed a clear separation between the wild type and mutant strain at each time point and underlined the high reproducibility of the biological replicas (**Fig. 2A)**. Moreover, hierarchical clustering indicated that for both strains changes at 3 h and 5 h clustered tighter than at 1 h (**Fig. 2B**). Next, we determined how the stimulus to hyphal

development affects gene expression in the wild type and in the mutant. **Dataset S1** shows genes that were up- (≥2 fold) or down–regulated (≥ 2-fold) with a False Discovery Rate (FDR) ≤ 0.05. This threshold was chosen to ensure that the analysis was stringent but would not miss significant genes. Among the 6346 probes, 537 genes were up-regulated at 1 h, 806 at 3 h and 1020 at 5 h in the wild type whereas 701, 780 and 964 genes were up-regulated in the *phr1* mutant. Moreover, 795, 956 and 1014 were down regulated at least 2-fold in the wild type and 953, 993 and 1128 in the mutant. Comparison of the data from wild type and mutant strains identified a common group of responsive genes (54%, 58% and 62% up-regulated and 59%, 72% and 72% down regulated at 1 h, 3 h and 5 h, respectively), suggesting that *phr1*Δ mutant cells trigger the hyphal expression program in spite of their failure to form hyphae.

The modulation of many genes reflects the extensive differentiation associated with induction of the hyphal program and, at least in the early stages, the shift from quiescence to growth and the change in culture conditions (media composition, pH and temperature). Up-regulated genes belonged to the functional categories expected for hyphal development: hyphal growth, pathogenesis, endoplasmic reticulum (ER)-Golgi transport, cell wall organization, Golgi-ER retrograde transport, ER-associated-protein degradation (ERAD) and biofilm formation. The typical signature up-regulated genes of hyphal growth, such as *ECE1, SOD5, ALS10, ALS3 RBT1, HWP1, HYR1 PRA1, ALS3 SAP4, SAP5, SAP6* and the typical down-regulated genes *RHD1*, *TYE7, NRG1* were present (Nantel *et al.*, 2002). *PHR1* itself is typically induced during hyphal growth and was up-regulated 1.4 fold at 1 h and 1.6 fold at 5 h in the wild type, in agreement with previous reports (Nantel *et al.*, 2002, Wilson *et al.*, 2009). As expected, *PHR1* transcript was undetectable. *PHR2* was repressed both in the wild type and in the mutant (**Dataset1**).

Many genes up or down-regulated in each strain appeared to be differentially modulated. To extract these differences, we used a relation factor (RF) representing the ratio between the expression ratio of each gene in the mutant and in the control. Thus, the value of the RF reflects the effect of the mutation on the abundance of a transcript. We set a threshold of RF ≥ 2 to select for transcript levels more abundant in the *phr1*Δ mutant than in the control (Class 1), and RF ≤ 0.5 for transcript levels reduced in the *phr1*Δ mutant compared to the control (Class 2). The complete list of Class 1 and Class 2 and their RF is reported in **Tables S1** and **S2** respectively.

Table 2 summarizes the functional categories of mutation-sensitive genes. Notably, in Class 1 many the categories “Metabolism and energy” and “Cell wall/surface”, indicates the cell’s

need of reorganizing the cell surface and redirecting metabolism. The categories "DNA replication", "Chromatin and chromosomes" and "Cell cycle control/morphogenesis" were also affected, suggesting perturbation of the coordination between cell cycle events and their coupling to morphogenesis. Class 2 contained many genes required for RNA processing and ribosome biogenesis primarily at 1 h. This response is likely to be a general reaction to defects in morphogenesis rather than to a specific cell wall stress, since it was also present in farnesol-treated cells (see Discussion).

As shown in **Fig. 2C**, the increase of transcripts of selected genes was confirmed by quantitative real time reverse transcriptase PCR (qRT-PCR). The RF values obtained from qRT-PCR were similar to the values obtained from the microarray analysis indicating the validity of the analysis.

Expression profile uncovers extensive rearrangement of the cell surface in cells lacking β(1,3)-glucan remodeling during induction of hyphal growth

As shown in **Table 3**, the Cell wall/surface category was among the largest and comprised: seven cell wall structural mannoproteins (*PGA23*, *RBR1*, *PGA13*, *PGA54, RHD3/PGA29,* orf19.750 and orf19.675) found only in *C. albicans* or *Candida* spp., and three cell wall proteins (*PGA6*, *RBT4, ECM331*) that have homologs in *S. cerevisiae*. Other induced genes were *CRH11*, encoding a GPI-anchored transglycosidase of GH16 family which catalyzes the cross-links between chitin and glucans, two chitin synthase isoforms (*CHS2, CHS8)* and *TOS1, EXG2, XOG1, SCW11,* orf19.7214 and *PLB3* that have enzymatic activity on glucans or lipids (*PLB3*). Interestingly, in the protein folding/modification category the presence of the ER chaperones involved in Chs3p-dependent chitin synthesis (*CHS7*) and in β(1,6)-glucan synthesis (*ROT1*) suggest their involvement in the chitin and glucan synthesis.

Two aspects of the expression data suggested that the absence of *PHR1* forces multiple adjustments in the cell's chitin synthesis process together with mannoproteins. Among the four genes encoding isoenzymes of chitin synthase (*CHS1, CHS2, CHS3* and *CHS8*) *CHS8* and *CHS2* transcript level was higher in the *phr1*Δ mutant (**Table 3**). *CHS2* and *CHS8* are also up-regulated by echinocandins (EC) (Walker *et al.*, 2008). Moreover, the transcript of *CHS7*, encoding a chaperone for Chs3p export from ER, was also more abundant in the mutant. Secondly, chitin cross-linking (*CRH11*) was also increased in the mutant suggesting that cross-linking between chitin and mannoproteins may occur.

CHS1 is an essential gene that is required for the formation of the septum and for cell wall integrity (Munro *et al.*, 2001). *CHS2* is preferentially expressed in the hyphal form and is

involved in septum formation (Walker *et al.*, 2013, Gow *et al.*, 1994, Lenardon *et al.*, 2007), whereas *CHS8* is responsible for the synthesis of a particular type of long fibrillar chitin at the septum (Walker *et al.*, 2013, Lenardon *et al.*, 2007). *CHS3* contributes the majority of cell wall chitin, which is deposited in the septal ring and lateral walls. Moreover, *CHS3* is responsible for the Calcofluor white/$CaCl_2$ induced stimulation of chitin accumulation that protects *C. albicans* cells from the killing effect of echinocandin (Walker *et al.*, 2008). *CHS2, CHS8* and *CHS3* are also responsible for the remedial septum, that is synthesized when Chs1p is inhibited, an indication of cross compensation (Walker *et al.*, 2013).

To evaluate the role of chitin synthases in the adaptive response of the *phr1* mutant, a *PHR1* homozygous null mutation was introduced into strains lacking *CHS2*, *CHS8*, *CHS2* and *CHS8* or *CHS3* (**Table 4**) and analyzed during the induction of hyphal growth. Two independent clones were used in all the analyses. The wild type strain and all *chs* mutants formed hyphae, although hyphae of the *chs* mutants were altered in morphology (**Fig. 3A** and **3 B**). Hyphae of the *chs3*Δ mutant were highly flocculant and at the microscopic level they were sometimes curved at the apex. As shown by CW-staining, the *chs3*Δ cells were CW-negative except at the thin line of the septa, an observation in agreement with Chs3p being responsible for the deposition of the majority of chitin located in the lateral wall and chitin ring but not in the chitin disk of the primary septum (Sanz *et al.*, 2005, Lenardon *et al.*, 2010b). Hyphae of *chs2*Δ and *chs8*Δ were also highly flocculant, were larger in diameter, and were curved and hyper-branched. These traits were accentuated in the double mutant *chs2*Δ *chs8*Δ cells. Despite these morphological differences, CW staining of these mutants was comparable to the wild type strain in distribution and intensity.

The *phr1*Δ mutant formed few germ tubes, most cells exhibiting short, enlarged, outgrowths with wide septa. CW-fluorescence was distinctly more intense than in control all over the walls and septum (**Fig. 3A**). Deletion of *PHR1* conferred the same morphological defects to the *chs*Δ mutants, but the combined mutations did not noticeably accentuate the morphological aberrations of *phr1*Δ cells after 5 h incubation. Unexpectedly, the *phr1*Δ *chs3*Δ mutants stained with similar intensity and distribution as the *phr1*Δ mutant. Conversely, the absence of either *CHS2* or *CHS8* resulted in reduced CW staining, whereas the simultaneous absence of both enhanced CW staining.

Variation in CW staining presumably reflects altered chitin content but can also be affected by damages to cell wall and alterations of permeability. To verify this, we measured the chitin content of the mutants after the induction of hyphal growth. As shown in **Fig. 3C**, the

deletion of *CHS3* in a wild type background dramatically reduced the chitin content of the cells while loss of either *CHS2* or *CHS8*, alone or in combination, resulted in a small reduction in chitin indicating that these genes provide a minor contribution to the total chitin of the wild type hyphae. In contrast, the chitin increase observed in the *phr1*Δ mutant was only slightly reduced in the absence *CHS3* or both *CHS2* and *CHS8*. However, the *phr1*Δ *chs2* Δand *phr1*Δ *chs8*Δ strains were deficient in chitin accumulation suggesting that the combined loss of *CHS2* and *CHS8* is compensated by other isoenzymes in the *phr1* mutant. In addition, chitin content of *phr1 chs3* at 3 h was about half that at 5 h, suggesting that extra chitin is progressively accumulated as a consequence of increasing stress during germination (Fig 3 D).

Microscopic examination of the *phr1*Δ*chs3* Δmutant after 24 h incubation revealed swollen, lysed cells and ghosts of cells into which CW had penetrated (**Fig. 3B, asterisks**). This prompted an examination of the viability of the various mutants using methylene blue staining. While only a few percent of *phr1*Δ cells were inviable at 5h and this increased to around 15% at 24 hr, 20% of the *phr1* Δ*chs3*Δ cells, or units of cells, were dead within 5 hr and this increased to about 82% by 24 h (Fig. 3D). When the *phr1* Δmutation was combined with deletions of *CHS2* and/or *CHS8* no relevant decline in viability was observed (Fig. 3D). Finally, no lysis phenotype for the hyphae of the parental strains was detected except for some apex of *chs3* mutant. Thus, Chs3p is required for long-term viability of *phr1* in liquid M199 alkaline pH.

Interestingly Chs2p and Chs8p appear to contribute to the synthesis of chitin during the initiation phase of hyphal development. However, chitin increment *per se* does not provide cell wall integrity in the absence of Phr1p. Although at 5 h the *phr1*Δ*chs3* Δmutant has a comparable increase in chitin content with respect to *phr1 chs2 chs8* mutant, the chitin accumulated in *phr1 chs3* mutant does not contribute to maintain cell integrity on a long temporal scale.

We next asked which isoenzyme/s contribute to chitin synthesis when *CHS3* or *CHS2* and *CHS8* are missing. Thus, we tested the cell sensitivity of mutants RO- 09-3143, a specific inhibitor of Chs1p (Sudoh *et al.*, 2000). The absence of visible growth of the *phr1* Δ*chs3* Δmutant, precluded testing the inhibitors against this strain confirming the severe lytic phenotype of this mutantI .f *phr1 chs2 chs8* mutant (remaining activities Chs1 and Chs3p) was more dependent on Chs1p, it would be correspondingly more sensitive to RO-09-3143 whereas if the mutant did not depend on Chs1p for viability, the sensitivity would be the same of the *phr1* mutant.

Fig. 4A shows that the growth of the *phr1* and *phr1 chs2 chs8* mutants was more susceptible to the inhibitor with respect to the parental strains but the mutants strains appeared to have a similar sensitivity to the drug suggesting that Chs1p is not required for the growth of *phr1 chs2 chs8* mutant. However, since the inhibitor causes an enlargement of the wild type and *chs2* hyphae and the appearance of "balloons" as previously described whereas *phr1* strains appeared as chains of septum-less cells and also swelling occurred, we also tested the killing effect by the XTT-reduction assay. Interestingly, the killing curves were similar for all the strains (**Fig. 4B**). These results indicate that Chs1p is not recruited in the triple mutant as the main compensatory chitin synthase.

The dependence of *phr1* cell integrity on Chs3p is attenuated in slow filamentation conditions

Because some mutations differentially influence filamentation in broth culture versus solid media (Lin et al, 1994; Sharkey et al, 1999), we tested the phenotype of *phr1chs* mutants also on agar solidified media. On solid M199-pH 7.5 at 37 °C, all the strains germinated and gave rise to visible colonies except *phr1*Δ*chs3*Δ mutant that did not produce colonies (**Fig.5A**). Upon microscopic observation of the agar surface, we concluded that *phr1*Δ*chs3*Δ cells did not undergo germination suggesting that cell death is an early event. Inclusion of 0.8 M sorbitol into the plates did not suppress the lethal phenotype (**Fig. 5B**). The defect of germination of the *phr1*Δ*chs3*Δ mutant was suppressed at pH 4.5 in agreement with the relation of the synthetic lethal phenotype to the presence of the *PHR1* deletion (data not shown).

We conducted a filamentation assay also on Spider medium, a less potent filamentation condition. At 37 °C and pH 7.5, all the strains formed colonies including *phr1*Δ *chs3*Δ mutant whose colonies became visible with a day of delay but progressively became bigger till the size of the single *phr1* mutants (**Fig. 5B**). The inclusion of 0.8 M sorbitol in the plates increased the number of CFU by 50%, supporting the notion that the reduced germination of *phr1*Δ *chs3*Δ mutant was due to lysis at the onset of blastospore germination (data not shown).

Next, we determined the effects of Spider medium buffered at pH 8. *phr1*Δ mutant gave rise to small colonies in agreement with the worsening of the phenotype at higher pH whereas

*phr1*Δ*chs3*Δ mutant did not produce colonies (**Fig. 5**). The lethal phenotype of *phr1*Δ*chs3*Δ mutant at pH 8 was not reverted by the inclusion of sorbitol in the plates (data not shown).

To understand the nature of the attenuation of the phenotype in Spider medium at pH 7.5, the four independent *phr1*Δ *chs3*Δ clones, named "adapted", were recovered from the plates at pH 7.5 and filamentation assays at pH 7.5 were repeated. The adapted clones were able to germinate and grow in Spider medium at pH 7.5 but not on M199 at pH 7.5 as the original *phr1*Δ *chs3*Δ mutant (data not shown). The phenotype in liquid M199 was indistinguishable from that of the original strain. These results indicate that attenuation of the *phr1*Δ *chs3*Δ phenotype on Spider medium at pH 7.5 results from physiological adaptation.

In conclusion, the phenotype of *phr1*Δ*chs3*Δ mutant is influenced by the filamentation conditions used in solid medium. On solid M199-pH 7.5 and Spider-pH 8 *phr1 chs3* cells die at the very early onset of germination. In Spider-pH 7.5 roughly 50 % of the population adapt after a long germination time. These results are consistent with M199 medium being a more demanding growth condition than Spider medium.

The block of hyphae elongation up-regulates DNA replication genes and accelerates the progression into the DNA division cycle

Next, we investigated the Class 1 genes related to "DNA replication and repair" (*POL30, POL3, RAD51, DUT1, MSH6, RFA2, RFA1,* orf19.7425, orf19.2796, *POL1, CDC54, RBR1, EXO1, orf19.4030, CDC46, MCM6*) and "Chromatin and chromosomes" (*HHF22, HHF1, HTA1*, *HTA2, HTB1, IRR1, ASF1, SMC6, NAT4*) (Tables S1). This transcriptional response occurred within 1 and 3 h and may be related to the block of filamentation, as a similar response was observed during the arrest of hyphal elongation by farnesol (Enjalbert & Whiteway, 2005). However, the actual effect of these changes on entry into S-phase has not been reported. Therefore, we analyzed by flow cytometry the DNA distribution profile of wild type and *phr1* mutant strains undergoing the Y-H transition. Blastospores from prolonged incubation in stationary phase (1.5 days) showed a very high degree of synchrony in germ tube formation when inoculated into hyphal induction conditions. The percentage of germ tubes was about 88% both for the wild type and *phr1* mutant at 1 h. By 1.5 h thin hyphae already appeared in the wild type whereas the germ tubes of the mutant developed a swollen apex. At this time, *phr1*Δ cells have already entered S-phase, earlier than control cells, and also an enrichment of cells at G_2/M was observed (**Fig. 6**). These results are in agreement with the early induction of DNA replication genes in the mutant.

Discussion

The present study describes the impact of the loss of cell wall assembly on the transcriptional program of *C. albicans* cells undergoing hyphal growth. To our knowledge this is the first report in which no inhibitor of glucan formation was used and where the impact on hyphal growth instead yeast growth was examined. Moreover, we performed a time-course analysis and obtained information both the short-term (1 h), medium-term (3h) and long-term (5h) exposure to hyphal wall stress. Cells lacking the glucan transferase/elongase ctivity Phr1p, that is fundamental for assembly and remodeling of β(1,3)-glucan, were the object of our study. Genes that are differentially modulated compared to the wild type provided a key to understand the consequences of the weakening of the cell wall on the abnormal morphogenetic effects, on the maintenance of cell integrity and contributed to explain some phenotypic traits typical of the mutant such as the defect of adhesion besides providing evidence of new unknown functions.

First, the results of our microarrays and genetic analyses indicated that cells deficient in β(1,3)-glucan remodeling under hyphal growth inducing conditions initiate the hyphal transcriptional program. The indication that *phr1* cells initiate the hyphal developmental program is provided not only by the ability to form germ tubes but also by the presence of typical hyphal-induced genes *ECE1, ALS10, ALS3, RBT1* (**Dataset 1**). The block in hyphal elongation that occurs o longer time causes a reduction of the expression of *ECE1*, as expected, although this reduction did not overcome the stringent parameters that were set in the microarray analysis and *ECE1* is not present among the modulated genes.

Another hint regards the *PHR* family. None of the *PHR* genes (*PHR2*, *PHR3*, *PGA4* and *PGA5*) was identified in our analysis indicating that no transcriptionally-mediated cross compensatory mechanism exists between these paralogs and *PHR1*. The recent finding that recombinant Pga4p is inactive also reinforces the unique role of *PHR1* at neutral-alkaline pH. adaptive response is triggered to survive.

A core set of 10 mannoproteins responds during time to the loss of β(1,3)-glucan assembly

Among the 10 genes encoding structural cell wall proteins, seven were found only in *C. albicans* or *Candida* spp. (*PGA23*, *RBR1*, *PGA13*, *PGA54, RHD3/PGA29,* orf19.750 and orf19.675) five of them are predicted to be modified by GPI (*PGA23*, *PGA13, RBR, PGA54*

and *RHD3/PGA29*) and were also partially characterized (Lotz *et al.*, 2004, de Boer *et al.*, 2010, Gelis *et al.*, 2012). We included one uncharacterized ORF, orf19.750, and one predicted ORF, orf19.675 that may be interesting for future studies. The first encodes a new mannoprotein since it has features in common with surface mannoproteins: the presence of a signal peptide, abundance of alanine, serine and threonine residues, a hydrophobicity plot similar to that of Ece1p, presence of internal repeats. Furthermore, it was also shown to be a substrate *in vitro* of the Kex2 protease (Bader *et al.*, 2008). Orf19.675 also encodes a putative extracellular protein.

Other two genes, *PGA6* and *ECM331*, have homologs in *S. cerevisiae* as do the remaining six genes encoding non-covalently linked cell wall proteins *RBT4*, *TOS1* and *ECM331* whose expression is sensitive to cell wall stress. *PGA6* is the ortholog of *CCW12*, a *S. cerevisiae* gene encoding a covalently linked cell wall mannoprotein required for cell wall integrity, and similarly Pga6p could be important for cell wall strength of *C. albicans* (Ragni *et al.*, 2011b, Ragni *et al.*, 2007).

As many mannoproteins have a structural role, this wide response could be related to the reinforcement of the extracellular matrix.

PGA13, ALS2 and ALS4 modulation and the defects in adhesion of phr1 mutant

PGA13 was reported to influence surface properties such as hydrophobicity and its deletion affects cell wall organization, increases adhesion to plastic and induces *ALS* gene expression (Gelis *et al.*, 2012). We postulate that, conversely, *PGA13* transcript increase in the mutant may result in reduced adhesion and this could contribute, together with the down-regulation of *ALS2* and *ALS4*, to the severe defect in adhesion to plastic and cell monolayers we previously described for *phr1* cells (Calderon *et al.*, 2010). Together with the inability to elongate, the adhesion defect contributes to the avirulence of the mutant in animal models of systemic infection and experimental keratomycosis (De Bernardis *et al.*, 1998, Yuan *et al.*).

CRH11 transglycosidase: the only member of the UTR2/CSF4 to respond to stress

Among genes encoding cell wall enzymes, *CRH11* was strongly induced. *CRH11* is the only member of a family of genes that includes *UTR2/CSF4* and *CRH12,* to respond to cell wall stress at the transcriptional level (Pardini *et al.*, 2006). Moreover, in vegetatively growing *C. albicans* cells treated with caspofungin, *CRH11* is up-regulated (Liu *et al.*, 2005). Thus, up-

regulation of *CRH11* in the *phr1* mutant during hyphal development is likely a response to the hyphal wall defects associated with the loss of *PHR1*. Interestingly, the homolog *ScCRH1* is also up-regulated in response to cell wall stress both in cell wall mutants, including a *gas1* mutant, and in cells treated with Congo red, or zymolyase (Lagorce *et al.*, 2003, Garcia *et al.*, 2004, Cabib, 2009). Biochemical and genetic studies have demonstrated that Crh1p of *S. cerevisiae* functions *in vitro* and *in vivo* in the cross-linking of chitin chains to β(1,3)-and β(1,6)-glucan which in turn can be linked to GPI-CWPs yielding a more resistant wall (Mazan *et al.*, Cabib *et al.*, 2007, Cabib *et al.*, 2008, Cabib, 2009). It is notable that in *gas1*Δ cells an increase in the transglycosylase activity mediated by these proteins has been reported (Cabib *et al.*, 2008). Assuming a functionally analogous role for *C. albicans* Crh11p, its induction in *phr1*Δ mutant, in conjunction with the observed increase in chitin would enhance the establishment of new cross-linkages and guarantee the robustness of the cell wall, protecting *phr1* cells from lysis (see model in **Fig. 7**).

Caspofungin (CS) induces cell wall stress by inhibiting β-1,3-glucan synthesis and the response to this cellular insult might be expected to partially overlap the response to loss of Phr1p. Bruno e*t al.* (2006) defined a core set of 34 CS-responsive genes by combining their results and those of Liu et al. (Liu *et al.*, 2005, Bruno *et al.*, 2006). Of the *PHR1*-responsive genes, 9 were in common with the core CS-responsive genes. Eight of these were up-regulated under both conditions. These included *CRH11*, *PGA13*, *ECM331*, *DDR48*, *ALS1*, orf19.3615, orf19.909, and orf19.2846. The CS-responsive genes were defined after 1 h treatment with CS and the last six of these common genes were induced at 1 h in the *phr1*Δ mutant, but their expression declined by 3 h. In contrast to this transitory response, *CRH11*, *PGA13*, *DDR48* showed a sustained expression in the *phr1*Δ mutant **(Table 3** and **S1**), suggesting these genes may be more critical to the cell's attempt to counteract cell wall damage. In addition, *PGA23* and *RTA4* (a putative fatty acid transporter), two additional CS-induced genes described by Bruno *et al.* (2006), are persistently up-regulated also in the *phr1* mutant. Only one down-regulated gene, orf19.5267, was in common at 1 h in the *phr1*Δ mutant and CS-treated cells. Notably, the expression of *CRH11*, *PGA13, PGA23, ECM331* is governed by *CAS5*, encoding a zinc-finger transcription factor that plays a major role in cell wall damage response in vegetative growth (Bruno *et al.*, 2006). Interestingly, *CAS5* transcript level increases in *phr1*Δ mutant after hyphal growth induction suggesting that this transcription factor is important also for hyphal wall stress.

In addition to the altered expression of mannoproteins and glucanases, the *phr1* mutant responded with an induction of genes encoding chitin synthases and an increase in chitin content. Of particular note is the induction of the genes encoding Class I chitin synthases, *CHS8* and *CHS2*. Similarly, *CHS2* and *CHS8* are up-regulated in CS-treated vegetatively growing *C. albicans* cells and these synthases constitute the major activities measured *in vitro* although the extra chitin was largely dependent on Chs3p (Walker *et al.*, 2008). Our analysis of *phr1 chs* mutants demonstrated that *CHS2* and *CHS8* are not required for the maintenance of *phr1* cell integrity during hyphal growth. On the contrary, *CHS3* is essential for the survival of *phr1* cells. The absence of Chs3p in the *phr1* mutant induces a progressive increase of chitin resulting from the recruitment of Chs2 and Chs8 that restore the chitin level of the *phr1* mutant by 5 h from the induction of hyphal growth (see Results). However, chitin increase per se does not appear enough to remedy the cell wall stress because *phr1 chs3* cells start to lyse (**Fig. 3D**). [the structure of this chitin must differ such that it is incapable of incorporation into a stable structure and cells die on a longer temporal scale.] An increase in chitin content is regarded as a typical response to cell wall stress (Fonzi, 1999, Popolo & Vai, 1998, Popolo *et al.*, 2001, Ram *et al.*, 1998).

These results can be reconciled by taking into account that different isoforms produce different fibrils of chitin that may be not equally effective in reinforcing the lateral cell wall. It has been shown that in *C. albicans* cells Chs8p is responsible for the synthesis of long chitin microfibrils at the septum whereas Chs3p synthesizes short chitin rodlets at both the septum and the rest of cell surface (Lenardon *et al.*, 2007, Walker *et al.*, 2013). Assuming that also in hyphae chitin fibrils produced by *CHS8* and *CHS2*, have a different structure than those produced by Chs3p, they may probably be able to compensate better the damage caused by lack of Phr1p at the level of the septum than that in lateral cell wall. This is supported by the fact that *phr1 chs3* cells usually lysed at the apex (data not shown).

The recruitment of other *CHS* isoforms by hyphal wall stress represents a difference between *C.albicans* and the yeast *S. cerevisiae* where absence of Chs3p does not lead to deposition of chitin by other isoforms, namely the Class I chitin synthase Chs1, despite *CHS1* is always up-regulated by cell wall stress (Lagorce *et al.*, 2003, Valdivieso *et al.*, 2000).

Regarding Chs3p, many reports suggest that Chs3p is regulated at a post-transcriptional level such as recruitment to the plasma membrane from the intracellular stores (chitosomes or ER) and regulation by phosphorylation of its localization. (Lenardon *et al.*, 2007) (Lenardon *et al.*, 2010a) (Chuang & Schekman, 1996, Bulik *et al.*, 2003). Interestingly, the level of the *CHS7* transcript in *phr1* cells is higher than in the wild type suggesting that Chs3p export from ER is increased in the *phr1* mutant Other biochemical mechanisms may contribute to increased

chitin synthase activity: the availability of the substrate (UDP-GlcNac), which is regarded as the limiting factor for chitin synthase activity, allosteric regulation by glucosamine, interaction with activators or protein modifications (Bulik *et al.*, 2003). Gfa1p was proposed to be the major control point in the chitin biosynthetic pathway (Lagorce *et al.*, 2002). Gfa1p could play a critical role in regulating Chs3p activity also in the *phr1* mutant. In *C.albicans* Gfa1p is a minor component of cytosolic proteins (0.0025%) (Milewski *et al.*, 1999). However, despite the transcriptional increase of GFA1 in the mutant, we did not find any correlation between the absolute *in vitro* activity of Gfa1p and the chitin levels, suggesting that the activity of this enzyme is not limiting in *C. albicans* (data not shown).

Overall, the results of our studies show for the first time the primary role of Chs3p in the response to wall stress in *Candida albicans* hyphae that differs in structure and composition from the yeast form cell wall on which most studies have concentrated. Our study also supports the hypothesis of a general mechanism of cellular response to wall stress. In fungi, a stress response is activated to counteract a weakening of the cell wall as shown in yeast constitutive cell wall mutants, or in cells under cell wall perturbing conditions such as treatment with echinocandins, Calcofluor, Congo Red, or high temperature (Liu *et al.*, 2005, Heilmann *et al.*, 2013, Popolo *et al.*, 2001, Meyer *et al.*, 2007).

Other functions affect cell cycle regulation

Finally, we demonstrated that the block in morphogenesis brings about an accelerated entry into S-phase and G2. In *C. albicans,* cells enter S-phase when germ tubes reach a critical length or size. Stabilization of the G1 cyclin and delayed accumulation of the mitotic cyclins Clb2 and Clb4 occurring during germ tube formation suggests an extended G1 phase with respect to yeast cells (Bensen *et al.*, 2005, Finley & Berman, 2005, Barton & Gull, 1988). The mechanism regulating this seems to be altered or negated in the presence of *phr1*Δ defects that block the hyphal morphogenic program. Moreover, in the mutant, genes involved in rRNA processing, maturation and transport are repressed at 1 h. We propose that premature entry into S-phase may bring about a temporary block in rDNA transcription and ribosome biogenesis. This response could be a consequence of the morphogenetic arrest as an early repression of ribosome biogenesis genes was also detected in the block of hyphae formation by farnesol (Enjalbert & Whiteway, 2005).

Interestingly, the cyclin genes *PCL1*, *PCL2* and *CCN1*, a homolog of *CLB3* in *S. cerevisiae*, normally repressed in cells induced to make hyphae, are up-regulated both in *phr1* and in

farnesol-arrested hyphae (**Table S1** and (Enjalbert & Whiteway, 2005). Also, the cyclin-dependent kinase *CDC28* is up-regulated at all three time points in the *phr1* mutant. Future studies will address the relations between the block of morphogenesis and cell cycle regulation under hyphal growth conditions.

This work highlights the existence of synthetic lethality between *PHR1* and *CHS3*, two fungal-specific genes. As the incidence of invasive fungal infections has been increasing, the current armamentarium of drugs is still limited both for therapy and for prophylaxis. The β(1,3)-glucanosyltransferases are essential in fungi either for viability or virulence. In *C. albicans* Phr proteins could be a promising target for new cell wall specific drugs taking also into account that the three dimensional-structure of the homologous protein *Sc*Gas2p was determined and a fluorescent enzyme assay for GH72 activity is available (Hurtado-Guerrero *et al.*, 2008, Mazan *et al.*, 2011). In *C. albicans* Chs3p is essential for survival of the *phr1* mutant suggesting that a combination therapy might be designed to hit the primary target together with the compensatory pathway.

The long-term adaptive response

These genes are included in the model of **Fig. 7.**
(TO BE COMPLETED)

Experimental procedures

Strains and growth conditions

The strains used in this work are listed in **Table 4.** To induce hyphal development, stationary phase cells from an overnight culture in YPD (1% yeast extract, 2% peptone, 2% glucose)-150 mM HEPES pH 6.0 incubated at 30 °C were pelleted. The pre-culture medium was buffered at pH 6 to limit the residual Phr2p since at this pH value, the expression of *PHR2* is extremely low whereas the phenotype of *phr1*Δ cells is not yet manifested (Muhlschlegel & Fonzi, 1997). Cells were suspended at an initial OD_{600} of about 0.25 in pre-warmed M199-150 mM HEPES buffered at pH 7.5 and supplemented with 1.9% glucose, and incubated under agitation at 37°C. For Ura^- strains, 25 μg ml^{-1} uridine was added to the growth medium of the pre-culture whereas 100μg ml^{-1} uridine was added to the M199 medium. The formation of hyphae was monitored every 30 min.

For the colony filamentation assay, M199-150 mM HEPES, supplemented with 2% agar, was adjusted to the desired pH and supplemented with 100 μg ml^{-1} uridine. Stationary phase cells from an overnight culture in YPD-pH 6 at 30° C were diluted to 10^3 cells ml^{-1} by two serial 1:100 dilutions in buffered liquid medium. From the last dilution, 100 and 150 μl were spread on top of solid M199. Plates were incubated at 37°C for 24 h. Plates were observed using a Leica MZ6 stereomicroscope.

Mutant strain construction

Strains C155 (*chs2/chs2*), NGY128 (*chs8/chs8*), Myco3 (*chs3/chs3*), and NGY138 (*chs2/chs2 chs8/chs8*) were kindly provided by Prof. Neil Gow (Aberdeen Fungal Group, University of Aberdeen, UK) and transformed with *Hin*dIII and *Pvu*II digested DNA of plasmid pSMS23 to delete one allele of *PHR1* (Saporito-Irwin *et al.*, 1995a, Fonzi & Irwin, 1993, Saporito-Irwin *et al.*, 1995b). Cell transformation was performed essentially as described in (Walther & Wendland, 2003). Ura^+ transformants were selected on SD agar. Linkage of the transforming DNA with the *PHR1* locus was verified by PCR amplification using primers PHR1-N7 and hisG3'P for the 5'-end and primers hisG-forward and PHR1rev(+1840) for the 3'-end. The primers used in this work are listed in **Table S3**.
Deletion of the second allele was achieved by transformation with *Btg*ZI and *Pvu*II digested DNA of plasmid pLit-PHR1-1NAT DNA. Plasmid pLit-PHR1-1NAT was constructed by cloning a 2.5 kb *Eco*RI-*Hin*dIII fragment from a genomic clone of *PHR1* (Yesland & Fonzi, 2000) into the like sites of pLITMUS38 (New England Biolabs). The resulting plasmid pLit38PHR1-1 was digested with *Sac*II and *Kpn*I, which removed nucleotides +167 to +853 of the *PHR1* coding region, and ligated with a 1265 bp *Sac*II-*Kpn*I fragment containing the nourseothricin resistance gene, *NAT1*, isolated from plasmid pJK795 (Shen *et al.*, 2005). Transformed cells were selected on SD medium containing 450 ugml-1 nourseothricin. Linkage to the *PHR1* locus was tested with PCR primers PHR1-N7 and NAT1_5'link_rev for the 5' end and NAT1-3'link_fwd and PHR1rev(+1840) for 3'-linkage. Absence of a wild type allele was verified with primers PHR1-N7 and PHR1-rev(+1840). Two independent *phr1* null mutants were constructed in each *chs* mutant background.

DNA microarray analysis

At 0, 1, 3 and 5 hours after the shift of stationary phase blastospores to the hyphal growth inducing medium, cells (200 OD_{600}) were collected by filtration on a Millipore 0.45 μm filter

110

disk. The filter was removed, transferred to a tube and the cells suspended in 1 ml of ice-cold H_2O. The washed cells were quickly frozen in liquid nitrogen and stored at -80°C until use. Cell samples were collected from two independent cultures.

Total RNA was extracted using the RNeasy Midi Kit (QIAGEN). Cell pellets were thawed and suspended in 600 µl of RTL buffer. After addition of an equal volume of cold, sterile glass beads, cells were broken by 5 cycles of 1 min agitation in a BeadBeater (Biospec) at 4°C and 1 min on ice. Total RNA was isolated from two independent experiments. RNA concentration and quality were assessed by spectrophotometric measurements and denaturing agarose gel electrophoresis. RNA samples were processed for further analysis at the Microarray Facility, Washington University at St. Louis, Mo U.S.A. (currently GTAC, Genome Technology Access Center).

DNA microarray hybridization

RNA integrity and quality were validated on an Agilent 2100 Bioanalyzer and reverse transcribed into cDNA in the presence of Cy3/Cy5 labeled dNTPs using the 3DNA array 350 detection system (Genisphere, Hatfield, PA) For each strain, data from 1, 3 and 5 h were compared to time zero. To exclude any influence due to the type of fluorophore used, the labeling of the samples was also inverted (dye-swap). In total 24 hybridizations were performed (12 for each strain).

DNA oligonucleotide microarrays represented 6,346 of the 6,354 predicted ORFs in the annotated *C. albicans* genome assembly 19. Probes consisted of unique ORF-specific 70-mer oligonucleotides, and oligonucleotide sequences were selected using an ArrayOligoSelector software and were obtained from Illumina (San Diego, CA). Each probe was spotted three times per slide, thus 19,308 spots were present on each array plus 10 specific control genes from *Arabidopsis thaliana*. A two-step protocol was used for hybridization (3DNA array 350 detection system). First, oligonucleotide arrays were hybridized to the cDNA probes in 2× formamide-based hybridization buffer overnight at 43°C and washed in 2× SSC (1× SSC is 0.15 M NaCl plus 0.015 M sodium citrate)-0.2% sodium dodecyl sulphate (SDS) according to the manufacturer's protocol. Fluorescent Cy3- and Cy5-capture reagents were combined in hybridization buffer and added to each array, which were incubated and washed again as described above. Slides were scanned immediately after hybridization on a ScanArray express HT scanner (Perkin-Elmer) to detect Cy3 and Cy5 fluorescence. The laser power was kept constant, and photomultiplier tube (PMT) values were set for optimal intensity with minimal background. An additional scan was done for each slide with the PMT such that

<1% of the elements are saturated in order to characterize spots which were saturated at the higher PMT setting. Gridding and analysis of images was performed with ScanArray software express V2.0 (Perkin-Elmer). Processing of the raw data and normalization were carried out at the Microarray Facility, Washington University at St. Louis, Mo using the LOWESS normalization. The Median of Ratios was used for further analyses.

Statistical analysis

For each strain, each time point (1, 3, 5 h) was compared with the respective time zero sample, once with each dye orientation (6 hybridizations per strain). For two biological replicas, a total of 24 hybridizations were performed. Microarray data were deposited at GEO database (GSE51064). The four expression ratios per comparison for each gene (2 biological replicates and 2 dye-swap) were averaged (arithmetic mean) and one-sample Limma analysis and False Discovery Rate (FDR, using a p-value ≤ 0.05) for multiple testing correction were applied (Smyth, 2005, Hochberg, 1995). This statistical analysis was performed with the web-software Babelomics (Medina *et al.*, 2010). Principal Component analysis was performed using the software Partek. Hierarchical cluster analysis was performed using Pearson correlation (average linkage) and the Multiple Viewer Experiment (MeV) software package developed by TIGR (Saeed *et al.*, 2003). The cutoff to consider transcriptional induction or repression with respect to time zero was a ratio ≥ 2 and ≤ 0.5, respectively. For the comparison of the transcriptional profile mutant versus the wild type strain, we calculated a Relation Factor (RF, ratio of the expression ratios) that measures the dependence of the transcript level on the mutation. All genes with available data in at least 3 replicates and FDR≤ 0.05 were considered in this analysis (Dataset S2 is available upon request). In order to select genes whose expression levels at different time were significantly altered in the *phr1* mutant we set a threshold of RF ≥ 2 to select transcripts at least twice more abundant in the *phr1* mutant than in the control (Class 1), and RF ≤ 0.5 for transcript at least twice less abundant in the *phr1*Δ mutant compared to the control (Class 2).

Verification of differential gene expression using quantitative real-time RT-PCR

Gene-specific primers were designed using Primer3 software (http://frodo.wi.mit.edu/primer3/) and further analyzed using the tool from Integrated DNA technologies (http://eu.idtdna.com/analyzer/applications/oligoanalyzer/). Primer sequences are shown in **Table 5**. Total RNA was extracted at time zero, 3 and 5 hours after induction of

hyphal growth. On-column DNase digestion was performed according to the manufacturer's instructions (QIAGEN). First strand cDNAs were synthesized from 1.6 µg of total RNA in 20 µl final volume, using the Reverse Transcription System A3500 (Promega). As a test for residual genomic DNA contamination, reactions were performed also in the absence of reverse transcriptase. Real time quantitative PCR reactions were carried out in a Bio-Rad IQ5 instrument. Each PCR reaction contained 5 µl of diluted cDNA, 7.5 µl of SsoFast™EvaGreen®Supermix with low ROX (Bio-Rad), 1.5 µl of oligos (final concentration each 0.5 µM) and 1 µl nuclease-free H_2O. Triplicates of all reactions were analysed. For quantification, the abundance of each transcript during induction conditions was determined relative to the standard *TDH3* RNA, as indicated in other reports (Fanning *et al.*, 2012, Blankenship *et al.*, 2010), for input cDNA normalization. Final data on relative gene expression between the two conditions (sample from time 3 or 5 h with respect to time zero for each strain) were calculated according to the $2^{-\Delta\Delta C}{}_T$ method (Livak & Schmittgen, 2001).

Microscopy

For Calcofluor White (CW) staining, 0.5 ml of culture (about 1-2 OD_{600}) were collected and the cells washed with 0.5 ml of dH_2O. The pellet was suspended in 0.5 ml of CW (0.1 mgml-1 dH_2O). After 5 min, the sample was washed twice with 1 ml of dH_2O and then examined by fluorescence microscopy. For DAPI staining, cells were collected, washed with dH_2O, fixed in 70% ethanol and stored at 4°C until examination. The sample was washed with dH_2O and suspended in DAPI solution (0.125 µg ml^{-1}) and incubated for 10 min in the dark. Then, the sample was washed twice with dH_2O and examined by fluorescence microscopy.
Fungal viability was assessed by methylene blue staining which identifies metabolically inactive or membrane compromised cells. Viable cells appear colorless while dead cells are blue. Cells were collected by centrifugation and suspended in the same volume of methylene blue solution (methylene blue 0.2 g/l, KH_2PO_4 27.2 g/l, K_2HPO_4 0.071 g/l, pH 4.6 stored at 4°C) and incubated for 20 min at RT prior to examination by bright-field microscopy.

Broth microdilution and XTT-reduction assay

To test sensitivity to the Chs1p inhibitor RO-09-3143, a microdilution assay at an inoculum size of 5 x 10^5 was performed according to the NCCLC guidelines M27-A2 and as previously described (Popolo & Vai, 1998). Briefly, cells were grown to stationary phase in YPD-

HEPES buffered at pH 6 at 25 °C. In a well of a 96-well micro titer plate, 100 µl of a suspension containing10^6 cells ml^{-1} in M199-HEPES pH 7.5, supplemented with 100 µg ml^{-1} of uridine if required, was added to an equal volume of medium containing RO-09-3143 (kindly donated by Roche) dissolved in DMSO. Two-fold serial dilutions of the inhibitor were made to achieve a range of concentrations from 0.012 µM to 25 µM. All determinations were made in duplicate. Control wells contained DMSO with no drug. The plates were incubated at 37 °C and inspected at 24 and 48 h. The effect of the treatment was evaluated both visually and also by reading the turbidity with a Tecan Infinite F200 PRO microtiter plate reader set to 5-reads of different areas per well. After centrifugation of the plate and removal of the medium a reduction assay of the tetrazolium salt 2,3-bis(2-methoxy-4-nitro-5-sulfophenyl)-5-[(phenylamino)carbonyl]-2*H*-tetrazolium hydroxide (XTT) was performed according to a previously published protocol (Ramage *et al.*, 2001) except for the ZTT concentration that was reduced to 0.250 µg/ml.

Enzymatic assay of the chitin content

Pellets corresponding to about 150-200 OD_{600} of cells were collected by centrifugation, suspended in 6 ml of H_2O, and divided into four equal aliquots, two of which were used to determine the dry weight. The other two were centrifuged and the pellets stored at −20°C for later chitin determinations.Total cellular chitin was measured by an enzymatic method, as described by Bulawa et al. (Bulawa, 1992). Washed cells (about 100 mg wet weight) were suspended in 1 ml 6% KOH and incubated at 80°C for 90 min. After cooling, 100 µl of glacial acetic acid were added and samples were centrifuged for 15 min at 13,000 x g. The pellet, containing the alkali-insoluble material, was washed twice with 50 mM phosphate buffer, pH 6.3 and suspended in 1 ml of the same buffer containing 1.7 mg of *Serratia marcescens* chitinase (Sigma). After 2 h at 37° C, 400 µl were transferred to a new tube and 25 µl of *Helix pomatia* β-glucuronidase (Roche) were added. Samples were incubated for 1 h at 37° C. After 1 min-incubation at 100°C, samples were centrifuged and the supernatants were saved. The amount of GlcNAc was determined with the Morgan-Elson reaction. To 100 µl of sample, 150 µl of H_2O were added. After 1 min-incubation at 100°C and addition of 250 µl of 0.27 M potassium tetraborate, pH 9, samples were boiled again for 8 min. After cooling, 3 ml of Ehrlich-solution (stock solution 10 times concentrated was prepared by mixing 10 g of p-dimethylaminobenzaldehyde (Sigma) in 12.5 ml of 10 N HCl and 87.5 ml of glacial acetic acid) was added and the samples were incubated for 40 min at 37°C.

The absorbance at 585 nm was measured and compared with a standard curve ranging from to 1 mg of N-acetylglucosamine. The micrograms of N-acetylglucosamine were normalized to the milligrams of dry weight of cells.

Flow cytometry analysis of DNA

CAI10 and CAS10 cells were grown to stationary phase at 30° C (1.5 days) in YPD pH 6 and then shifted to M199-pH 7.5 at 37°C at an initial density of 0.25 OD_{600}. At different time intervals after induction of hyphal growth, 1 OD_{600} of cells were mildly sonicated, collected by centrifugation, fixed in ice-cold 70% ethanol and stored at 4°C. The samples were suspended in 0.5 ml of RNase A (1 mg ml^{-1} in 50 mM Tris-HCl pH 7.5) and incubated at 37°C overnight. The next day, the samples were centrifuged and suspended in 0.5 ml of Proteinase K (2 mg ml^{-1} in 50 mM Tris-HCl pH 7.5). After 2 h at 42°C, the samples were centrifuged, suspended in FACS buffer (200 mM Tris-HCl pH 7.5, 200 mM NaCl, 78 mM $MgCl_2$) and stored at 4°C. At the time of the analysis, 100 µl of sample was added to 1 ml of Sytox Green 1x, a nucleic acid stain (diluted 1:5000 in 50 mM Tris-HCl pH 7.5; Invitrogen), subjected to a brief sonication and analyzed with a FACScan flow cytofluorimeter (BD Biosciences, San Jose, Ca). We analyzed 10^4 cells for each sample.

Accession numbers

Information for the *C. albicans* genes can be found at the Candida genome Database (CGD) Web site (http://www.candidagenome.org). Microarray data seta can be found at the Gene Expression Omnibus Web Site (http://www.ncbi.nlm.nih.gov/geo/) under the accession number GSE51064.

Acknowledgements

The authors wish to thank Dr. Elena Galati for the FACS analysis and Mr. Roberto Cavatorta for the help in the preparation of the figures. This work was supported by the EU-RTN project “Cantrain” N.512481, FP 7 to LP. Work at JA lab was supported by grant BIO2010-22146 (Ministerio de Ciencia e Innovación, Spain) and S2010/BDM-2414 (Comunidad de Madrid). Collaboration between JA and LP was also supported by the LLP-ERASMUS Teaching mobility program between Universidad Complutense de Madrid and Università degli Studi di Milano. We thank Roche for the gift of RO-09-3143. We also wish to thank

Jennifer Jerome and Barath Ramasubramanian for assistance in the construction of the strains.

Legends

Figure 1. Morphological responses to the lack of β(1,3)-glucan remodeling during induction of hyphal growth in *C. albicans*. A. Specificity of the anti-Phr1p antibody in immunoblot analysis of total extract. B. Detection of Phr1p during hyphal growth by immunoblot analysis after induction of hyphal growth. C. Morphology of the indicated strains at different time after induction of hyphal growth by shifting blastospores to M199-150 mM HEPES buffered at pH 7.5 at 37°C.

Figure 2. Global comparison of the transcriptional profile of wild type and *phr1* cells during induction of hyphal growth. (A) Principal component analysis. Each of the four blocks for each strain represents one of the sets of hybridization results. The median of ratios was used. (▲), CAI 10; (■) CAS10. **(B)** Hierarchical clustering analysis of gene expression. The top part of the complete analysis is shown. C. qRT-PCR of some selected genes. The mutant was refereed to wild type at time zero set equal to 1.

Figure 3. Effects of deletion of *CHS3, CHS2, CHS8* or *CHS2* and *CHS8* on the *PHR1* null mutant. (A) Strains CAI4 (wild type), Myco3 (*chs3*), C155 (*chs2*), NGY128 (*chs8*) and NGY138 (*chs2 chs8*) and their respective *phr1*Δ derivatives CAS8 (*phr1*), FP3 (*phr1 chs3*), FP155 (*phr1 chs2*), FP128 (*phr1 chs8*) and FP138 (*phr1 chs2 chs8*) were induced to switch to hyphal growth in M199-150 mM HEPES buffered at pH 7.5 at 37°C and 5 hours later aliquots of culture were processed for calcofluor white (CW) staining. Pictures were taken using the same exposure time (2.5 s). For *chs3* and *phr1 chs3* the corresponding bright field image is also shown. **(B)** Same as in A but cells were collected 24 hours after induction of hyphal growth. Exposure time of *phr1 chs3* cells was reduced to 1 s as indicated in the figure and the corresponding bright field image shows cell ghosts into which CW penetrated. Magnification, x 1,300. **(C)** Chitin content at 5 h. Mean values ± standard deviations (SD) are shown, n = 3. **(D)** Determination of the percentage of dead cells. Data are mean values of two independent experiments that gave very similar results.

Figrue 4. Evaluation of the Chs1p inhibition on the viability of *phr1 chs2 chs8* mutant.

The indicated mutants and the wild type were analyzed for sensitivity to the Chs1p inhibition by microdilution assay. A. profiles of the growth measured by turbidity. All data were referred to wild type set 100%. B. Killing effect of the inhibitor. The viability of the strains was evaluated by the XTT assay as described in Materials and methods.

Figure 5. Synthetic lethal phenotype of *CHS3* and *PHR1* on solid M199-pH 7.5 and Spider medium pH 8. Blastospores were plated on solid M199-150 mM HEPES medium buffered at pH 7.5, with the inclusion of sorbitol (*right panel*) or at pH 4.5 and images were taken after 24 h of incubation at 37 °C. Blastospores were also plated on Spider-150 mM HEPES medium buffered at pH 7.5 or pH 8 and images were taken afte 7 days at 37 °C.

Figure 6. Cytofluorimetric analysis of DNA distribution. Cells were analyzed at the indicated time after induction of hyphal growth at 37°C in M199 buffered at pH 7.5. 1C and 2C indicate the DNA content.

Figure 7 Model of the long-term adaptive response to the wall stress in *phr1* on induction of hyphal growth.

In this model the core response of adaptation at 5 h from the induction of hyphal growth is reported. The suffix * indicates the genes that are repressed in the wild type and induced in the mutant (green/red) whereas ** indicates the genes that are not modulated in the wild type and induced in the mutant (white/red). Only up-regulated genes were examined. Genes encoding predicted GPI-anchored mannoproteins are underlined.
The figure highlights genes involved in the signaling pathways, in the reshape of the surface (Cell wall/surface, Filamentous growth, protein folding), in the control of the cell cycle and morphogenesis (cell cycle) as those with the most striking difference between the mutant and the wild type at long term.

Supporting Information

Dataset S1. Transcriptional profile of wild type and *phr1*Δ cells during induction of hyphal growth. (available UPON REQUEST OF THE COMMISION)

Figure S1. Progress curves of Gfa1p reaction. Crude extracts that had been gel-filtered through a Sephadex G25 column to remove low molecular mass molecules, were incubated under the conditions described in Materials and Methods. The amount of glucosamine-6P formed (in nmoles) is referred to the protein content (in mg) of the sample. Values are mean ± standard deviations of three different experiments.

Table S1. Class 1: transcripts that are more abundant in the *phr1*Δ mutant than in the wild type.

Table S2. Class 2: transcripts that are less abundant in the *phr1*Δ mutant than in the wild type.

Table S3. Comparison of data from microarray and qRT-PCR analyses. [a] and [b] Expression ratio of each gene at the indicated time compared to time zero in the same strain. [c] RF, Relation Factor, ratio of the expression ratios or fold-change MUT/WT. [d] and [e] Fold-change of the transcript level of each gene at the indicated time with respect to time zero.

Table S4. Oligonucleotides used in this work

References

Alvarez, F.J., L.M. Douglas, A. Rosebrock & J.B. Konopka, (2008) The Sur7 protein regulates plasma membrane organization and prevents intracellular cell wall growth in Candida albicans. *Mol Biol Cell* **19**: 5214-5225.

Bader, O., Y. Krauke & B. Hube, (2008) Processing of predicted substrates of fungal Kex2 proteinases from Candida albicans, C. glabrata, Saccharomyces cerevisiae and Pichia pastoris. *BMC Microbiol* **8**: 116.

Barton, R. & K. Gull, (1988) Variation in cytoplasmic microtubule organization and spindle length between the two forms of the dimorphic fungus Candida albicans. *J Cell Sci* **91 (Pt 2)**: 211-220.

Bensen, E.S., A. Clemente-Blanco, K.R. Finley, J. Correa-Bordes & J. Berman, (2005) The mitotic cyclins Clb2p and Clb4p affect morphogenesis in Candida albicans. *Mol Biol Cell* **16**: 3387-3400.

Blankenship, J.R., S. Fanning, J.J. Hamaker & A.P. Mitchell, (2010) An extensive circuitry for cell wall regulation in Candida albicans. *PLoS Pathog* **6**: e1000752.

Brown, A.J., F.C. Odds & N.A. Gow, (2007) Infection-related gene expression in Candida albicans. *Curr Opin Microbiol* **10**: 307-313.

Bruno, V.M., S. Kalachikov, R. Subaran, C.J. Nobile, C. Kyratsous & A.P. Mitchell, (2006) Control of the C. albicans cell wall damage response by transcriptional regulator Cas5. *PLoS Pathog* **2**: e21.

Bulawa, C.E., (1992) CSD2, CSD3, and CSD4, genes required for chitin synthesis in Saccharomyces cerevisiae: the CSD2 gene product is related to chitin synthases and to developmentally regulated proteins in Rhizobium species and Xenopus laevis. *Mol Cell Biol* **12**: 1764-1776.

Bulik, D.A., M. Olczak, H.A. Lucero, B.C. Osmond, P.W. Robbins & C.A. Specht, (2003) Chitin synthesis in Saccharomyces cerevisiae in response to supplementation of growth medium with glucosamine and cell wall stress. *Eukaryot Cell* **2**: 886-900.

Cabib, E., (2009) Two novel techniques for determination of polysaccharide cross-links show that Crh1p and Crh2p attach chitin to both beta(1-6)- and beta(1-3)glucan in the Saccharomyces cerevisiae cell wall. *Eukaryot Cell* **8**: 1626-1636.

Cabib, E., N. Blanco, C. Grau, J.M. Rodriguez-Pena & J. Arroyo, (2007) Crh1p and Crh2p are required for the cross-linking of chitin to beta(1-6)glucan in the Saccharomyces cerevisiae cell wall. *Mol Microbiol* **63**: 921-935.

Cabib, E., V. Farkas, O. Kosik, N. Blanco, J. Arroyo & P. McPhie, (2008) Assembly of the yeast cell wall. Crh1p and Crh2p act as transglycosylases in vivo and in vitro. *J Biol Chem* **283**: 29859-29872.

Calderon, J., M. Zavrel, E. Ragni, W.A. Fonzi, S. Rupp & L. Popolo, (2010) PHR1, a pH-regulated gene of Candida albicans encoding a glucan-remodelling enzyme, is required for adhesion and invasion. *Microbiology* **156**: 2484-2494.

Chuang, J.S. & R.W. Schekman, (1996) Differential trafficking and timed localization of two chitin synthase proteins, Chs2p and Chs3p. *J Cell Biol* **135**: 597-610.

Davis, D.A., (2009) How human pathogenic fungi sense and adapt to pH: the link to virulence. *Curr Opin Microbiol* **12**: 365-370.

De Bernardis, F., F.A. Muhlschlegel, A. Cassone & W.A. Fonzi, (1998) The pH of the host niche controls gene expression in and virulence of Candida albicans. *Infect Immun* **66**: 3317-3325.

de Boer, A.D., P.W. de Groot, G. Weindl, M. Schaller, D. Riedel, R. Diez-Orejas, F.M. Klis, C.G. de Koster, H.L. Dekker, U. Gross, O. Bader & M. Weig, (2010) The Candida albicans cell wall protein Rhd3/Pga29 is abundant in the yeast form and contributes to virulence. *Yeast* **27**: 611-624.

de Medina-Redondo, M., Y. Arnaiz-Pita, C. Clavaud, T. Fontaine, F. del Rey, J.P. Latge & C.R. Vazquez de Aldana, (2010) beta(1,3)-glucanosyl-transferase activity is essential for cell wall integrity and viability of Schizosaccharomyces pombe. *PLoS One* **5**: e14046.

Eckert, S.E., W.J. Heinz, K. Zakikhany, S. Thewes, K. Haynes, B. Hube & F.A. Muhlschlegel, (2007) PGA4, a GAS homologue from Candida albicans, is up-regulated early in infection processes. *Fungal Genet Biol* **44**: 368-377.

Ene, I.V., A.K. Adya, S. Wehmeier, A.C. Brand, D.M. MacCallum, N.A. Gow & A.J. Brown, (2012) Host carbon sources modulate cell wall architecture, drug resistance and virulence in a fungal pathogen. *Cell Microbiol* **14**: 1319-1335.

Enjalbert, B. & M. Whiteway, (2005) Release from quorum-sensing molecules triggers hyphal formation during Candida albicans resumption of growth. *Eukaryot Cell* **4**: 1203-1210.

Fanning, S., W. Xu, N. Solis, C.A. Woolford, S.G. Filler & A.P. Mitchell, (2012) Divergent targets of Candida albicans biofilm regulator Bcr1 in vitro and in vivo. *Eukaryot Cell* **11**: 896-904.

Finley, K.R. & J. Berman, (2005) Microtubules in Candida albicans hyphae drive nuclear dynamics and connect cell cycle progression to morphogenesis. *Eukaryot Cell* **4**: 1697-1711.

Fonzi, W.A., (1999) PHR1 and PHR2 of Candida albicans encode putative glycosidases required for proper cross-linking of beta-1,3- and beta-1,6-glucans. *J Bacteriol* **181**: 7070-7079.

Fonzi, W.A. & M.Y. Irwin, (1993) Isogenic strain construction and gene mapping in Candida albicans. *Genetics* **134**: 717-728.

Garcia, R., C. Bermejo, C. Grau, R. Perez, J.M. Rodriguez-Pena, J. Francois, C. Nombela & J. Arroyo, (2004) The global transcriptional response to transient cell wall damage in Saccharomyces cerevisiae and its regulation by the cell integrity signaling pathway. *J Biol Chem* **279**: 15183-15195.

Gastebois, A., T. Fontaine, J.P. Latge & I. Mouyna, beta(1-3)Glucanosyltransferase Gel4p is essential for Aspergillus fumigatus. *Eukaryot Cell* **9**: 1294-1298.

Gelis, S., P.W. de Groot, L. Castillo, M.D. Moragues, R. Sentandreu, M.M. Gomez & E. Valentin, (2012) Pga13 in Candida albicans is localized in the cell wall and influences cell surface properties, morphogenesis and virulence. *Fungal Genet Biol* **49**: 322-331.

Ghannoum, M.A., R.J. Jurevic, P.K. Mukherjee, F. Cui, M. Sikaroodi, A. Naqvi & P.M. Gillevet, (2010) Characterization of the oral fungal microbiome (mycobiome) in healthy individuals. *PLoS Pathog* **6**: e1000713.

Gow, N.A., P.W. Robbins, J.W. Lester, A.J. Brown, W.A. Fonzi, T. Chapman & O.S. Kinsman, (1994) A hyphal-specific chitin synthase gene (CHS2) is not essential for growth, dimorphism, or virulence of Candida albicans. *Proc Natl Acad Sci U S A* **91**: 6216-6220.

Heilmann, C.J., A.G. Sorgo, S. Mohammadi, G.J. Sosinska, C.G. de Koster, S. Brul, L.J. de Koning & F.M. Klis, (2013) Surface stress induces a conserved cell wall stress response in the pathogenic fungus Candida albicans. *Eukaryot Cell* **12**: 254-264.

Hochberg, B.a., (1995) Controlling the false discovery rate: a practical and powerful approach to multiple testing. *J.R.Stat.Soc. Ser. B* **57**: 289-300.

Hurtado-Guerrero, R., A.W. Schuttelkopf, I. Mouyna, A.F. Ibrahim, S. Shepherd, T. Fontaine, J.P. Latge & D.M. van Aalten, (2008) Molecular mechanisms of yeast cell wall glucan remodelling. *J Biol Chem* **284**: 8461-8469.

Klis, F.M., G.J. Sosinska, P.W. de Groot & S. Brul, (2009) Covalently linked cell wall proteins of Candida albicans and their role in fitness and virulence. *FEMS Yeast Res* **9**: 1013-1028.

Kovacova, K., G. Degani, E. Stratilova, V. Farkas & L. Popolo, (2015) Catalytic properties of Phr family members of cell wall glucan remodeling enzymes: implications for the adaptation of Candida albicans to ambient pH. *FEMS Yeast Res* **15**.

Kubitschek-Barreira, P.H., N. Curty, G.W. Neves, C. Gil & L.M. Lopes-Bezerra, (2013) Differential proteomic analysis of Aspergillus fumigatus morphotypes reveals putative drug targets. *J Proteomics* **78**: 522-534.

Lagorce, A., N.C. Hauser, D. Labourdette, C. Rodriguez, H. Martin-Yken, J. Arroyo, J.D. Hoheisel & J. Francois, (2003) Genome-wide analysis of the response to cell wall mutations in the yeast Saccharomyces cerevisiae. *J Biol Chem* **278**: 20345-20357.

Lagorce, A., V. Le Berre-Anton, B. Aguilar-Uscanga, H. Martin-Yken, A. Dagkessamanskaia & J. Francois, (2002) Involvement of GFA1, which encodes glutamine-fructose-6-phosphate amidotransferase, in the activation of the chitin synthesis pathway in response to cell-wall defects in Saccharomyces cerevisiae. *Eur J Biochem* **269**: 1697-1707.

Lane, S., C. Birse, S. Zhou, R. Matson & H. Liu, (2001) DNA array studies demonstrate convergent regulation of virulence factors by Cph1, Cph2, and Efg1 in Candida albicans. *J Biol Chem* **276**: 48988-48996.

Latge, J.P., (2007) The cell wall: a carbohydrate armour for the fungal cell. *Mol Microbiol* **66**: 279-290.

Lenardon, M.D., S.A. Milne, H.M. Mora-Montes, F.A. Kaffarnik, S.C. Peck, A.J. Brown, C.A. Munro & N.A. Gow, (2010a) Phosphorylation regulates polarisation of chitin synthesis in Candida albicans. *J Cell Sci* **123**: 2199-2206.

Lenardon, M.D., C.A. Munro & N.A. Gow, (2010b) Chitin synthesis and fungal pathogenesis. *Curr Opin Microbiol* **13**: 416-423.

Lenardon, M.D., R.K. Whitton, C.A. Munro, D. Marshall & N.A. Gow, (2007) Individual chitin synthase enzymes synthesize microfibrils of differing structure at specific locations in the Candida albicans cell wall. *Mol Microbiol* **66**: 1164-1173.

Liu, T.T., R.E. Lee, K.S. Barker, L. Wei, R. Homayouni & P.D. Rogers, (2005) Genome-wide expression profiling of the response to azole, polyene, echinocandin, and pyrimidine antifungal agents in Candida albicans. *Antimicrob Agents Chemother* **49**: 2226-2236.

Livak, K.J. & T.D. Schmittgen, (2001) Analysis of relative gene expression data using real-time quantitative PCR and the 2(-Delta Delta C(T)) Method. *Methods* **25**: 402-408.

Lotz, H., K. Sohn, H. Brunner, F.A. Muhlschlegel & S. Rupp, (2004) RBR1, a novel pH-regulated cell wall gene of Candida albicans, is repressed by RIM101 and activated by NRG1. *Eukaryot Cell* **3**: 776-784.

Mazan, M., N. Blanco, K. Kovacova, Z. Firakova, P. Rehulka, V. Farkas & J. Arroyo, A novel fluorescence assay and catalytic properties of Crh1 and Crh2 yeast cell wall transglycosylases. *Biochem J* **455**: 307-318.

Mazan, M., E. Ragni, L. Popolo & V. Farkas, (2011) Catalytic properties of the Gas family beta-(1,3)-glucanosyltransferases active in fungal cell-wall biogenesis as determined by a novel fluorescent assay. *Biochem J* **438**: 275-282.

Medina, I., J. Carbonell, L. Pulido, S.C. Madeira, S. Goetz, A. Conesa, J. Tarraga, A. Pascual-Montano, R. Nogales-Cadenas, J. Santoyo, F. Garcia, M. Marba, D. Montaner & J. Dopazo, (2010) Babelomics: an integrative platform for the analysis of transcriptomics, proteomics and genomic data with advanced functional profiling. *Nucleic Acids Res* **38**: W210-213.

Meyer, V., R.A. Damveld, M. Arentshorst, U. Stahl, C.A. van den Hondel & A.F. Ram, (2007) Survival in the presence of antifungals: genome-wide expression profiling of Aspergillus niger in response to sublethal concentrations of caspofungin and fenpropimorph. *J Biol Chem* **282**: 32935-32948.

Milewski, S., D. Kuszczak, R. Jedrzejczak, R.J. Smith, A.J. Brown & G.W. Gooday, (1999) Oligomeric structure and regulation of Candida albicans glucosamine-6-phosphate synthase. *J Biol Chem* **274**: 4000-4008.

Mouyna, I., M. Monod, T. Fontaine, B. Henrissat, B. Lechenne & J.P. Latge, (2000) Identification of the catalytic residues of the first family of beta(1-3)glucanosyltransferases identified in fungi. *Biochem J* **347 Pt 3**: 741-747.

Muhlschlegel, F.A. & W.A. Fonzi, (1997) PHR2 of Candida albicans encodes a functional homolog of the pH-regulated gene PHR1 with an inverted pattern of pH-dependent expression. *Mol Cell Biol* **17**: 5960-5967.

Munro, C.A., K. Winter, A. Buchan, K. Henry, J.M. Becker, A.J. Brown, C.E. Bulawa & N.A. Gow, (2001) Chs1 of Candida albicans is an essential chitin synthase required for synthesis of the septum and for cell integrity. *Mol Microbiol* **39**: 1414-1426.

Nantel, A., D. Dignard, C. Bachewich, D. Harcus, A. Marcil, A.P. Bouin, C.W. Sensen, H. Hogues, M. van het Hoog, P. Gordon, T. Rigby, F. Benoit, D.C. Tessier, D.Y. Thomas & M. Whiteway, (2002) Transcription profiling of Candida albicans cells undergoing the yeast-to-hyphal transition. *Mol Biol Cell* **13**: 3452-3465.

Oberholzer, U., A. Nantel, J. Berman & M. Whiteway, (2006) Transcript profiles of Candida albicans cortical actin patch mutants reflect their cellular defects: contribution of the Hog1p and Mkc1p signaling pathways. *Eukaryot Cell* **5**: 1252-1265.

Pardini, G., P.W. De Groot, A.T. Coste, M. Karababa, F.M. Klis, C.G. de Koster & D. Sanglard, (2006) The CRH family coding for cell wall glycosylphosphatidylinositol proteins with a predicted transglycosidase domain affects cell wall organization and virulence of Candida albicans. *J Biol Chem* **281**: 40399-40411.

Popolo, L., T. Gualtieri & E. Ragni, (2001) The yeast cell-wall salvage pathway. *Med Mycol* **39 Suppl 1**: 111-121.

Popolo, L. & M. Vai, (1998) Defects in assembly of the extracellular matrix are responsible for altered morphogenesis of a Candida albicans phr1 mutant. *J Bacteriol* **180**: 163-166.

Ragni, E., J. Calderon, U. Fascio, M. Sipiczki, W.A. Fonzi & L. Popolo, (2011a) Phr1p, a glycosylphosphatidylinsitol-anchored beta(1,3)-glucanosyltransferase critical for hyphal wall formation, localizes to the apical growth sites and septa in Candida albicans. *Fungal Genet Biol* **48**: 793-805.

Ragni, E., H. Piberger, C. Neupert, J. Garcia-Cantalejo, L. Popolo, J. Arroyo, M. Aebi & S. Strahl, (2011b) The genetic interaction network of CCW12, a Saccharomyces cerevisiae gene required for cell wall integrity during budding and formation of mating projections. *BMC Genomics* **12**: 107.

Ragni, E., M. Sipiczki & S. Strahl, (2007) Characterization of Ccw12p, a major key player in cell wall stability of Saccharomyces cerevisiae. *Yeast* **24**: 309-319.

Ram, A.F., J.C. Kapteyn, R.C. Montijn, L.H. Caro, J.E. Douwes, W. Baginsky, P. Mazur, H. van den Ende & F.M. Klis, (1998) Loss of the plasma membrane-bound protein Gas1p in Saccharomyces cerevisiae results in the release of beta1,3-glucan into the medium and induces a compensation mechanism to ensure cell wall integrity. *J Bacteriol* **180**: 1418-1424.

Ramage, G., K. Vande Walle, B.L. Wickes & J.L. Lopez-Ribot, (2001) Standardized method for in vitro antifungal susceptibility testing of Candida albicans biofilms. *Antimicrob Agents Chemother* **45**: 2475-2479.

Richard, M.L. & A. Plaine, (2007) Comprehensive analysis of glycosylphosphatidylinositol-anchored proteins in Candida albicans. *Eukaryot Cell* **6**: 119-133.

Rossignol, T., B. Kelly, C. Dobson & C. d'Enfert, (2011) Endocytosis-mediated vacuolar accumulation of the human ApoE apolipoprotein-derived ApoEdpL-W antimicrobial peptide contributes to its antifungal activity in Candida albicans. *Antimicrob Agents Chemother* **55**: 4670-4681.

Saeed, A.I., V. Sharov, J. White, J. Li, W. Liang, N. Bhagabati, J. Braisted, M. Klapa, T. Currier, M. Thiagarajan, A. Sturn, M. Snuffin, A. Rezantsev, D. Popov, A. Ryltsov, E. Kostukovich, I. Borisovsky, Z. Liu, A. Vinsavich, V. Trush & J. Quackenbush, (2003) TM4: a free, open-source system for microarray data management and analysis. *Biotechniques* **34**: 374-378.

Sanz, M., L. Carrano, C. Jimenez, G. Candiani, J.A. Trilla, A. Duran & C. Roncero, (2005) Candida albicans strains deficient in CHS7, a key regulator of chitin synthase III, exhibit morphogenetic alterations and attenuated virulence. *Microbiology* **151**: 2623-2636.

Saporito-Irwin, S.M., C.E. Birse, P.S. Sypherd & W.A. Fonzi, (1995a) *PHR1*, a pH-regulated gene of *Candida albicans*, is required for morphogenesis. *Mol. Cell. Biol.* **15**: 601-613.

Saporito-Irwin, S.M., C.E. Birse, P.S. Sypherd & W.A. Fonzi, (1995b) PHR1, a pH-regulated gene of Candida albicans, is required for morphogenesis. *Mol Cell Biol* **15**: 601-613.

Shen, J., W. Guo & J.R. Kohler, (2005) CaNAT1, a heterologous dominant selectable marker for transformation of Candida albicans and other pathogenic Candida species. *Infect Immun* **73**: 1239-1242.

Sillo, F., C. Gissi, D. Chignoli, E. Ragni, L. Popolo & R. Balestrini, (2013) Expression and phylogenetic analyses of the Gel/Gas proteins of Tuber melanosporum provide insights into the function and evolution of glucan remodeling enzymes in fungi. *Fungal Genet Biol* **53**: 10-21.

Smyth, (2005) Limma: linear models in microarray data. In: Bioinformatics and Computational Biology Solutions using R and Bioconductor

C.V. Gentleman R, Dudoit S, Izrizarry R, Huber W (ed). Springer, New York, pp. 397-420.

Sudoh, M., T. Yamazaki, K. Masubuchi, M. Taniguchi, N. Shimma, M. Arisawa & H. Yamada-Okabe, (2000) Identification of a novel inhibitor specific to the fungal chitin synthase. Inhibition of chitin synthase 1 arrests the cell growth, but inhibition of chitin synthase 1 and 2 is lethal in the pathogenic fungus Candida albicans. *J Biol Chem* **275**: 32901-32905.

Valdivieso, M.H., L. Ferrario, M. Vai, A. Duran & L. Popolo, (2000) Chitin synthesis in a gas1 mutant of Saccharomyces cerevisiae. *J Bacteriol* **182**: 4752-4757.

Walker, L.A., M.D. Lenardon, K. Preechasuth, C.A. Munro & N.A. Gow, (2013) Cell wall stress induces alternative fungal cytokinesis and septation strategies. *J Cell Sci* **126**: 2668-2677.

Walker, L.A., C.A. Munro, I. de Bruijn, M.D. Lenardon, A. McKinnon & N.A. Gow, (2008) Stimulation of chitin synthesis rescues Candida albicans from echinocandins. *PLoS Pathog* **4**: e1000040.

Walther, A. & J. Wendland, (2003) An improved transformation protocol for the human fungal pathogen Candida albicans. *Curr Genet* **42**: 339-343.

Weig, M., K. Haynes, T.R. Rogers, O. Kurzai, M. Frosch & F.A. Muhlschlegel, (2001) A GAS-like gene family in the pathogenic fungus Candida glabrata. *Microbiology* **147**: 2007-2019.

Wilson, D., S. Thewes, K. Zakikhany, C. Fradin, A. Albrecht, R. Almeida, S. Brunke, K. Grosse, R. Martin, F. Mayer, I. Leonhardt, L. Schild, K. Seider, M. Skibbe, S. Slesiona, B. Waechtler, I. Jacobsen & B. Hube, (2009) Identifying infection-associated genes of Candida albicans in the postgenomic era. *FEMS Yeast Res* **9**: 688-700.

Yesland, K. & W.A. Fonzi, (2000) Allele-specific gene targeting in *Candida albicans* results from heterology between alleles. *Microbiology* **146**: 2097-2104.

Yuan, X., B.M. Mitchell, X. Hua, D.A. Davis & K.R. Wilhelmus, The RIM101 signal transduction pathway regulates Candida albicans virulence during experimental keratomycosis. *Invest Ophthalmol Vis Sci* **51**: 4668-4676.

Table 1. Functional categories and number of genes in Class1 or Class 2

	Functional category	1h	3h	5h
Class 1				
	Unknown function	38	11	32
	Cell wall/surface	13	14	11
	Metabolism and energy	11	6	4
	Filamentous growth	10	3	8
	DNA replication and repair	10	10	2
	Chromatin and chromosomes	5	7	0
	Transcription	5	3	4
	Cell cycle control/morphogenesis	4	6	6
	Transport	4	3	3
	Signal transduction	3	2	4
	Cell polarity/cytoskeleton	3	1	2
	Oxido-reduction processes	6	2	2
	Protein modification/folding	2	1	4
	Adhesion	1	0	0
	Stress response	1	2	2
	RNA processing and biogenesis	1	0	0
	Pathogenesis	0	0	1
Class 2				
	RNA processing and biogenesis	21	2	6
	Unknown function	11	16	31
	Transport	5	5	9
	Metabolism and energy	3	6	16
	Transcription	3	3	8
	Protein modification/folding	2	4	3
	Cell wall/surface	1	2	2
	Oxido-reduction processes	1	1	6
	Adhesion	1	0	3
	Signal transduction	0	0	2
	Stress response	0	2	2

Table 2. Selected genes modulated in the *PHR1* null mutant ordered into different biological processes.

Functional category	Systematic name	*Locus name*	*S.cerevisiae best hit*	1h RF	3h RF	5h RF	Description
CLASS 1							
Cell wall/surface	orf19.3740	*PGA23*	-	21.5	22.2	65.6	GPI protein
	orf19.750			6.4	11.1	36.0	In vitro substrate of Kex2p
	orf19.535	*RBR1*	-		2.4	6.7	GPI protein
	orf19.5384	*CHS8*	*CHS1*	2.2	2.0	4.3	Chitin synthase
	orf19.6420	*PGA13*	-		4.1	3.7	GPI protein
	orf19.2706	*CRH11*	*CRH1*	4.7	4.2	3.3	GPI transglycosylase
	orf19.4225	*ECM331*	*PST1*	2.3	5.2	5.3	GPI protein
	orf19.4765	*PGA6*	*CCW12*	2.8	6.8	3.4	GPI protein
	orf19.2685	*PGA54*	-	2.0	3.5		GPI protein
	orf19.1690	*TOS1*	*TOS1*		2.5		Putative β(1,3)-glucanase
	orf19.6594	*PLB3*	*PLB1*		2.3		GPI anchored phospholipase B
	orf19.7298	*CHS2*	*CHS1*	2.4	2.0		Chitin synthase
	orf19.2952	*EXG2*	*EXG2*	2.2			GPI-anchored exo-β-1,3-glucosidase cell wall protein
	orf19.2990	*XOG1*	*EXG1*	2.3		5.9	Exo-β(1,3)-glucanase
	orf19.3893	*SCW11*	*SCW11*			2.8	Cell wall protein similar to glucanases
	orf19.5305	*RHD3*			3.4	n.a.	Yeast associated GPI-protein
	orf19.675			6			Cell wall protein
	orf19.7214		*YBR056W*	2.4			Glucan 1,3-β-glucosidase
	orf19.6202	*RBT4*	*PRY3*	2.2	10	8.9	PRY family protein
Protein folding modification	orf19.1665	*MNT1*	*KTR1*	2.4			Golgi α(1,2)-mannosyltransferase
	orf19.6864			2.5		3.5	Protein ubiquitylation
	orf19.2444	*CHS7*	*CHS7*	n.a.	n.a.	2.4	Export Chs3p from ER
	orf19.6029	*ROT1*	*ROT1*		2.8	2.3	ER chaperone- β(1,6)-glucan synthesis
	orf19.3682	*CWH8*				2	Dol-P-P) phosphatase
Metabolism	orf19.9186	*GFA1*	*GFA1*	2.8	2.1	2.3	Glucosamine-6P synthase
	orf19.979	*FAS1*	*FAS1*	2.9	2.0		β-subunit of fatty acid synthase
	orf19.7466	*ACC1*	*ACC1*	2.6	2.0		Acetyl-coenzyme-A carboxylase
	orf19.5949	*FAS2*	*FAS2*	2.5	2.0		α-subunit of fatty acid synthase
	orf19.6459	*DPP3*	*DPP1*	3.1			DGPP phosphatase; farnesol synthesis
	orf19.837	*GNA1*	*GNA1*	2.1			Glucosamine-6P acetyltransferase
	orf19.24	*RTA2*	*RSB1*	4.8	3.3	3.9	Flippase for sphingolipid release
Stress response	orf19.4082	*DDR48*	*DDR48*		4.5	3.4	Immunogenic stress-associated protein
	orf19.2125			2.1	3.1	2.4	CipC-like ant biotic response protein
Signal transduction	orf19.4866	*CPP1*	*MSG5*			5.2	MAPK phosphatase
	orf19.3775	*SSK2*	*SSK2*		2.1	4.7	MAPKKK
	orf19.3216			2.5	3.0	3.6	Rab GTPase activatorr
	orf19.5797	*PLC2*		5.3		3.0	PI-PLC
	Orf19.7504		*RST3*	2.6			Phosphatase type 2A complex
DNA replication/repair	orf19.4616	*POL30*	*POL30*	2.6		2.6	PCNA
	orf19.5182	*POL3*	*POL3*			2.2	Catalytic subunit of DNA pol delta
	orf19.3752	*RAD51*	*RAD51*		3.3		Homologous recombination and repair
	orf19.3322	*DUT1*	*DUT1*	2.3	3.2		dTTP *de novo* biosynthesis
	orf19.4945	*MSH6*	*MSH6*		3.1		Mismatch repair
	orf19.2267	*RFA2*	*RFA2*		2.4		Putative DNA replication factor A
	orf19.2093	*RFA1*	*RFA1*	2.2	2.1		Putative DNA replication factor A
	orf19.7425		UNG1	2			Base-excision repair
	orf19.2796		POL12	3.5	n.a.	n.a.	DNA replication initiation
	orf19.5873	*POL1*	*POL1*	3.2	n.a.	n.a.	DNA polymerase α
	orf19.3761	*CDC54*	*MCM4*	2.4			Pre-replication complex helicase subunit
	orf19.5779	*RNR1*	*RNR1*	2	3.4		Subunit of r bonucleotide reductase
	orf19.926	*EXO1*	*EXO1*		3.2		Exodeoxyr bonuclease
	orf19.4030		*PRI1*		2.7		Orthologs have DNA primase activity
	orf19.5487	*CDC46*	*MCM5*	2.6	2.5		MCM helicase complex subunit
	orf19.2611	*MCM6*	*MCM6*	2	2.3		MCM replication initiation complex subunit
Chromatin	orf19.1854	*HHF22*	*HHF2*	2.2	2.6		Putative histone H4
	orf19.1052		*HTB1*		3.2		Putative histone H2B
	orf19.1059	*HHF1*	*HHF1*		3.2		Putative histone H4
	orf19.6924	*HTA1*	*HTA1*	2.1	2.9		Histone H2A
	orf19.1051	*HTA2*	*HTA1*		2.4		Putative histone H2A
	orf19.6925	*HTB1*	*HTB1*		2.2		Histone H2B
	orf19.7232	*IRR1*	*IRR1*	2.3			Putative cohesin complex subunit
	orf19.3715	*ASF1*	*ASF1*	2.2			Chromatin assembly complex
	orf19.6568	*SMC6*	*SMC6*		2.0		SMC protein
	orf19.4664	*NAT4*	*NAT4*	2.6	n.a.		Putative histone acetyl transferase

CLASS 2							
Adhesion	orf19.1097	*ALS2*	*SAG1*			0.2	GPI protein; Adhesin
	orf19.4555	*ALS4*	*SAG1*		n.a.	0.4	GPI protein; Adhesin
	orf19.5267			0.4	n.a.		Putative adhesion-like protein

RF is the ratio between the expression ratio of each gene in the *phr1* mutant and in the control
CLASS 1: RF ≥ 2 refer to transcripts that are at least 2 times more abundant in the mutant than in the wild type and that passed the statistical criteria (see Table S1 and Material and methods). Among the genes of Table S1, only genes that were upregulated by two-fold in the mutant (expression ratio ≥ 2) are shown.

CLASS 2: RF ≤ 0.5 indicate transcripts that are less abundant in the mutant than in the wild type (see Table S2).
The lack of value indicates that RF is present but does not pass the cut-off.
n.a.: value not available because the expression ratio is statistically not significant or technically incomplete (less than three replicates) in either one of the strains or both.

Table 3. *Candida albicans* strains used in this work

Strain	Parental Strain	Genotype*	Source or reference
CAF2-1	SC5314	*URA3/ura3*Δ::*λimm434*	[Fonzi &Irwin, 1993]
CAI4	CAF2-1	*ura3* Δ::*λimm434*/*ura3*Δ:: *λimm434*	[Fonzi &Irwin, 1993]
CAF3-1	CAF2-1	*ura3* Δ::*λimm434*/*ura3*Δ:: *λimm434*	[Fonzi &Irwin, 1993]
CAS8	CAF3-1	*phr1*Δ*::hisG/phr1*Δ	[Saporito-Irwin *et al.*, 1995]
CAI10	CAF3-1	*URA3/ura3* Δ::*λimm434*	[Fonzi &Irwin, 1993]
CAS10	CAS8	*phr1*Δ*::hisG/phr1*Δ *URA3/ura3* Δ::*λimm434*	[Saporito-Irwin *et al.*, 1995]
C155	CAI4	*chs2*Δ::*hisG/chs2*Δ::*hisG*	[Walker *et al*., 2008]
FP155-14-21	C155	*phr1*Δ*::hisG-URA3-hisG/phr1*Δ*::NAT1 chs2*Δ*::hisG/chs2*Δ*::hisG*	This work
FP155-19-21	C155	*phr1*Δ*::hisG-URA3-hisG/phr1*Δ*::NAT1 chs2*Δ*::hisG/chs2*Δ*::hisG*	This work
Myco3	CAI4	*chs3*Δ::*hisG/chs3*Δ::*hisG*	[Walker *et al*., 2008]
FP3-19-211	Myco3	*phr1*Δ*::hisG-URA3-hisG/phr1*Δ*::NAT1 chs3*Δ*:: hisG/chs3*Δ*::hisG*	This work
FP3-118-25	Myco3	*phr1*Δ*::hisG-URA3-hisG/phr1*Δ*::NAT1 chs3*Δ*:: hisG/chs3*Δ*::hisG*	This work
NGY128	CAI4	*chs8*Δ::*hisG/chs8*Δ::*hisG*	[Walker *et al*., 2008]
FP128-19-21	NGY128	*phr1*Δ*::hisG-URA3-hisG/phr1*Δ*::NAT1 chs8*Δ*::hisG/chs8*Δ*::hisG*	This work
FP128-111-21	NGY128	*phr1*Δ*::hisG-URA3-hisG/phr1*Δ*::NAT1 chs8*Δ*:: hisG/chs8*Δ*::hisG*	This work
NGY138	CAI4	*chs2*Δ*::hisG/chs2*Δ*::hisG chs8*Δ*:: hisG/chs8*Δ*::hisG*	[Walker *et al*., 2008]
FP138-16-22	NGY138	*phr1*Δ*::hisG-URA3-hisG/phr1*Δ*::NAT1 chs2*Δ*::hisG/chs2*Δ*::hisGchs8*Δ*::hisG/chs8*Δ*::hisG*	This work
FP138-114-21	NGY138	*phr1*Δ*::hisG-URA3-hisG/phr1*Δ*::NAT1 chs2*Δ*::hisG/chs2*Δ*::hisGchs8*Δ*::hisG/chs8*Δ*::hisG*	This work

*all strains apart from CAF2-1, CAI10 and CAS10 are homozygous for the *ura3* Δ::*λimm434* mutation [Fonzi & Irwin, 1993]

Figure 1

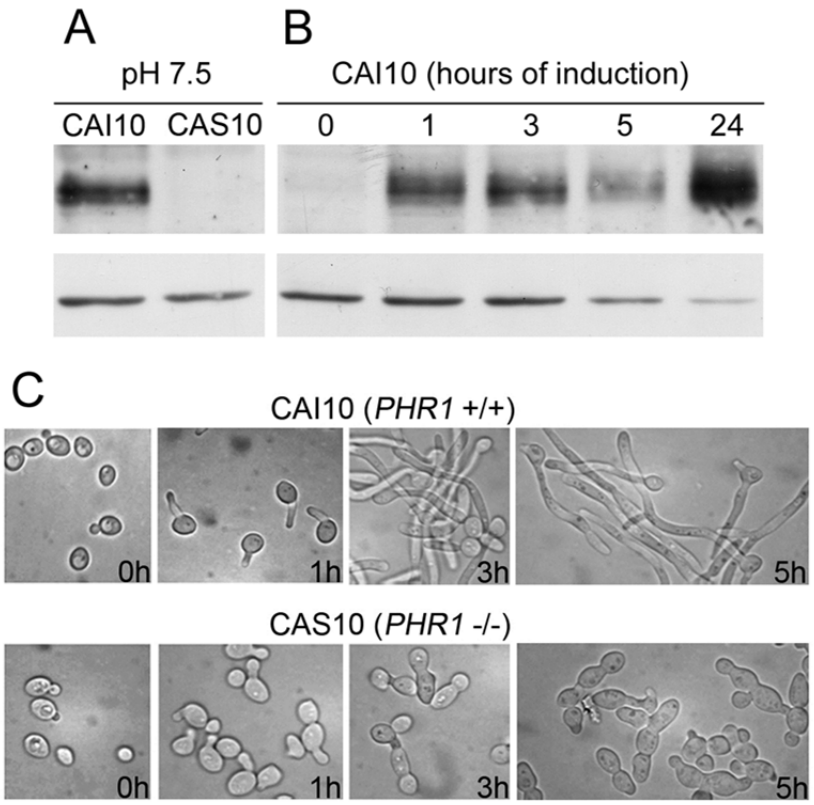
A
pH 7.5
CAI10
CAS10
B
CAI10 (hours of induction)
0
1
3
5
24
C
CAI10 (PHR1 +/+)
0h
1h
3h
5h
CAS10 (PHR1 -/-)
0h
1h
3h
5h

Figure 2

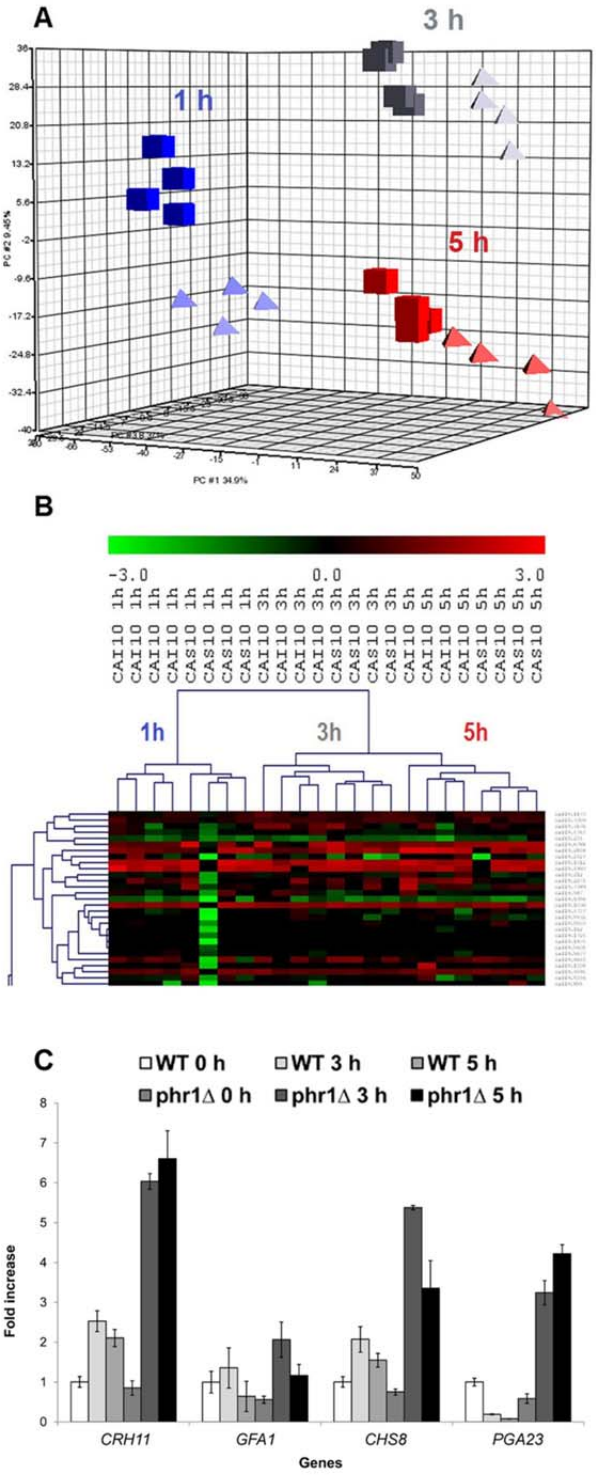
A
3 h
1 h
5 h
B
-3.0
0.0
3.0
1h
3h
5h
C
WT 0 h
WT 3 h
WT 5 h
phr1Δ 0 h
phr1Δ 3 h
phr1Δ 5 h
Fold increase
CRH11
GFA1
CHS8
PGA23
Genes

Figure 3

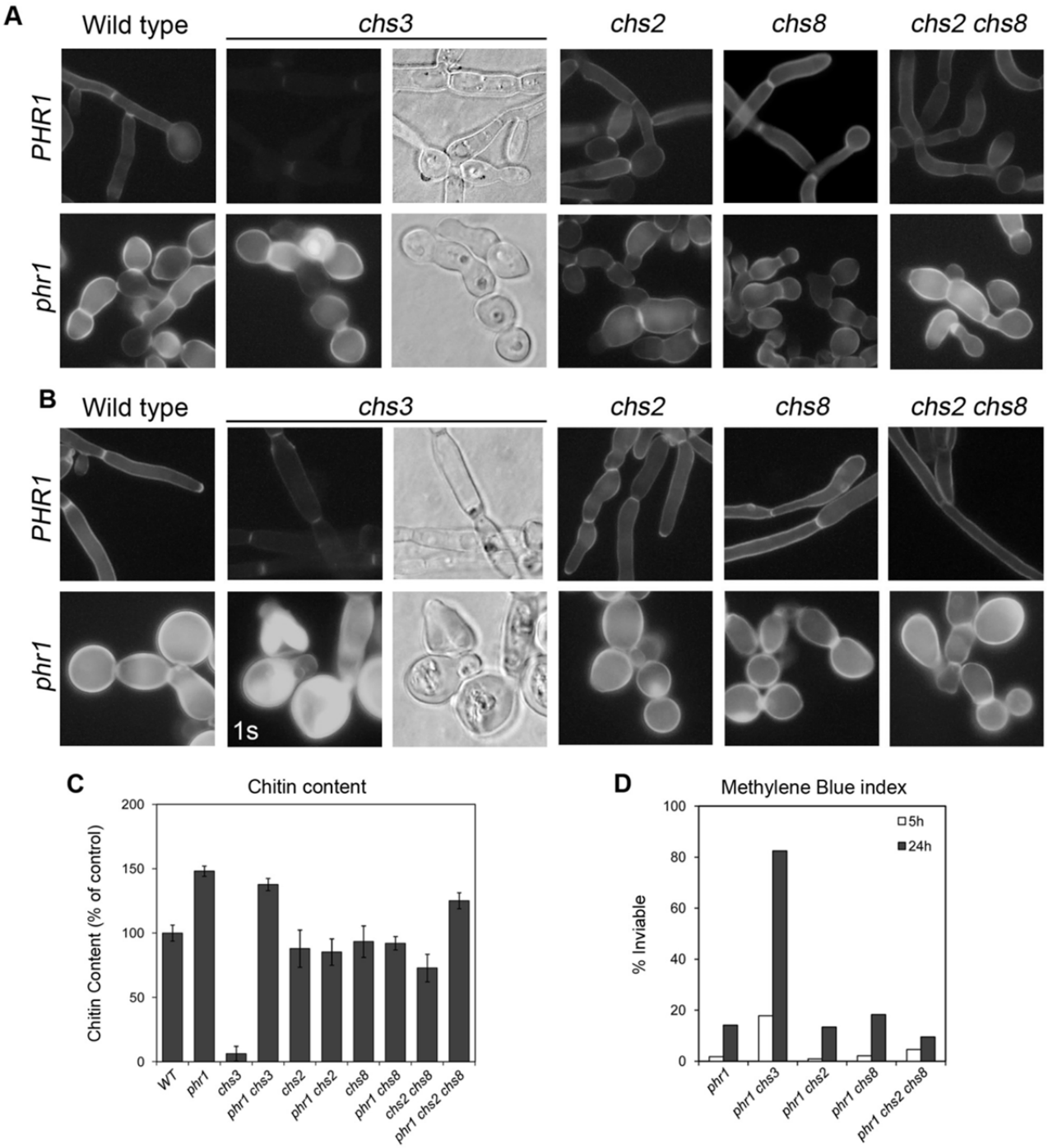
A
Wild type
chs3
chs2
chs8
chs2 chs8
PHR1
phr1
B
Wild type
chs3
chs2
chs8
chs2 chs8
PHR1
phr1
1s
C
Chitin content
Chitin Content (% of control)
200
150
100
50
0
WT
phr1
chs3
phr1 chs3
chs2
phr1 chs2
chs8
phr1 chs8
chs2 chs8
phr1 chs2 chs8
D
Methylene Blue index
% Inviable
100
80
60
40
20
0
5h
24h
phr1
phr1 chs3
phr1 chs2
phr1 chs8
phr1 chs2 chs8

Figure 4

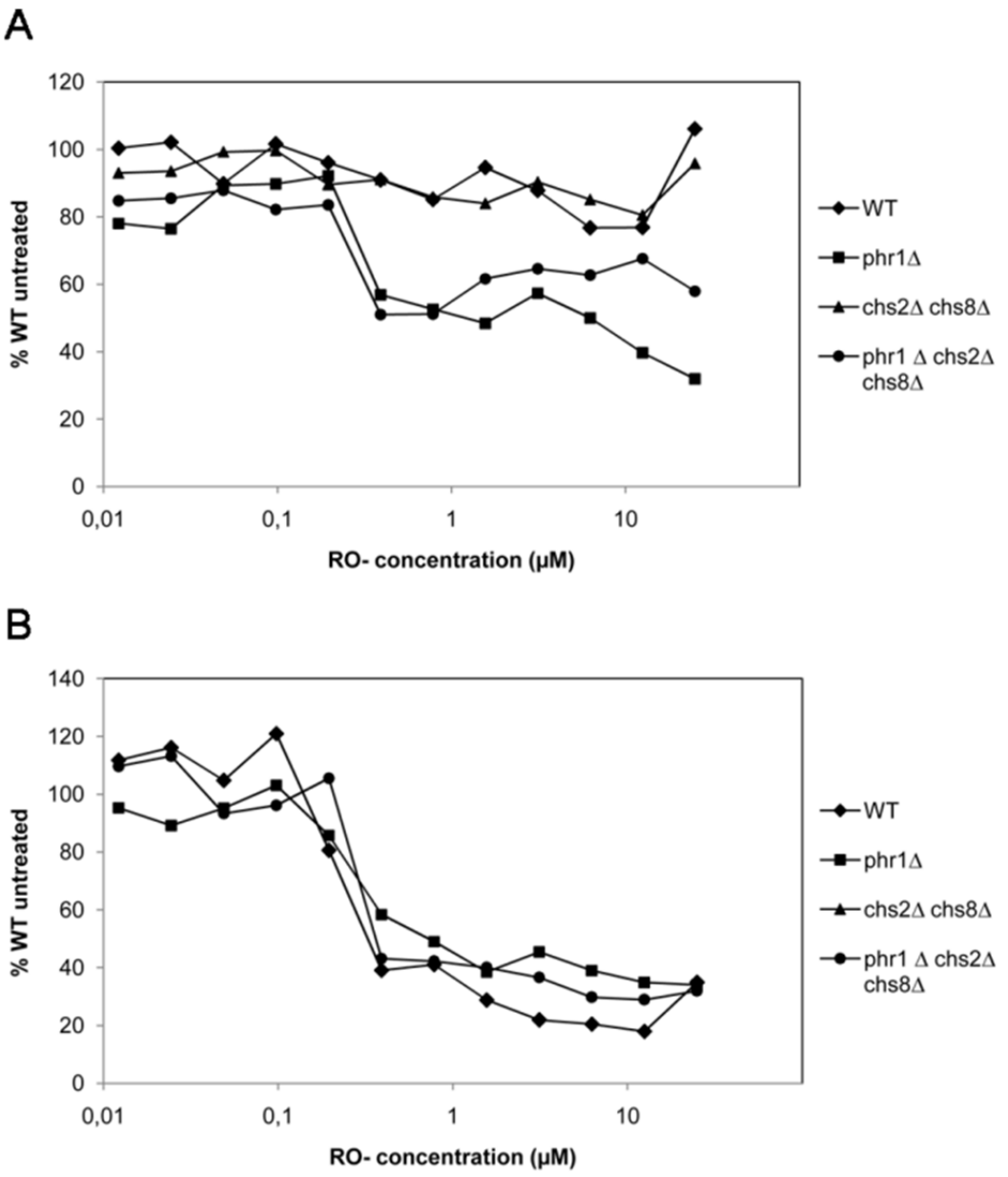
A
120
100
80
60
40
20
0
% WT untreated
0,01
0,1
1
10
RO- concentration (µM)
WT
phr1Δ
chs2Δ chs8Δ
phr1 Δ chs2Δ chs8Δ
B
140
120
100
80
60
40
20
0
% WT untreated
0,01
0,1
1
10
RO- concentration (µM)
WT
phr1Δ
chs2Δ chs8Δ
phr1 Δ chs2Δ chs8Δ

Figure 5

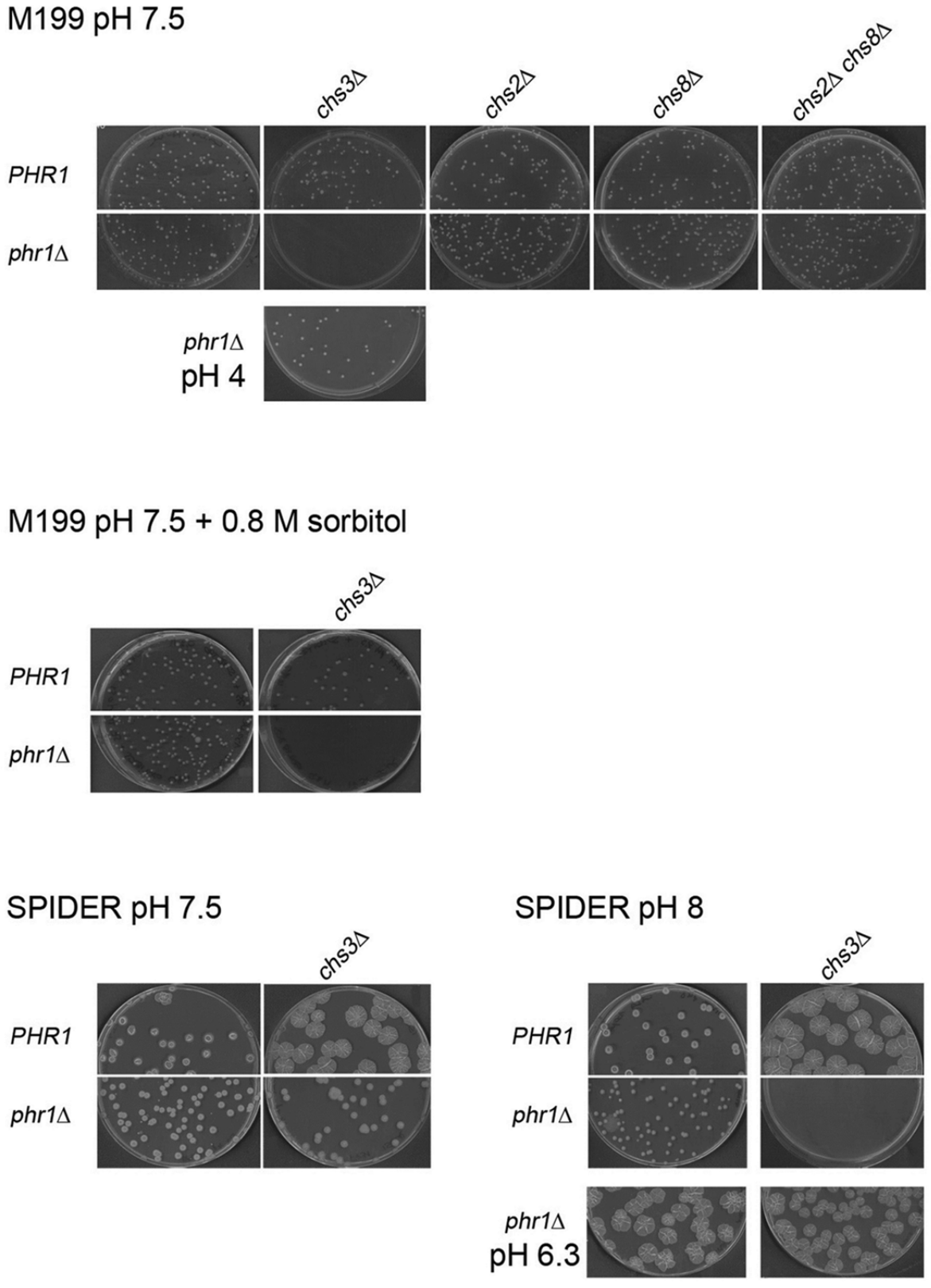
M199 pH 7.5
chs3Δ
chs2Δ
chs8Δ
chs2Δ chs8Δ
PHR1
phr1Δ
phr1Δ
pH 4
M199 pH 7.5 + 0.8 M sorbitol
chs3Δ
PHR1
phr1Δ
SPIDER pH 7.5
chs3Δ
PHR1
phr1Δ
SPIDER pH 8
chs3Δ
PHR1
phr1Δ
phr1Δ
pH 6.3

Figure 6

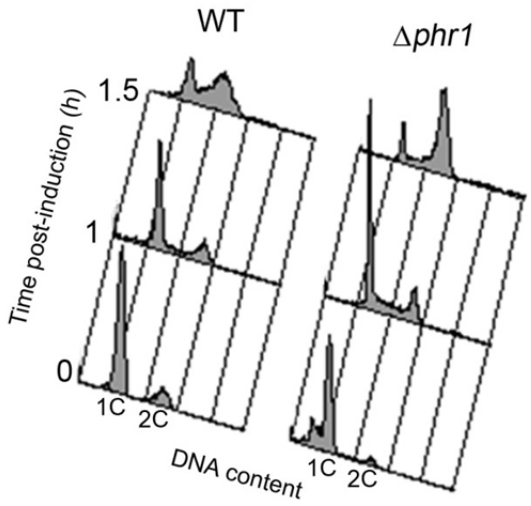

Figure 7

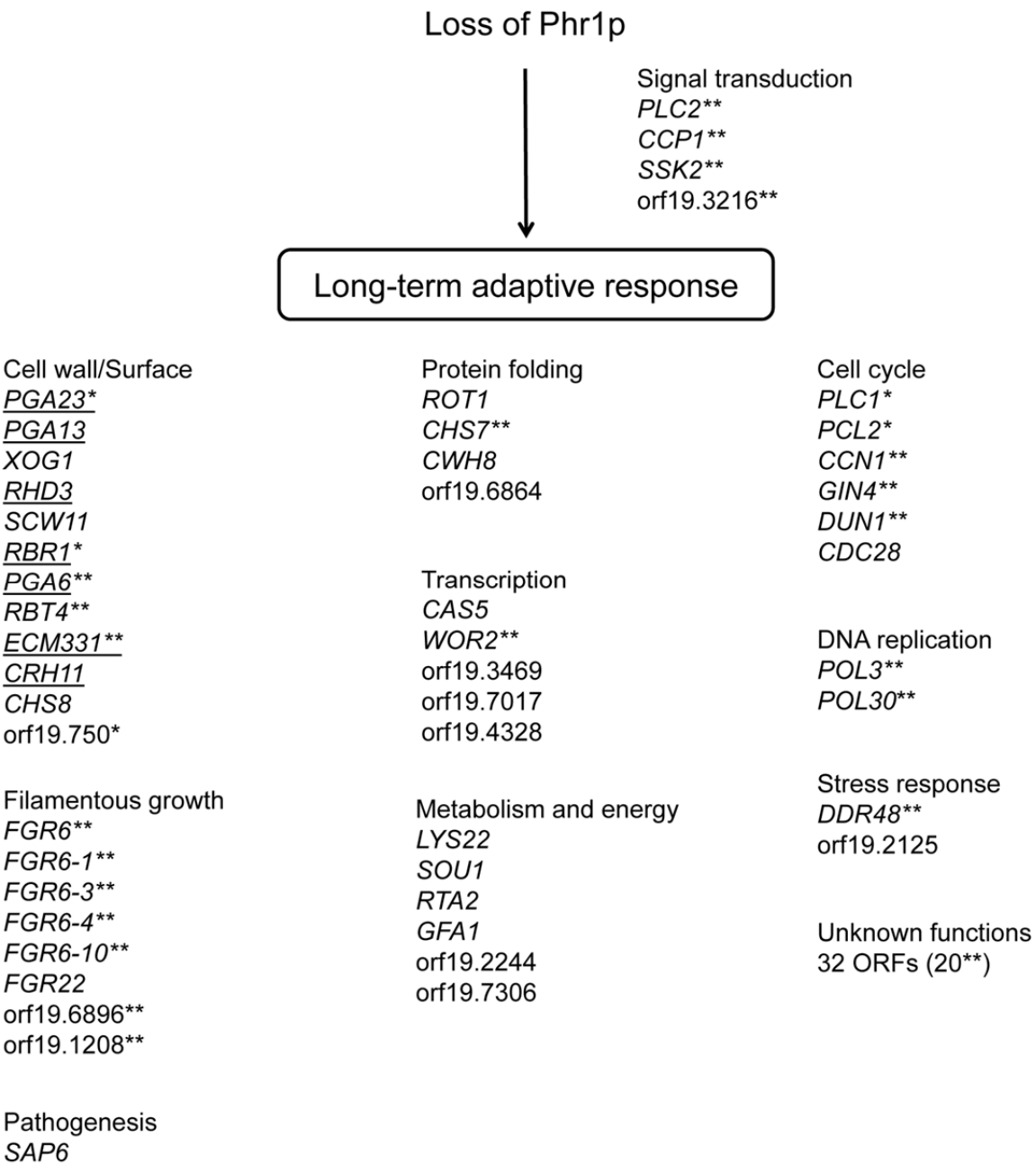
Loss of Phr1p
Signal transduction
PLC2**
CCP1**
SSK2**
orf19.3216**
Long-term adaptive response
Cell wall/Surface
PGA23*
PGA13
XOG1
RHD3
SCW11
RBR1*
PGA6**
RBT4**
ECM331**
CRH11
CHS8
orf19.750*
Filamentous growth
FGR6**
FGR6-1**
FGR6-3**
FGR6-4**
FGR6-10**
FGR22
orf19.6896**
orf19.1208**
Pathogenesis
SAP6
Protein folding
ROT1
CHS7**
CWH8
orf19.6864
Transcription
CAS5
WOR2**
orf19.3469
orf19.7017
orf19.4328
Metabolism and energy
LYS22
SOU1
RTA2
GFA1
orf19.2244
orf19.7306
Cell cycle
PLC1*
PCL2*
CCN1**
GIN4**
DUN1**
CDC28
DNA replication
POL3**
POL30**
Stress response
DDR48**
orf19.2125
Unknown functions
32 ORFs (20**)

Table S1. Class 1 - transcripts that are more abundant in the phr1Δ than in the wild type

Green: expression ratio ≤ 0.5 each time was compared to time zero in the same strain
Red: expression ratio ≥ 2
Light blue: mutant/wild type ≥ except values obtained from two expression rations ≤ 0.5 (green/green)

Time after induction			1 h			3 h			5 h			
ORF	**GeneName**	**Functional category**	**WT**	***phr*1**	***phr*1/WT (RF)**	**WT**	***phr*1**	***phr*1/WT (RF)**	**WT**	***phr*1**	***phr*1/WT (RF)**	**Description**
orf19.5741	ALS1	Adhesion	0,5	1,4	2,8	0,2	0,2	1,4	0,4	0,1	0,2	Adhesin, ALS family
orf19.2649	PCL1	Cell cycle control/morphogenesis							0,3	3,8	11,7	Cyclin homolog
orf19.403	PCL2	Cell cycle control/morphogenesis	0,5	1,9	3,9	0,1	1,6	10,7	0,3	2,3	6,7	Cyclin homolog
orf19.3856	CDC28	Cell cycle control/morphogenesis	2,9	4,6	1,6	1,6	3,1	2,0	2,2	5,3	2,4	Cyclin-dependent protein kinase
orf19.3207	CCN1	Cell cycle control/morphogenesis	0,7	2,4	3,5	0,4	2,5	6,0	0,7	5,7	7,9	G1 cyclin; Cdc28p-Ccn1p initiates Cdc11p phosphorylation on hyphal induction
orf19.663	GIN4	Cell cycle control/morphogenesis	2,0	3,9	2,0	0,6	2,4	4,0	1,0	3,2	3,2	Septin ring assembly; phosphorylates septin Cdc11
orf19.4002	DUN1	Cell cycle control/morphogenesis	2,0	2,2	1,1				1,0	2,1	2,1	Protein kinase involved in DNA damage cell-cycle checkpoint
orf19.4308	HSL1	Cell cycle control/morphogenesis	1,8	5,3	2,9	1,5	3,3	2,2	1,9	3,6	1,9	Protein kinase involved in determination of morphology via regulation of Swe1p andCdc28p
orf19.4257	INT1	Cell cycle control/morphogenesis	1,7	2,2	1,3	1,0	2,0	2,1	1,3	2,3	1,8	Structurally similar to human leukocyte integrin; involved in adhesion and morphogenesis regulation
orf19.3501		Cell polarity/cytoskeleton	2,4	4,1	1,7	1,0	2,0	2,1	1,6	2,7	1,7	Sc ortholog Pxl1 localizes to sites of polarized growth; required for selection and/or maintenance of polarized growth sites
orf19.2416.1	MLC1	Cell polarity/cytoskeleton	5,2	10,3	2,0	3,3	5,8	1,8	4,0	5,7	1,4	Microtubule-dependent localized protein to Spitzenkorper and cytokinetic ring in hyphae
orf19.17	SCP1	Cell polarity/cytoskeleton	0,5	1,1	2,2	0,7	1,1	1,5	0,4	1,2	2,7	Putative cortical actin cytoskeleton protein
orf19.5544	SAC6	Cell polarity/cytoskeleton	0,3	0,9	2,6	1,3	1,7	1,3	1,6	2,2	1,4	Fimbrin; actin filament bundling protein
orf19.6610		Cell polarity/cytoskeleton	1,2	1,6	1,3	0,6	1,4	2,1	0,7	2,2	2,9	Microtubule binding
orf19.3740	PGA23	Cell wall/surface	0,1	1,8	21,5	0,2	4,2	22,2	0,2	10,2	65,6	Predicted GPI-anchored cell surface protein
orf19.750		Cell wall/surface	0,2	1,2	6,4	0,3	3,6	11,1	0,2	7,6	36,0	Predicted cell wall protein; *in vitro* substrate for Kex2p
orf19.535	RBR1	Cell wall/surface	0,2	0,2	1,4	0,3	0,7	2,4	0,3	2,3	6,7	GPI-anchored cell wall protein, repressed by Rim101
orf19.5384	CHS8	Cell wall/surface	3,8	8,3	2,2	3,0	5,9	2,0	2,6	11,1	4,3	Chitin synthase for long fibrils, induced by cell wall regeneration
orf19.6420	PGA13	Cell wall/surface	0,1	0,4	3,4	1,8	7,2	4,1	8,9	32,8	3,7	GPI-anchored cell wall protein
orf19.2706	CRH11	Cell wall/surface	2,0	9,3	4,7	1,2	5,1	4,2	2,3	7,6	3,3	GPI-cell wall transglycosylase of GH16 family, CS-induced
orf19.4255	ECM331	Cell wall/surface	2,3	5,4	2,3	1,0	5,4	5,2	1,2	6,3	5,3	GPI-anchored plasma membrane and cell wall protein, CS-induced
orf19.4765	PGA6	Cell wall/surface	2,2	6,2	2,8	0,5	3,4	6,8	0,9	3,2	3,4	GPI-cell wall protein, similar to *Sc* CCW12
orf19.2685	PGA54	Cell wall/surface	8,5	16,9	2,0	6,3	22,1	3,5	14,1	24,3	1,7	Putative GPI-anchored protein
orf19.1690	TOS1	Cell wall/surface	4,3	7,5	1,8	1,0	2,5	2,5	2,7	5,0	1,9	Protein similar to alpha agglutinin anchor subunit
orf19.6594	PLB3	Cell wall/surface	0,8	1,2	1,5	1,0	2,4	2,3	2,1	3,2	1,5	GPI-anchored cell surface phospholipase B
orf19.7298	CHS2	Cell wall/surface	2,0	4,8	2,4	1,3	2,6	2,0	2,5	3,3	1,3	Chitin synthase; required for wild-type chitin deposition in hyphae; transcription is regulated during dimorphic transition
orf19.2952	EXG2	Cell wall/surface	3,0	6,6	2,2	2,3	3,1	1,4	2,9	3,8	1,3	GPI-anchored cell wall protein,similar to Sc exo-1,3-beta-glucosidase Exg2p;predicted Kex2p substrate
orf19.2990	XOG1	Cell wall/surface	0,5	1,2	2,3	0,1	0,3	3,1	0,2	1,3	5,9	Major exo-β(1,3)-glucanase family GH5
orf19.3893	SCW11	Cell wall/surface	1,0	0,6	0,6	0,6	0,8	1,4	0,3	0,8	2,8	Cell wall protein; downregulated in core caspofunginresponse
orf19.5305	RHD3	Cell wall/surface	0,8	1,7	2,0	0,4	1,5	3,4				GPI-anchored yeast-associated cell wall protein
orf19.675		Cell wall/surface	0,1	0,8	6,0	0,3	0,4	1,2	0,7	0,8	1,2	Cell wall protein of unknown function; induced in core CS-response
orf19.7214		Cell wall/surface	0,2	0,6	2,4	2,3	2,1	0,9	4,5	5,7	1,3	β(1,3)-glucan endoglucosidase; induced during cell wall regeneration
orf19.6202	RBT4	Cell wall/surface	2,9	6,2	2,2	0,4	4,1	10,0	1,0	9,3	8,9	Extracellular Pry family member
orf19.1854	HHF22	Chromatin and chromosomes	2,3	5,2	2,2	2,1	5,4	2,6	3,1	4,2	1,3	Putative histone H4
orf19.1052		Chromatin and chromosomes	2,0	3,4	1,7	1,3	4,3	3,2	2,1	2,5	1,2	Predicted histone H2B
orf19.1059	HHF1	Chromatin and chromosomes	2,7	4,5	1,7	1,7	5,5	3,2	3,1	4,0	1,3	Putative histone H4
orf19.6924	HTA1	Chromatin and chromosomes	2,3	5,0	2,1	1,5	4,2	2,9	2,3	3,1	1,3	Histone H2A
orf19.1051	HTA2	Chromatin and chromosomes	2,9	4,4	1,5	1,7	4,2	2,4	2,3	2,3	1,0	Putative histone H2A
orf19.6925	HTB1	Chromatin and chromosomes	2,2	3,8	1,7	1,6	3,7	2,2	2,4	2,1	0,9	Histone H2B
orf19.7232	IRR1	Chromatin and chromosomes	1,9	4,5	2,3	0,8	1,7	2,0	1,0	1,5	1,6	Putative cohesin complex subunit
orf19.3715	ASF1	Chromatin and chromosomes	1,4	3,2	2,2				0,7	1,2	1,8	Protein similar to S.cerevisiae Asf1p, which is a chromatin assembly complex component
orf19.6568	SMC6	Chromatin and chromosomes	0,9	1,3	1,5	0,3	0,7	2,0	0,6	0,8	1,4	Putative structural maintenance of chromosomes (SMC) protein
orf19.4664	NAT4	Chromatin and chromosomes	0,4	1,2	2,6				0,2	0,2	0,8	Putative histone acetyl transferase
orf19.4616	POL30	DNA replication and repair	1,5	4,0	2,6	0,5	1,9	3,5	0,9	2,4	2,6	Putative DNA pol processivity factor
orf19.5182	POL3	DNA replication and repair	1,2	1,6	1,4	0,9	1,5	1,6	0,9	2,0	2,2	Catalytic subunit of DNA pol delta
orf19.3752	RAD51	DNA replication and repair	2,5	3,4	1,3	0,9	3,0	3,3	1,7	2,3	1,3	Protein involved in homologous recombination and DNA repair
orf19.3322	DUT1	DNA replication and repair	2,0	4,6	2,3	0,7	2,3	3,2	0,9	1,8	2,0	dUTP-pyrophosphatase, dTTP *de novo* biosynthesis
orf19.4945	MSH6	DNA replication and repair	2,2	3,1	1,5	1,2	3,9	3,1				Protein similar to Sc Msh6p, which isinvolved in mismatch repair
orf19.2267	RFA2	DNA replication and repair	1,8	3,0	1,7	0,9	2,1	2,4	1,3	1,5	1,2	Putative DNA replication factor A
orf19.2093	RFA1	DNA replication and repair	1,2	2,7	2,2	1,0	2,1	2,1	1,1	2,2	1,9	Putative DNA replication factor A
orf19.7425		DNA replication and repair	2,3	4,6	2,0	2,2	4,2	1,9	3,0	3,6	1,2	Base-excision repair
orf19.2796		DNA replication and repair	1,2	4,2	3,5							DNA replication initiation
orf19.5873	POL1	DNA replication and repair	1,8	5,6	3,2							Putative DNA directed DNA polymerase α

orf19.3761	CDC54	DNA replication and repair	0,9	2,1	2,4	0,3	0,5	1,4	0,5	0,9	1,7	Putative pre-replication complex helicase subunit
orf19.5779	RNR1	DNA replication and repair	2,1	4,1	2,0	0,4	1,4	3,4	1,0	1,8	1,7	Large subunit of ribonucleotide reductase
orf19.926	EXO1	DNA replication and repair	1,1	1,7	1,5	0,4	1,1	3,2	0,7	0,9	1,3	Exodeoxyribonuclease
orf19.4030		DNA replication and repair	1,4	2,2	1,6	0,4	1,2	2,7	0,9	1,1	1,2	Orthologs have DNA primase activity
orf19.5487	CDC46	DNA replication and repair	0,8	2,1	2,6	0,3	0,7	2,5	0,6	1,2	1,9	Putative hexameric MCM helicase complex subunit
orf19.2611	MCM6	DNA replication and repair	1,3	2,5	2,0	0,5	1,1	2,3	0,6	1,0	1,7	Putative MCM DNA replication initiation complex component
orf19.1208		Filamentous growth	1,5	3,9	2,6	0,6	1,9	3,4	1,1	3,3	3,1	Member of FGR6 family
orf19.6896		Filamentous growth	1,4	4,7	3,4	0,6	1,9	3,2	1,0	3,0	2,9	Member of FGR6 family
orf19.5191	FGR6-1	Filamentous growth	1,4	5,5	3,9	0,6	2,5	4,3	1,2	3,6	2,9	Member of FGR6 family
orf19.5315	FGR6	Filamentous growth	1,8	5,2	2,9	0,6	2,6	4,6	1,3	3,3	2,5	Member of FGR6 family; transposon mutation affects filamentous growth
orf19.4712	FGR6-3	Filamentous growth	1,4	3,5	2,5	0,8	2,1	2,7	1,2	2,7	2,2	Member of FGR6 family
orf19.1234	FGR6-10	Filamentous growth	1,4	4,6	3,3	0,6	1,8	3,0	1,3	2,8	2,1	Member of FGR6 family
orf19.5775		Filamentous growth	1,2	8,0	6,7							Member of a family encoded by FGR6-related genes
orf19.4246		Filamentous growth	0,9	2,5	2,7	2,4	2,0	0,8	2,6	4,8	1,9	Protein similar to Sc Ykr070wp; transposon mutation affects filamentous growth
orf19.1586	FGR22	Filamentous growth	0,1	0,8	5,5	0,6	1,8	2,9	0,4	1,4	3,3	Putative PtdIns-specificphospholipase C (PI-PLC)
orf19.3490	FGR6-4	Flamentous growth	1,3	3,2	2,6				1,3	2,7	2,0	Member of a family encoded by FGR6-related genes in the RB2 repeat sequence
orf19.1618	GFA1	Metabolism and energy	3,1	8,8	2,8	2,3	4,8	2,1	3,3	7,6	2,3	Glucosamine-6-phosphate synthase
orf19.979	FAS1	Metabolism and energy	1,5	4,4	2,9	3,6	7,3	2,0	1,9	3,0	1,6	β-subunit of fatty acid synthase
orf19.7466	ACC1	Metabolism and energy	1,1	3,0	2,6	3,9	7,6	2,0	1,7	1,7	1,0	Putative acetyl-coenzyme-A carboxylase; CS-repressed
orf19.5949	FAS2	Metabolism and energy	1,9	4,6	2,5	5,3	10,4	2,0	2,6	3,0	1,2	α-subunit of fatty acid synthase
orf19.6459	DPP3	Metabolism and energy	3,1	9,6	3,1	5,3	8,9	1,7	10,2	14,1	1,4	Diacylglycerol Pyrophosphate phosphatase (DGPP); required for farnesol biosynthesis
orf19.2761		Metabolism and energy	2,5	5,6	2,3				2,1	3,0	1,4	Putative GPI anchor assembly protein
orf19.837	GNA1	Metabolism and energy	2,1	4,3	2,1	1,8	2,0	1,1	0,6	1,5	2,4	Glucosamine-6-phosphate acetyltransferase
orf19.4506	LYS22	Metabolism and energy	3,6	3,7	1,0	0,3	0,8	2,6	0,1	0,7	5,5	Putative homocitrate synthase
orf19.2896	SOU1	Metabolism and energy	0,2	0,9	5,2	0,3	0,4	1,2	0,3	1,3	5,0	Enzyme involved in utilization of L-sorbose
orf19.24	RTA2	Metabolism and energy	0,4	2,0	4,8	0,2	0,6	3,3	0,4	1,6	3,9	Putative flippase for sphingolipids; sphingoid metabolic process; CS-induced
orf19.3827		Metabolism and energy	0,5	1,1	2,2	1,2	1,2	1,0	1,0	0,9	0,9	Metalloprotease of the mitochodnrial inner membrane
orf19.7227		Metabolism and energy	0,4	0,8	2,0	1,0	0,8	0,8	3,0	1,1	0,4	Protein type 1 phosphatase regulatory subunit, similar to ScYIP1
orf19.1340		Oxidation-reduction processes	2,3	3,3	1,4	3,6	11,0	3,1	4,8	6,0	1,2	Putative aldose reductase
orf19.2244		Oxidation-reduction processes	0,4	1,3	3,5	3,9	3,3	0,8	1,0	3,5	3,6	Similar to oxidoreductases and to Sc Yjr096wp
orf19.4309	GRP2	Oxidation-reduction processes	0,2	0,6	2,8	1,3	1,4	1,1	1,5	2,2	1,4	Methylglyoxalreductase induced in stress response
orf19.2192	GDH2	Oxidation-reduction processes	0,5	1,2	2,3	1,5	2,0	1,3	2,4	2,0	0,8	Putative NAD-specific glutamate dehydrogenase
orf19.4274	PUT1	Oxidation-reduction processes	1,8	4,1	2,3				2,0	1,8	0,9	Putative proline oxidase, proline catabolism, alkaline-regulated by Rim101p
orf19.1910		Oxidation-reduction processes	0,5	1,0	2,1	0,8	0,7	0,9	0,5	0,7	1,3	Predicted NADH-dependent flavin oxidoreductase
orf19.5806	ALD5	Oxidation-reduction processes	0,4	0,8	2,0	2,3	2,4	1,1	1,7	2,7	1,6	NAD-aldehyde dehydrogenase
orf19.7306		Oxidation-reduction processes	0,5	0,9	1,9	2,4	2,5	1,0	3,9	7,8	2,0	Aldo-keto reductase family protein
orf19.4716	GDH3	Oxidation-reduction processes	16,6	19,5	1,2	9,7	24,0	2,5	35,5	46,7	1,3	NADP-glutamate dehydrogenase, Rim101-induced at pH 8
orf19.5542	SAP6	Pathogenesis	45,9	23,8	0,5				10,8	28,8	2,7	Secreted aspartyl protease
orf19.1665	MNT1	Protein folding/modification	1,4	3,3	2,4	1,0	1,2	1,3	1,2	1,7	1,4	Golgi α(1,2)-mannosyltransferase
orf19.6864		Protein folding/modification	1,4	3,5	2,5	0,2	0,4	2,2	0,3	1,1	3,5	Putative ubiquitination
orf19.2444	CHS7	Protein folding/modification							1,2	2,9	2,4	Protein required for ER export of Chs3p
orf19.6029	ROT1	Protein folding/modification	0,7	1,4	1,9	0,3	1,0	2,8	0,5	1,0	2,3	Similar to the ER protein Sc Rot1p, which is involved in cell wall 1,6-beta-glucan biosynthesis and protein glycosylation
orf19.3682	CWH8	Protein modification/folding	0,3	0,3	0,8	0,5	0,7	1,3	2,7	5,3	2,0	Putative dolichyl pyrophosphate (Dol-P-P) phosphatase; protein N-glycosylation
orf19.5334		RNA processing and biogenesis	0,2	0,5	3,6	0,9	1,0	1,2	1,3	0,8	0,6	Ortholog of S. cerevisiae Tis11, a mRNA-binding protein
orf19.4866	CPP1	Signal transduction	0,8	0,9	1,2	0,8	1,7	2,2	0,8	4,0	5,2	MAPK phosphatase, represses Y-H switch, regulates Cph1p filamentation pathway
orf19.3775	SSK2	Signal transduction	1,0	1,5	1,6	1,2	2,4	2,1	1,1	5,0	4,7	MAP kinasekinase kinases; regulates Hog1 activation and signaling
orf19.3216		Signal transduction	2,2	5,6	2,5	0,8	2,3	3,0	1,1	3,9	3,6	Rab GTPase activator
orf19.5797	PLC2	Signal transduction	0,2	0,8	5,3	0,6	1,6	2,7	0,4	1,4	3,0	(PtdIns)-specificphospholipase C (PI-PLC)
orf19.7504		Signal transduction	0,5	1,2	2,6	1,2	1,7	1,4	1,2	1,7	1,4	Ortholog of Sc Rts3p, a component of the protein phosphatase type 2A complex; induced in core CS-response
orf19.2125		Stress response	7,8	16,2	2,1	6,6	20,4	3,1	10,4	25,1	2,4	CipC-like antibiotic response protein; fungal specific
orf19.4082	DDR48	Stress response	0,1	0,5	7,6	0,5	2,2	4,5	1,9	6,6	3,4	Immunogenic stress-associated protein, CS-induced
orf19.7017		Transcription	1,7	3,8	2,2	2,4	5,7	2,3	2,5	9,6	3,8	Putative homeodomain-containing repressor of transcription
orf19.5992	WOR2	Transcription	1,3	1,0	0,8	1,0	2,2	2,3	1,0	5,0	5,1	Transcriptional regulator of white-opaque switching
orf19.4725	SWI6	Transcription	1,5	3,6	2,4				1,1	1,4	1,3	Putative component of transcription complexes
orf19.4670	CAS5	Transcription	0,7	1,4	2,1	0,4	0,8	2,0	0,4	1,3	3,0	Transcription factor, cell wall damage response
orf19.3469		Transcription	0,5	1,4	3,0	0,4	0,6	1,3	0,5	1,0	2,0	Component of transcription complexes
orf19.7359	CRZ1	Transcription	0,4	1,0	2,4	0,3	0,4	1,1	0,5	0,6	1,3	Calcineurin-regulated transcription factor
orf19.5286	YCP4	Transcription	0,2	0,6	2,4	0,9	1,0	1,0	0,9	1,8	2,0	Putative flavodoxin; FMN binding protein
orf19.4328	CCC2	Transport	0,5	0,7	1,3	0,5	1,2	2,3	0,6	2,7	4,2	Copper-transporting P-type ATPase of Golgi; CS-repressed
orf19.2209	YVC1	Transport	2,0	3,8	2,0	0,9	2,5	2,8	1,8	4,3	2,4	Calcium transport
orf19.1813	FLC2	Transport	1,1	2,9	2,5	1,0	2,5	2,5	1,3	2,8	2,2	Protein involved in heme uptake; putative FADtransporter, similar to ScFlc2p
orf19.1702	ARF3	Transport	5,3	10,2	1,9	2,0	4,0	2,0	3,2	4,3	1,4	Intracellular protein transport
orf19.1224	FRP3	Transport	1,2	3,1	2,5	1,1	1,2	1,1	1,1	1,6	1,4	Ammonium transport

orf19.5022		Transport	1,8	3,5	2,0	5,2	6,0	1,2	6,3	6,3	1,0	Ion transport
orf19.5037	HRQ2	Unknown function; gene named							2,4	5,5	2,3	Protein not essential for viability
orf19.3417	ACF2	Unknown function; gene named							1,8	4,9	2,7	Putative endo-1,3-beta-glucanase; fungal-specific
orf19.1120	FAV2	Unknown function; gene named	6,4	7,2	1,1	0,8	2,5	3,2				Adhesin-like protein
orf19.4867	SWE1	Unknown function; gene named	1,1	2,3	2,1							Functional homolog of Sc Swe1p
orf19.668	TOS4	Unknown function; gene named	1,1	2,2	2,1	0,6	1,3	2,3	0,8	1,0	1,2	Putative forkhead transcription factor
orf19.2344	ASR1	Unknown function; gene named	0,04	0,1	1,6	0,1	0,1	1,5	0,1	0,6	4,2	Putative heat shock protein
orf19.4688	DAG7	Unknown function; gene named	0,2	0,5	2,2	0,03	0,04	1,5	0,03	0,2	5,2	Secretory protein
orf19.7350	RCT1	Unknown function; gene named	0,3	0,6	2,1	0,7	0,6	0,9	0,7	1,3	1,9	Predicted ORF
orf19.4706		Unknown function; gene not named	0,7	1,9	2,9	0,6	1,5	2,7	1,1	3,8	3,4	Predicted ORF
orf19.3007.2		Unknown function; gene not named	0,4	1,4	3,5	1,6	2,2	1,4	1,2	3,9	3,3	Predicted ORF
orf19.5518		Unknown function; gene not named	1,0	3,5	3,3	0,7	3,6	5,0	1,1	3,8	3,3	Predicted ORF
orf19.3145		Unknown function; gene not named	1,5	4,5	2,9	0,7	1,8	2,7	1,4	4,3	3,1	Predicted ORF
orf19.4485		Unknown function; gene not named	1,3	4,4	3,3	0,6	2,5	4,3	1,0	3,1	3,1	Predicted ORF
orf19.1144		Unknown function; gene not named							4,0	11,0	2,8	Predicted ORF with SEL-1 like protein domain
orf19.1344		Unknown function; gene not named	4,1	13,6	3,3	13,5	24,1	1,8	5,5	15,0	2,7	Predicted ORF; fluconazole-induced
orf19.5295		Unknown function; gene not named				3,4	3,3	1,0	2,6	6,2	2,4	Potential member of endo/exonuclease/phosphatase family
orf19.7297		Unknown function; gene not named	1,3	1,9	1,5	4,4	4,7	1,1	3,9	8,9	2,3	Putative cystathionine gamma-synthase; Hog1p-induced; Gcn4p-regulated
orf19.3737		Unknown function; gene not named	1,4	3,0	2,1	1,8	2,7	1,5	2,1	4,9	2,3	Protein with a Vps9 vacuolar protein sorting protein domain
orf19.1830		Unknown function; gene not named	0,9	1,7	1,9				3,0	6,3	2,1	Predicted ORF
orf19.4922		Unknown function; gene not named	2,6	2,7	1,0	3,1	3,2	1,0	2,5	5,0	2,0	Predicted ORF
orf19.2959.1		Unknown function; gene not named	0,1	0,9	7,4	1,3	2,1	1,6	3,0	5,9	2,0	Predicted ORF
orf19.5799		Unknown function; gene not named	0,4	1,8	4,5	0,3	0,7	2,8	0,5	2,6	5,2	Predicted ORF
orf19.4531		Unknown function; gene not named	0,7	0,7	1,0	0,5	1,5	3,0	0,6	2,5	4,1	Putative PDR subfamily ABC transporter
orf19.3694		Unknown function; gene not named							0,7	2,7	3,9	Predicted ORF
orf19.727		Unknown function; gene not named	1,3	4,5	3,5				1,3	3,4	2,7	Member of a family encoded by FGR6-related genes in the RB2 repeat sequence
orf19.914		Unknown function; gene not named	1,2	4,7	3,8	0,6	1,9	3,3	1,2	3,2	2,6	Predicted ORF
orf19.6929		Unknown function; gene not named	1,2	1,6	1,3				0,8	2,1	2,6	Predicted ORF:orthologs have phosphatase activity
orf19.7506		Unknown function; gene not named	1,1	1,4	1,3	0,9	2,2	2,4	0,9	2,2	2,6	Predicted ORF
orf19.7005		Unknown function; gene not named	1,4	4,9	3,5	0,6	1,9	3,3	1,1	2,8	2,4	Predicted ORF
orf19.6960		Unknown function; gene not named	1,3	3,7	2,8	0,7	2,3	3,5	1,3	3,0	2,4	Predicted ORF
orf19.4553		Unknown function; gene not named	0,8	0,9	1,1	0,8	0,8	1,0	1,1	2,2	2,0	Predicted ORF
orf19.5777		Unknown function; gene not named	0,9	1,5	1,8				1,5	3,1	2,0	Predicted ORF
orf19.1099		Unknown function; gene not named	1,7	4,5	2,6				1,6	3,3	2,0	Predicted ORF
orf19.3144		Unknown function; gene not named	1,7	3,6	2,1	0,6	2,1	3,3	1,1	2,3	2,0	Predicted ORF
orf19.4014		Unknown function; gene not named	2,0	3,6	1,8	4,2	9,3	2,2	5,9	11,1	1,9	Putative ER phospholipid phosphatase, similar to ScCDC1
orf19.3615		Unknown function; gene not named	0,6	2,2	3,4	1,8	3,8	2,2	2,3	4,0	1,7	Predicted ORF; CS-induced
orf19.5137.1		Unknown function; gene not named	1,9	2,5	1,3	1,2	2,3	2,0	2,3	2,0	0,9	Predicted ORF
orf19.6843		Unknown function; gene not named	2,5	5,5	2,2				2,0	1,9	1,0	Putative role in nucleosome assembly
orf19.5514		Unknown function; gene not named	2,1	4,4	2,1							Predicted ORF
orf19.3793		Unknown function; gene not named	3,6	7,4	2,1	6,1	7,6	1,2	6,5	9,5	1,5	Predicted ORF
orf19.95		Unknown function; gene not named	0,7	4,9	6,7							Predicted ORF
orf19.4666		Unknown function; gene not named	1,6	4,8	2,9	1,5	2,8	1,9	1,9	3,6	1,9	Predicted ORF
orf19.6474		Unknown function; gene not named	0,9	2,5	2,8	1,3	1,3	1,0	1,9	2,9	1,5	Protein with chitin synthesis regulation, resistance to Congo red domain
orf19.4390		Unknown function; gene not named	0,9	2,3	2,7				1,2	1,7	1,4	Predicted ORF
orf19.6737		Unknown function; gene not named	1,1	2,6	2,3	1,1	1,8	1,6	2,6	2,8	1,0	Predicted ORF
orf19.3983		Unknown function; gene not named	1,7	3,6	2,2	2,3	1,8	0,8	1,4	2,4	1,7	Predicted ORF
orf19.1825		Unknown function; gene not named	1,5	3,0	2,1							Protein not essential for viability; filament induced
orf19.1935		Unknown function; gene not named	1,0	2,0	2,0							Predicted ORF, dubious
orf19.6527		Unknown function; gene not named	0,2	0,4	1,8	0,2	0,2	1,2	0,3	0,6	2,6	Predicted ORF
orf19.1565		Unknown function; gene not named	0,6	0,6	1,0	0,2	0,5	2,3	0,3	0,7	2,3	Protein with unknown function
orf19.1862		Unknown function; gene not named	0,1	0,2	2,7	0,2	0,1	0,7	0,3	0,6	2,0	Possible stress protein
orf19.2030		Unknown function; gene not named	0,2	1,0	4,5	1,0	1,1	1,1	2,0	2,4	1,2	Predicted ORF
orf19.3932		Unknown function; gene not named	0,1	0,6	4,4	1,4	1,7	1,2	2,4	4,0	1,6	Predicted RNA binding protein; induced in core CS response
orf19.1632		Unknown function; gene not named	0,2	0,9	4,4	0,5	1,1	2,2	0,5	1,9	3,5	Predicted ORF
orf19.5282		Unknown function; gene not named	0,2	0,8	3,3	0,5	0,3	0,7	1,2	0,5	0,4	Predicted ORF
orf19.246		Unknown function; gene not named	0,5	1,5	3,1	0,7	1,0	1,4	0,7	1,5	2,1	Predicted metalloendopeptidase
orf19.3110		Unknown function; gene not named	0,2	0,6	2,9				0,2	0,5	3,3	Possible mannosyltransferase
orf19.94		Unknown function; gene not named	0,2	0,6	2,6	1,2	1,4	1,2	2,1	2,6	1,2	Predicted ORF
orf19.462		Unknown function; gene not named	0,5	1,0	2,1	1,8	1,7	1,0	1,4	1,9	1,4	Predicted ORF

Table S2. Class 2 - transcripts that are less abundant in the *phr1* Δ than in the wild type

Green: expression ratio ≤ 0.5 each time was compared to time zero in the same strain
Red: expression ratio ≥ 2
Light blue: mutant/wild type ≤ 0.5 except values obtained from two xpression rations ≥ 2 (red/red)

Time after induction			1 h			3 h			5 h			
ORF	**GeneName**	**Functional category**	**WT**	***phr* 1**	***phr* 1/WT (RF)**	**WT**	***phr* 1**	***phr* 1/WT (RF)**	**WT**	***phr* 1**	***phr* 1/WT (RF)**	**Description**
orf19.1097	ALS2	Adhesion	0,6	1,1	1,7	0,2	0,2	0,9	0,4	0,1	0,2	ALS family protein, role in adhesion
orf19.4555	ALS4	Adhesion	0,2	0,1	0,7				0,03	0,01	0,4	ALS family protein
orf19.2121	ALS2	Adhesion	0,9	1,4	1,5	0,3	0,2	0,7	0,9	0,2	0,2	ALS family
orf19.5267		Adhesion	0,6	0,3	0,4				0,3	0,5	1,7	Putative cell wall adhesin-like protein, CS-repressed
orf19.5032	SIM1	Cell wall/surface	0,5	0,4	0,9	0,1	0,02	0,3				Cell wall bigoenesis; SUN family member
orf19.4651	PGA53	Cell wall/surface	0,5	0,6	1,2	0,4	0,2	0,5	0,3	0,3	1,1	GPI-anchored cell surface protein
orf19.2758	PGA38	Cell wall/surface	0,6	0,2	0,4	1,1	1,1	1,0	1,0	1,3	1,3	Putative adhesin-like GPI-anchored protein; repressed during cell wall regeneration
orf19.5760	IHD1	Cell wall/surface	3,2	4,6	1,4	1,3	1,0	0,7	2,4	0,8	0,3	GPI-anchored protein
orf19.6782	BMT1	Cell wall/surface	0,9	0,5	0,6	2,5	1,6	0,6	3,2	1,7	0,5	β-mannosyltransferase for cell wall phopshopeptidomannan
orf19.3670	GAL1	Metabolism and energy	0,2	0,2	1,0	0,6	0,4	0,7	2,2	0,5	0,2	Galactokinase
orf19.5288	IFE2	Metabolism and energy	0,01	0,01	1,1	0,1	0,04	0,6	0,2	0,02	0,1	Alcohol dehydrogenase, decreased expression in hyphae
orf19.3707	YHB1	Metabolism and energy	0,1	0,1	1,2	0,1	0,1	0,8	0,2	0,02	0,1	Nitric oxide dioxygenase, nitric oxidescavenging/detoxification
orf19.3710	YHB5	Metabolism and energy	2,0	1,2	0,6	0,1	0,03	0,2	0,4	0,1	0,2	Protein related to flavohemoglobins, filament induced
orf19.3656	COX15	Metabolism and energy	0,5	0,6	1,1	0,4	0,4	1,0	0,3	0,1	0,5	Cytochrome oxidase assembly protein
orf19.7593		Metabolism and energy	0,5	0,4	0,7	0,1	0,1	0,8	0,2	0,1	0,5	Putative asparaginase
orf19.6343	*FEN1*	Metabolism and energy	0,4	0,2	0,6	0,1	0,1	0,8	0,2	0,1	0,5	Putative fatty acid elongase
orf19.3483		Metabolism and energy	0,03	0,03	1,0	0,05	0,03	0,7	0,1	0,04	0,5	Glycorophosphodiester phopshodiesterase
orf19.7314	CDG1	Metabolism and energy	0,2	0,2	1,2	0,7	0,5	0,7	1,6	0,4	0,2	Putative cysteine dioxygenases
orf19.3675	GAL7	Metabolism and energy	0,1	0,1	0,7	0,2	0,2	0,9	0,8	0,2	0,3	Putative galactose-1-phoshphate uridyl transferase
orf19.3672	GAL10	Metabolism and energy	0,2	0,1	0,9	0,4	0,3	0,8	1,4	0,4	0,3	UDP-glucose 4-epimerase
orf19.1517	ARO3	Metabolism and energy	4,7	4,3	0,9	1,3	1,3	1,0	0,7	0,4	0,5	3-deoxy-D-arabinoheptulosonate-7-phosphate synthase; aromatic amino acid synthesis
orf19.5394.1		Metabolism and energy	0,8	0,7	0,9	0,8	0,6	0,7	0,9	0,5	0,5	Ortholog(s) have role in mitochondrial respiratory chain complex IV assembly
orf19.2251	AAH1	Metabolism and energy	0,1	0,1	0,7	0,1	0,02	0,5	0,03	0,02	0,7	Adenine deaminase involved in purine salvage and nitrogen catabolism
orf19.1847	ARO10	Metabolism and energy	0,2	0,1	0,4	0,6	0,6	1,1	0,5	0,6	1,2	Aromatic decarboxylase, alkaline downregulated
orf19.6844	ICL1	Metabolism and energy	0,01	0,01	0,5	0,03	0,02	0,9	0,03	0,04	1,3	Isocitrate lyase
orf19.7227		Metabolism and energy	0,4	0,8	2,0	1,0	0,8	0,8	3,0	1,1	0,4	Protein type 1 phosphatase regulatory subunit, similar to ScYIP1
orf19.3669	SHA3	Metabolism and energy	0,5	0,8	1,6	2,3	2,2	0,9	4,8	1,9	0,4	Putative serine/threonine kinase involved in glucose transport
orf19.2050		Metabolism and energy	0,8	0,7	0,9	2,0	1,0	0,5	3,5	1,9	0,5	Ortholog(s) have sterol esterase activity; lipid metabolism
orf19.449		Metabolism and energy				3,5	1,5	0,4	7,6	2,4	0,3	Putative phosphatidyl synthase
orf19.85	GPX2	Metabolism and energy	5,1	4,7	0,9	3,0	1,3	0,4	17,2	2,6	0,1	Glutathione peroxidase activity
orf19.3412	ATG15	Metabolism and energy	1,0	1,2	1,2	3,2	1,7	0,5	3,4	3,1	0,9	Putative lipase required for intravacuolar lysis of autophagic bodies; similar to ScAtg15p
orf19.385	GCV2	Metabolism and energy	8,6	1,9	0,2	3,6	2,3	0,7	5,4	3,2	0,6	Role in glycine catabolism
orf19.732		Oxidoreduction processes				0,3	0,3	1,1	0,5	0,3	0,5	Possible dehydrogenase
orf19.5842		Oxidoreduction processes	1,1	1,0	0,8				0,8	0,3	0,4	Protein with predicted siroheme synthase middle domains NAD(P)-binding
orf19.3331	ABC1	Oxidoreduction processes	0,6	0,4	0,8	0,9	1,0	1,1	0,9	0,5	0,5	Putative ubiquinol-cytochrome-c reductase
orf19.4631	ERG251	Oxidoreduction processes	0,4	0,6	1,4	1,1	0,8	0,7	2,0	0,6	0,3	C-4 sterol methyl oxidase; erogosterol synthesis
orf19.7077	*FRE7*	Oxidoreduction processes	0,9	0,3	0,4	3,3	1,2	0,4	2,4	0,8	0,4	Putative ferric reductase
orf19.3521	ARH2	Oxidoreduction processes							3,9	1,7	0,4	Adenodroxin-NADPH oxidoreductase, heme biosynthesis
orf19.4279	MNN1	Protein folding/modification	0,1	0,03	0,4				0,04	0,02	0,4	Putative α(1,3)-mannosyltransferase
orf19.3301		Protein folding/modification	0,3	0,1	0,4	0,3	0,1	0,5	0,4	0,2	0,4	Putative ubiquitin ligase
orf19.4871	ERO1	Protein folding/modification	0,2	0,2	0,9	0,3	0,1	0,5	0,3	0,1	0,4	Protein with role in formation of disulfide bonds
orf19.7654	CPR6	Protein folding/modification	1,3	1,4	1,1	3,3	1,8	0,5	1,2	1,0	0,8	Peptidyl-prolyl cis-trans isomerase,protein refolding
orf19.5961		Protein folding/modification	0,6	0,5	0,8	3,1	1,6	0,5	3,0	1,9	0,6	Chaperone for proteasome assembly
orf19.3479		RNA processing and biogenesis	0,6	0,6	1,0	0,2	0,2	1,1	0,2	0,1	0,5	snRNA pseudouridine synthesis
orf19.2735	*SEN2*	RNA processing and biogenesis	1,2	0,6	0,5				0,3	0,2	0,5	Putative tRNA splicing endonuclease subunit
orf19.494		RNA processing and biogenesis	0,3	0,1	0,4	0,1	0,1	0,5	0,1	0,1	0,5	Putative RNA binding protein, role in pre-rRNA processes
orf19.6736		RNA processing and biogenesis	0,5	0,5	0,9	0,3	0,3	0,9	0,4	0,2	0,5	Protein required for mitochondrial ribosome small subunit biogenesis

orf19.6862		RNA processing and biogenesis	1,1	0,7	0,6	0,4	0,3	0,7	0,5	0,2	0,5	Processing rRNA
orf19.7369	TRM12	RNA processing and biogenesis	0,7	0,5	0,8	0,4	0,3	0,8	0,8	0,4	0,5	S-adenosylmethionine-dependent methyl transferase
orf19.3303		RNA processing and biogenesis	0,4	0,2	0,5	0,2	0,1	0,5	0,2	0,1	0,8	tRNA methyltransferase
orf19.6873.1	KTI11	RNA processing and biogenesis	0,4	0,1	0,4	0,04	0,02	0,7	0,04	0,02	0,6	Zn-ribbon protein; synthesis of diphthamide on translation factor eEF2;invovled in tRNA modification
orf19.2934		RNA processing and biogenesis	0,4	0,2	0,4	0,1	0,04	0,7	0,1	0,1	0,9	Ribosomal large subunit export from nucleous; similar to Sc Bud20p reuired for bus site selection
orf19.6234		RNA processing and biogenesis	0,5	0,2	0,4	0,1	0,1	1,1	0,1	0,1	0,8	Putative U2 snRNP, rRNA processing and prereplicative complex
orf19.4746	JIP5	RNA processing and biogenesis	0,5	0,2	0,4	0,1	0,1	0,8	0,1	0,1	0,8	Role in biogenesis of ribosomal large subunit, repressed in core stress response
orf19.5500	*MAK16*	RNA processing and biogenesis	0,4	0,2	0,4	0,1	0,03	0,6	0,1	0,04	0,6	Putative constituent of 66S prerimosomal particles
orf19.154		RNA processing and biogenesis	0,3	0,2	0,5	0,1	0,1	0,8	0,1	0,1	1,4	Biogenesis ribosomal small subunit, ortholog of Sc UTP30
orf19.1642		RNA processing and biogenesis	0,4	0,2	0,5	0,1	0,1	0,8	0,1	0,1	0,9	Ortholog of Sc loc1p, Involved in assymetric RNA localization and in rRNA biogenesis
orf19.2185	NSA1	RNA processing and biogenesis	0,4	0,2	0,5	0,1	0,1	0,8	0,1	0,1	1,0	Ribosomal large subunit biogenesis, similar to Sc NSA1
orf19.809		RNA processing and biogenesis	0,3	0,2	0,5	0,1	0,1	1,0	0,1	0,1	0,9	Involved in maturation of LSU-rRNA precursor, similar to ScNOP12
orf19.5732	NOG2	RNA processing and biogenesis	0,4	0,2	0,5	0,1	0,1	0,9	0,1	0,1	0,8	Nucleolar GTPase; export of large ribosomal subunit from nucleus
orf19.3630	RRP8	RNA processing and biogenesis	0,5	0,2	0,5	0,1	0,1	1,1	0,2	0,2	0,7	Ribosomal protein; large ribosomal subunit biogenesis
orf19.3756	CHR1	RNA processing and biogenesis	0,4	0,2	0,5	0,1	0,2	1,3	0,2	0,2	1,0	ATP-dependent RNA helicase
orf19.2830	*RRP9*	RNA processing and biogenesis	0,5	0,3	0,5	0,1	0,1	0,9	0,1	0,1	1,1	Ribosomal protein similar to ScRrp9
orf19.5678		RNA processing and biogenesis	0,8	0,3	0,4				0,4	0,3	0,7	Protein required for synthesis of diphthamide on eEF2 possibily with KIT11
orf19.5507	ENP1	RNA processing and biogenesis	0,6	0,2	0,4	0,1	0,1	0,9	0,1	0,1	0,9	Required for pre rRNA processing
orf19.2654	RMS1	RNA processing and biogenesis	0,6	0,3	0,5				0,2	0,2	1,3	Putative ribosomal lysine methyl transferase; regulation of translation
orf19.2314		RNA processing and biogenesis	0,6	0,3	0,5	0,1	0,1	0,9	0,2	0,2	0,9	Protein involved in nucleolar integrity and processing of pre-rRNA; similar to ScCgr1p
orf19.6831	PRP5	RNA processing and biogenesis	0,7	0,3	0,5				0,6	0,6	1,0	pre mRNA processing helicase activity
orf19.7154	*UTP18*	RNA processing and biogenesis	0,6	0,3	0,5	0,1	0,1	0,9	0,1	0,1	0,9	U3 SnoRNA-associated protein
orf19.1673	PPT1	Signal transduction	1,1	0,6	0,6	0,4	0,3	0,6	0,5	0,2	0,5	Putative ser/thr protein phosphatase
orf19.1760	RAS1	Signal transduction	2,6	2,7	1,0	2,2	1,4	0,6	3,7	1,8	0,5	Small GTPase; regulates cAMP and MAP kinase pathways
orf19.822	HSP21	Stress response	0,01	0,02	1,4	0,1	0,02	0,3	0,9	0,1	0,1	Small heat-shock protein
orf19.882	HSP78	Stress response	0,2	0,3	1,2	0,7	0,3	0,4	0,8	0,4	0,5	Heat-shock protein
orf19.6824		Transcription	0,1	0,05	0,5	0,03	0,02	0,6	0,1	0,02	0,3	h-L-h-transcription factor regulator of cell adhesions,
orf19.2356	CRZ2	Transcription	0,03	0,01	0,4				0,04	0,02	0,4	Putative transcription factor, zinc finger,similar to ScCrz1p
orf19.4941	TYE7	Transcription	0,1	0,3	4,1	0,6	0,5	0,8	1,6	0,4	0,2	Putative bHLH (basic region, helix-loop-helix)transcription factor; CS-repressed
orf19.6514	CUP9	Transcription	0,5	0,3	0,6	0,3	0,2	0,7	0,8	0,3	0,3	Transcription factor, Y-H switched repressed
orf19.1168	ZCF3	Transcription	1,7	0,5	0,3	0,6	0,2	0,4	0,8	0,3	0,4	Zn(II)2Cys6 domain transcription factor required for filamentous growth
orf19.2748	ARG83	Transcription	1,4	2,6	1,8	0,5	0,5	1,0	0,9	0,4	0,5	GAL4-like Zn(II)2Cys6 transcription factor
orf19.1187	CPH2	Transcription	0,2	0,3	1,3	0,3	0,3	1,0	0,7	0,4	0,5	Myc-bHLH transcription factor; promotes hyphal growth
orf19.7374	CTA4	Transcription	0,3	0,2	0,7	0,3	0,2	0,5	0,2	0,2	1,0	Zn(II)2Cys6 transcription factor
orf19.3912	GLN3	Transcription	0,9	0,6	0,7	0,6	0,3	0,5	0,7	0,6	0,9	GATA transcription factor, regulation of nitrogen starvation-induced filamentous growth
orf19.1826	MDM34	Transcription	0,8	0,5	0,6	0,7	0,5	0,7	2,3	0,7	0,3	Putative transcription factor
orf19.508	QDR1	Transport	0,1	0,1	1,4	0,1	0,04	0,5	0,1	0,03	0,2	Putative Transporter of antibiotic resistance
orf19.7313	SSU1	Transport	0,2	0,1	0,4	0,2	0,1	0,3	0,2	0,1	0,3	Protein similar to ScSsu1p sulfiteTransport protein
orf19.6817	FCR1	Transport	0,5	0,5	1,0				0,1	0,04	0,3	Zinc cluster transcription factor, fluconazole resistance
orf19.6937	PTR2	Transport	0,1	0,1	0,6	0,1	0,03	0,6	0,1	0,03	0,4	Putative oligopeptide Transporter, repressed by RIM101 at pH 8
orf19.4599	*PHO89*	Transport	0,3	0,2	0,5	0,03	0,03	0,8	0,1	0,05	0,5	Phosphate permease
orf19.1978	GIT2	Transport	0,3	0,2	0,7	0,2	0,1	0,5	0,2	0,1	0,5	Putative glycerophosphoinositol permease
orf19.2020	HGT6	Transport	0,1	0,1	1,4	0,4	0,3	0,8	1,0	0,3	0,3	Putative high-affinity MFS glucose transporter
orf19.2942	DIP5	Transport	0,5	0,3	0,6	0,1	0,1	0,9	0,9	0,5	0,5	Dicarboxylic amino acid permease
orf19.473	TPO4	Transport	1,0	0,8	0,8	1,0	0,5	0,5	0,6	0,5	0,8	Putative sperimidine transporter
orf19.5905		Transport	0,6	0,3	0,5	0,1	0,1	1,0	0,1	0,1	0,8	Sterol transport; similar to Sc OSH2
orf19.6578		Transport	0,6	0,3	0,5	1,4	1,1	0,7	3,5	1,4	0,4	Predicted membrane transporter; repressed in core CS-response
orf19.7219	FTR1	Transport	3,0	1,6	0,5	3,6	1,8	0,5	8,9	7,3	0,8	High-affinity iron permease; involved in pathogenesis
orf19.2107.1	MUQ1	Unknown function; gene named	0,04	0,1	2,9	2,1	1,6	0,7	5,9	1,7	0,3	ATP biosynthetic process
orf19.4044	MUM2	Unknown function; gene named	2,1	1,7	0,8	0,8	0,4	0,5				Protein similar to *Sc* Mum2p
orf19.2723	HIT1	Unknown function; gene named	0,4	0,1	0,4	0,3	0,2	0,6	0,4	0,2	0,6	Protein similar to Sc Hit1p, which is required for growth at hightemperature
orf19.3369	MOH1	Unknown function; gene named	0,5	0,4	1,0				3,5	1,5	0,4	Similar to *ScMOH1*
orf19.171	DBP2	Unknown function; gene named	0,3	0,2	0,6	0,1	0,1	0,9	0,2	0,1	0,5	Putative DEAD-box family ATP-dependent RNA helicase invovled in mRNA decay
orf19.2462	PRN3	Unknown function; gene named	0,6	0,3	0,5	0,5	0,7	1,4	0,9	0,5	0,5	Protein similar to pirin
orf19.5496	AVT1	Unknown function; gene named	0,9	0,8	0,9	0,7	0,7	0,9	0,7	0,4	0,5	Putative vacuolar transporter
orf19.1285		Unknown function; gene not named	0,5	0,3	0,7	0,9	0,3	0,4	1,1	0,7	0,6	Putative lipid binding protein
orf19.6688		Unknown function; gene not named	0,7	0,5	0,6	0,7	0,4	0,5	0,6	0,3	0,6	Predictive ORF

orf19.1363		Unknown function; gene not named	0,1	0,04	0,6	0,02	0,01	0,7	0,04	0,02	0,5	Predicted ORF; Plc1p-regulated
orf19.4445		Unknown function; gene not named	0,1	0,1	1,5	0,1	0,1	0,7	0,1	0,1	0,5	Predicted ORF; Plc1p-regulated
orf19.7296		Unknown function; gene not named	0,1	0,4	2,7	0,2	0,1	0,4	0,3	0,2	0,5	Putative cation conductance protein
orf19.5607		Unknown function; gene not named	0,7	0,5	0,7	0,3	0,3	1,0	0,3	0,2	0,5	Predicted ORF
orf19.4280		Unknown function; gene not named	0,3	0,2	0,8	0,2	0,2	0,8	0,4	0,2	0,5	Predicted ORF
orf19.4450.1		Unknown function; gene not named	0,03	0,1	4,1	0,4	0,2	0,5	0,8	0,05	0,1	Predicted ORF
orf19.5626		Unknown function; gene not named	0,1	0,1	1,1	0,6	0,4	0,6	1,6	0,5	0,3	Plc1-regulated
orf19.5069		Unknown function; gene not named	0,3	0,5	1,7	0,8	0,4	0,6	1,1	0,4	0,3	Similar to *Sc* meiotic DNA recombinase
orf19.6556		Unknown function; gene not named	0,5	0,3	0,5	0,9	0,3	0,4	1,1	0,4	0,4	Predicted ORF
orf19.1368		Unknown function; gene not named				1,1	0,5	0,5	1,0	0,4	0,4	Predicted ORF
orf19.4816		Unknown function; gene not named	0,6	0,3	0,5	0,7	0,5	0,7	1,1	0,5	0,4	Predicted ORF;induced by nitric oxide
orf19.4580		Unknown function; gene not named	1,0	0,9	0,9	1,4	0,9	0,7	0,9	0,5	0,5	Predicted ORF
orf19.3360		Unknown function; gene not named	0,4	0,3	0,9	0,3	0,2	0,5	0,6	0,3	0,5	Predicted ORF
orf19.2724		Unknown function; gene not named	0,2	0,1	0,5	0,3	0,1	0,4	0,8	0,4	0,5	Predicted ORF
orf19.3644		Unknown function; gene not named	0,3	0,3	1,1	0,4	0,2	0,5	0,5	0,3	0,7	Predicted ORF
orf19.775		Unknown function; gene not named	0,4	0,4	0,9	0,9	0,5	0,5	1,3	0,8	0,6	Probable protein involved in vacuolar protein sorting
orf19.1287		Unknown function; gene not named	0,3	0,1	0,3	0,1	0,1	0,6	0,2	0,1	0,6	Predicted ORF
orf19.6316.4		Unknown function; gene not named	0,5	0,2	0,4	0,1	0,1	1,0	0,1	0,1	0,9	Predicted ORF
orf19.1090		Unknown function; gene not named	0,7	0,3	0,4	0,4	0,4	1,0	0,3	0,3	1,0	Predicted ORF
orf19.670.2		Unknown function; gene not named	0,03	0,1	1,9	1,0	1,1	1,0	7,0	1,3	0,2	Predicted ORF; hypoxia
orf19.4828		Unknown function; gene not named	0,8	0,6	0,8	1,5	1,0	0,7	2,8	1,0	0,3	WD repeat domain protein
orf19.7085		Unknown function; gene not named	0,3	0,2	1,0	2,4	0,9	0,4	2,9	1,1	0,4	Predicted ORF;induced in core stress response
orf19.6683		Unknown function; gene not named	2,7	1,8	0,7	1,3	1,0	0,8	3,1	1,2	0,4	Predicted vacuolar protein with a calcineurin-like phosphoesterase domain
orf19.1964		Unknown function; gene not named	2,2	2,6	1,1	4,9	4,2	0,8	3,6	1,6	0,4	Predicted ORF
orf19.6448		Unknown function; gene not named	2,5	2,2	0,9	2,9	1,9	0,7	3,1	1,5	0,5	Similar to ubiquitin ligase
orf19.1861		Unknown function; gene not named	0,6	0,8	1,2				3,3	1,7	0,5	Predicted ORF
orf19.6586		Unknown function; gene not named	0,3	0,4	1,1	1,9	1,3	0,7	2,6	1,4	0,5	Predicted ORF
orf19.1505		Unknown function; gene not named	1,6	1,1	0,7	2,4	1,2	0,5	2,0	1,2	0,6	Predicted ORF
orf19.2515		Unknown function; gene not named	0,3	0,4	1,3	3,3	1,8	0,5	5,1	5,0	1,0	Predicted ORF
orf19.3142		Unknown function; gene not named	2,5	1,1	0,4							Predicted ORF
orf19.334		Unknown function; gene not named	2,1	0,9	0,4	16,9	4,5	0,3	21,7	8,9	0,4	Late stage biofilm-induced gene
orf19.7396		Unknown function; gene not named	0,1	0,1	0,6	0,1	0,04	0,7	0,1	0,1	0,4	Predicted ORF
orf19.6770		Unknown function; gene not named	0,2	0,2	0,8	0,2	0,1	0,4	0,3	0,1	0,4	Predicted ORF
orf19.7283		Unknown function; gene not named	0,02	0,01	0,6	0,03	0,01	0,5	0,04	0,01	0,4	Predicted ORF
orf19.699		Unknown function; gene not named	0,2	0,1	0,4				0,2	0,1	0,3	Predicted ORF

Table S3. Comparison of data from microarray and qRT-PCR analyses.

Gene	Time	DNA Microarray			qRT-PCR		
	3 hr	**WT[a]**	***phr1*[b]**	**RF[c]**	**WT fold-change[d]**	***phr1* fold-change[e]**	**RF**
CRH11		1.2	5.1	4.2	2.5 ± 0.3	7.2 ± 0.2	2.8 ± 0.1
GFA1		2.3	4.8	2.1	1.4 ± 0.5	3.7 ± 0.8	2.8 ± 0.4
CHS8		3.0	5.9	2.0	2.1 ± 0.3	7.2 ± 0.1	3.5 ± 0.2
PGA23		0.2	4.2	22.2	0.2 ± 0.01	5.6 ± 0.5	29.2 ± 0.1
	5 hr						
CRH11		2.3	7.6	3.3	2.1 ± 0.2	6.6 ± 2.7	3.1 ± 0.4
GFA1		3.3	7.6	2.3	0.6 ± 0.4	2.1 ± 0.5	3.3 ± 0.6
CHS8		2.6	11.1	4.3	1.6 ± 0.2	4.5 ± 0.9	2.9 ± 0.2
PGA23		0.2	10.2	65.6	0.1 ± 0.01	7.3 ± 0.4	93.1 ± 0.1

[a] and [b] Expression ratio of each gene at the indicated time compared to time zero in the same strain.
[c] RF, Relation Factor, ratio of the expression ratios or fold-change MUT/WT
[d] and [e] Fold-change of the transcript level of each gene at the indicated time with respect to time zero.

Table S4. Oligonucleotides used in this work

Primer	Sequence
Primers for strain construction	
PHR1-N7	5'-CCATGGCCTCCTTAGATCAAATCATTCC-3'
hisG3'P	5'-GCCAAGCGCTTTCAGTTTCTC-3'
hisG-forward	5'-CCTCATATCCGCACCTCCTC-3'
PHR1rev(+1840)	5'-CACCAATTGAGAAACTTAGGGAT-3'
NAT1_5'link_rev	5-GAGCCGTAATTTTTGCTTCG-3'
NAT1-3'link_fwd	5'-TGGTCGCTATACTGCTGTCG-3'
Primers for Q-RT-PCR	
CRH11-F	5'-CTACCGTTACCAGTTCTTCG-3'
CRH11-R	5'-CAGTGGAGGCAGTACTTGAA-3'
GFA1-F	5'-ATCTGCTGGGGAATCTACTG-3'
GFA1-R	5'-GCAGAATCTGGTTGTTCG-3'
CHS8-F	5'-GGTAGTGGTGGAATACATGC-3'
CHS8-R	5'-ATCTCTTCACCAGTGTCCAG-3'
TDH3-F	5'-GGTTTCGGTAGAATCGGTAG-3'
TDH3-R	5'-CACCCTTGTATCTACCGTGA-3'
PGA23-F	5'-GGAAGCTTAGTTGGTGGTCT-3'
PGA23-R	5'-TCTAGATCCTGAACCACTGC-3'